SYNTHESIS AND CHARACTERIZATION OF LANTHANIDE BASED NANOMATERIALS FOR RADIATION DETECTION AND BIOMEDICAL APPLICATIONS

by

MINGZHEN YAO

Presented to the Faculty of the Graduate School of

The University of Texas at Arlington in Partial Fulfillment

of the Requirements

for the Degree of

DOCTOR OF PHILOSOPHY

THE UNIVERSITY OF TEXAS AT ARLINGTON

May 2011

ACKNOWLEDGEMENTS

First and foremost, I would like to express my sincere gratitude and respect to my research and dissertation advisor, Prof. Dr. Wei Chen, for his invaluable guidance and constant encouragement during my research and study. His insight and expertise in nanotechnology has been my greatest source of inspiration.

I would like to thank Professors Dr. Ping Liu, Dr. Andrew Brandt, Dr. Weidong Zhou and Dr. Yaowu Hao for serving on my dissertation committee. I am grateful to them for their careful and critical reading of my dissertation and invaluable suggestions. Their comments and suggestions not only helped me to improve my research skills but also led me to a deeper insight into future research. I also would like to thank Dr. Alex Weiss, Dr. John L. Fry, Dr. Qiming Zhang, Dr. Zdzislaw Musielak, Dr. Jian Yang and Dr. Georgios Alexandrakis for their invaluable suggestions, guidance, and encouragement for my study and research.

I would like to thank the current and former members in Dr. Chen's group: Dr. Marius Hossu, Dr. Ke Jiang, Dr. Zhongxin Liu, Dr. Xiaoju Zou, Lun Ma, Bob Zhang, David Li, Prof. Zhong Sun, Boonkuan Woo and Jose Barona, for their help and friendship.

Thanks to all the faculties and stuffs in physics department especially to Margie, Doug, Victor, Stacy and Bethany, for their help during my Ph.D study in UTA.

Finally I would like to thank my family. I wish to express my deepest and most heartfelt gratitude to my parents for their constant encouragement and love. I am grateful to my sister and brother for their love and support. My special thanks go to my husband Tianfu Wu, for always being there for me with great love and constant support; to my dearest son Albon Wu, his smile and love is my strongest backbone in this journey. This dissertation could not have been done without them.

March 30, 2011

ABSTRACT

SYNTHESIS AND CHARACTERIZATION OF LANTHANIDE BASED NANOMATERIALS FOR RADIATION DETECTION AND BIOMEDICAL APPLICATIONS

Mingzhen Yao, PhD

The University of Texas at Arlington, 2011

Supervising Professor: Wei Chen

Lanthanide based nanomaterials have shown a great potential in various areas such as luminescence imaging, luminescent labels, and detection of cellular functions. Due to the f-f transitions of the metal ion, luminescence of lanthanide ions is characterized by sharp and narrow emissions. In this dissertation lanthanide based nanoparticles such as Ce^{3+}, Eu^{3+} and other lanthanide ions doped LaF_3 were synthesized, their characterization, encapsulation and embedding into hybrid matrix were investigated and some of their biomedical and radiological applications were studied.

DMSO is a common solvent which has been used widely for biological applications. LaF_3:Ce nanoparticles were synthesized in DMSO and it was found that their fluorescent emission originates from the metal-to-ligand charge-transfer excited states. After conjugation with PpIX and then encapsulation within PLGA, the particles show efficient uptake by cancer cells and great cytotoxicity, which is promising for applications in cancer treatments. However, the emission of Eu^{3+} in DMSO is totally different from LaF_3:Ce, very strong characteristic

luminescence is observed but no emissions from metal-to-ligand charge-transfer excited states as observed in LaF_3:Ce in DMSO. Besides, it is very interesting to see that the coupling of Eu^{3+} with O-H oscillations after water was introduced has an opposite effect on emission peaks at 617 nm and its shoulder peak at 613 nm. As a result, the intensity ratio of these two emissions has a nearly perfect linear dependence on increasing water concentration in Eu-DMSO, which provides a very convenient and valuable method for water determination in DMSO.

Ce^{3+} has been well known as an emitter for radiation detection due to its very short decay lifetime. However, its emission range limited the environment in which the detection system works. Whereas, Quantum dots have high luminescence quantum efficiency but their low stopping power results in very weak scintillation luminescence. Nanocompounds formed with CdTe quantum dots and LaF_3:Ce nanoparticles optimize both stopping power and scintillation efficiency based on energy transfer from LaF_3:Ce to CdTe. Hybrid matrix materials such as ORMOSIL have superior mechanical properties and a better processability than pure molecular material which could be used as carrier of radiation material. Moreover, embedding a lanthanide complex in a hybrid matrix enhances its thermal stability and luminescence output. LaF_3:Ce doped ORMOSIL was synthesized by using two different LaF_3:Ce, the nanoparticle doping concentration can reach up to 15.66% while its transparency and luminescent properties were maintained. These materials are very promising for radiation detection.

TABLE OF CONTENTS

LIST OF ILLUSTRATIONS

LIST OF TABLES

Table Page

CHAPTER 1

INTRODUCTION

1.1 Nanotechnology

Nanotechnology has produced a significant impact on our economy and society. The convergence of several scientific disciplines across chemistry, physics, biology, electronics, and engineering etc. is leading to a multiplication of applications in materials manufacturing, medical diagnosis and health care, biotechnology, security, computer chips and so on. Scientific and technological discoveries in nanotechnology are growing at an unprecedented rate.

Nanotechnology is a relatively new but quickly evolving field. It is originated on December 29, 1959, when Richard Feynman, the late preeminent physicist (Nobel Prize for Physics 1965), gave a speech at the annual meeting of the American Physical Society at the California Institute of Technology. His speech, entitled “There’s Plenty of Room at the Bottom, An Invitation to Enter a New Field of Physics,” was remarkably prescient. Feynman proposed employing “machine tools to make smaller machine tools, these in turn to be used in making still smaller machine tools and so on all the way down to the atomic level.” This discussion was the earliest vision of nanotechnology.

From a strictly historical point of view, the first to mention of nanotechnology was by J. C. Maxwell, who in 1867 imagined in a thought experiment a tiny entity that could manipulate individual molecules. A catalyst for the development of the modern field of nanoscience and technology was the discovery of subatomic particles, particles smaller than the atom. The work of G. J. Stoney and J. J. Thompson led to the discovery of electrons and to the development of the field of particle physics. This work led to enquiry into the nature and substance of small particles. In the 1920s, Irving Langmuir introduced the concept of a monolayer, which is a layer

of material one molecule thick. Over the next half century, the development of various scanning microscopes enabled visualization and even manipulation of nano-sized structures.

Today, broadly defined, nanotechnology refers to technological study and application involving nanoscale materials. The term 'nanotechnology' was first used by Taniguchi *et al* in 1974;[1] they defined it as the processing, separation, consolidation, and deformation of materials by one atom or by one molecule. Drexler then popularized the field of nanotechnology by publishing two of the earliest books on the field: *Engines of Creation: The Coming Era of Nanotechnology and Nanosystems and Molecular Machinery, Manufacturing and Computation*. Later on, 'nanoscience' and 'nanotechnologies' have been defined by the Royal Society and Royal Academy of Engineering[2] as follows: "*Nanoscience is the study of phenomena and manipulation of materials at atomic, molecular and macromolecular scales, where the properties differ significantly from those at a larger scale*"; likewise, "*Nanotechnologies are the design, characterization, production and application of structures, devices and systems by controlling shape and size at nanometer scale*".

The term 'nanoparticle' is generally used to refer to a small particle with all three dimensions less than 100 nanometers.[2] Nanoparticles are of great scientific interest as they are effectively a bridge between bulk materials and atomic or molecular structures. A bulk material should have constant physical properties regardless of its size, but at the nano-scale this is often not the case. Size-dependent properties are observed such as quantum confinement in semiconductor particles, surface plasmon resonance in some metal particles and superparamagnetism in magnetic materials.

What is unique about nanoscale particulate matter is that, at the nanoscale level, the known physical and chemical properties of substances are altered, providing new possibilities for using the same substances only in nanosizes rather than in microsized particles. For example, the bending of bulk copper (wire, ribbon, etc.) occurs with movement of copper atoms/clusters at about the 50 nm scale. Copper nanoparticles smaller than 50 nm are

considered super-hard materials that do not exhibit the same malleability and ductility as bulk copper. The change in properties is not always desirable. Ferroelectric materials smaller than 10 nm can switch their magnetization direction using room-temperature thermal energy, thus making them useless for memory storage. Suspensions of nanoparticles are possible because the interaction of the particle surface with the solvent is strong enough to overcome differences in density, which usually result in a material either sinking or floating in a liquid. Nanoparticles often have unexpected visible properties because they are small enough to confine their electrons and produce quantum effects. For example, gold nanoparticles appear deep red to black in solution.

The main reason for this difference between nanoparticles and macroparticles of the same substance is the different surface-area-to-volume ratio, which is increased in the case of the nanoparticle. Nanoparticles have a very high surface-area-to-volume ratio. This provides a tremendous driving force for diffusion, especially at elevated temperatures. Sintering can take place at lower temperatures, over shorter time scales than for larger particles. This theoretically does not affect the density of the final product, though flow difficulties and the tendency of nanoparticles to agglomerate complicate matters. The large surface-area-to-volume ratio also reduces the incipient melting temperature of nanoparticles.[3]

1.2 Applications of Nanotechnology

Recently, the use of nanotechnology has increased in many scientific disciplines, including electronics, stain-resistant clothing manufacture, and cosmetics. Nanotechnology may especially hold the promise of significant improvements in human health and well-being. Research has repeatedly shown that nanotechnology has many potential medical applications, such as in bioimaging, drug delivery, and new cancer-fighting drugs.

Molecular imaging of live cells and whole organisms is an important tool for studying cancer biology and determining the efficacy of tumor therapies. This type of visualization has been helped tremendously by the development of fluorescent probes such as nanoparticles. In

the fight against the pain, suffering, and death due to cancer, nanoparticles have been used in living subjects to target tissue-specific vascular biomarkers[4] and cancer cells[5-8] and to identify sentinel lymph nodes in cancer[9-12]. In addition, the use of nanoparticles as fluorescent tags in cell biology[13,14] will continue to make an impact.

Another major area of application is drug delivery. The goal is to improve contact between a drug and its target, enabling the drug to combat the disease state more efficiently. Certain characteristics of nanoparticles make them useful as carriers of active drugs. For example, their small size allows them to pass through certain biological barriers. Also, they often allow a high density of therapeutic agent to be encapsulated, dispersed, or dissolved within them. This capability depends on the preparation process, during which nanoparticles can be engineered to yield different properties and release characteristics for the entrapped agent. Because of the versatility of chemistries and preparation methods in these systems, surface functionalities can sometimes be incorporated into the nanoparticle. This facilitates additional attractive possibilities, such as the attachment of 'shielding' ligands that prolong the circulation of the nanoparticles in the blood stream, or the targeting of ligands for interaction with specific cells or tissue.

The field of nano-sized labels has generated a great deal of attention, due to their high photostability, biocompatibility, size, and composition-tunable luminescence emission from visible to near-infrared wavelengths.[15-19] Numerous articles have been devoted to more recent developments, such as plasmon resonance, surface-enhanced phenomena, metal nanoshells and semiconductor quantum dots.[20-23] In the last decade, several optical biosensors have been designed that can detect changes in the optical properties of the evanescent field of an optical surface wave, which allows the quantification of molecular recognition processes, notably antibody–antigen interactions.[24-26] So far, this field has also been extended to single-molecule detection techniques.[27]

1.3 Synthesis of Nanoparticles

There are various liquid-phase methods for preparing nanoparticles, such as chemical reduction, sol-gel, reversed micelle, hot-soap, pyrolysis, and spray pyrolysis. Chemical synthesis of nanoparticles is a rapidly growing field with great potential for making useful materials.[28] Chemical synthesis permits the manipulation of matter at the molecular level. Because of mixing at the molecular level, good chemical homogeneity can be achieved. Also, by understanding the relationship between how matter is assembled on an atomic and molecular level and the material's macroscopic properties, molecular synthetic chemistry can be designed to prepare novel starting components. Better control of particle size, shape, and size distribution can be achieved in particle synthesis.

1.3.1 Nucleation and Growth from Solutions

Precipitation of a solid from a solution is a common technique for the synthesis of fine particles. The general procedure involves reactions in aqueous or non-aqueous solutions containing the soluble or suspended salts. Once the solution becomes supersaturated with the product, a precipitate is formed by either homogeneous or heterogeneous nucleation. Homogeneous and heterogeneous nucleation refers to the formation of stable nuclei with or without foreign species respectively. After the nuclei are formed, their growth usually proceeds by diffusion. In diffusion-controlled growth, concentration gradients and temperature are important in determining the growth rate. To form mono-dispersed particles, i.e. unagglomerated particles with a very narrow size distribution, all the nuclei must form at nearly the same time, and subsequent growth must occur without further nucleation[29] or agglomeration of the particles.

In general, particle size and particle-size distribution, amount of crystallinity, crystal structure, and degree of dispersion can be affected by reaction kinetics. Factors influencing the rate of reactions include the concentration of reactants, reaction temperature, pH, and the order in which the reagents are added to the solution. A multi-element material is often made by co-

precipitation of the batched ions. However, it is not always easy to simultaneously co-precipitate all the desired ions, since different species may precipitate at different pH levels. Thus, special attention is required to control chemical homogeneity and stoichiometry. Phase separation may be avoided during liquid precipitation and homogeneity at the molecular level improved by converting the precursor to powder form by using spray drying[30] or freeze drying.[31]

1.3.2 Stabilization of Fine Particles against Agglomeration

Fine particles, particularly nanoscale particles, since they have large surface areas, often agglomerate to form either lumps or secondary particles, thus minimizing the total surface or interfacial energy of the system. When the particles are strongly stuck together, these hard agglomerates are called *aggregates*. Many materials containing fine particles, some examples of which include paints, pigments, electronic inks, and ferrofluids, are useful if the particles in the fluid suspension remain unagglomerated or dispersed. Agglomeration of fine particles can occur at the synthesis stage or during drying and subsequent processing of the particles. Thus it is very important to stabilize the particles against adverse agglomeration at each step of particle production and powder processing. Surfactants are used to produce dispersed particles in the synthesis process or to disperse synthesized agglomerated fine particles.

Many technologies use surfactants.[32,33] A surfactant is a surface-active agent that has an amphipathic structure in that solvent, i.e. a lyophobic (solvent repulsive) and lyophilic group (solvent attractive). Depending on the charges at the surface-active portions, surfactants are classified as either anionic, cationic, zwitterionic (bearing both positive and negative charges), or non-ionic (no charges). At low concentrations, the surfactant molecules absorb on the surfaces or interfaces in the system, and can significantly alter the interfacial energies.

Agglomeration of fine particles is caused by the attractive van der Waals force and/or the driving force that tends to minimize the total surface energy of the system. Repulsive interparticle forces are required to prevent the agglomeration of these particles. Two methods are commonly used. The first stabilization method causes dispersion using electrostatic

repulsion. Repulsion results from the interactions between a particle's surface and the solvent. Electrostatic stabilization of a dispersion occurs when the electrostatic repulsive force overcomes the attractive van der Waals forces between particles. This stabilization method is generally effective in dilute systems of aqueous or polar organic media. It is very sensitive to the electrolyte concentration, since a change in concentration may destroy the electric double layer, resulting in particle agglomeration.

The second stabilization method involves the use of steric forces. Surfactant molecules can adsorb onto the surfaces of particles and their lyophilic chains will then extend into the solvent and interact with each other. The solvent chain interaction, which is a mixing effect, increases the free energy of the system and produces an energy barrier to the closer approach of particles. When particles come into closer contact with each other, the motion of the chains extending into the solvent is restricted, producing an effective barrier in both aqueous and non-aqueous media, one less sensitive to impurities or trace additives than when using electric stabilization. The steric stabilization method is particularly effective in dispersing high concentrations of particles.

1.4 Characterization of Nanoparticles

Nanoparticle characterization is necessary for establishing understanding and control of nanoparticle synthesis and applications. Characterization uses a variety of different techniques, mainly drawn from materials science. Common techniques are electron microscopy [TEM,SEM], atomic force microscopy [AFM], dynamic light scattering [DLS], x-ray photoelectron spectroscopy [XPS], powder x-ray diffractometry [XRD], Fourier transform infrared spectroscopy [FTIR], Matrix-Assisted Laser-Desorption Time-of-flight mass spectrometry [MALDI-TOF], and ultraviolet-visible spectroscopy.

X-ray diffraction is the preferred method for examining the formation of the crystalline assembly, provided the sample size is sufficient. The diffraction spectrum at the high-angle range is directly related to the atomic structure of the nanoparticles, whereas the spectrum at

the lower angle region is directly associated to the ordered assembly of nanocrystals.[34,35] By examining the diffraction peaks that are extinct in the spectrum, one may identify the crystallography of the packing. This analysis is based on the assumption that each particle is identical in size, shape, and even orientation, so that the extinction rules derived from diffraction physics apply.

Scanning electron microscopy (SEM) is a powerful technique for imaging the surfaces of almost any material. It is likely the most popular tool for material characterization. A modern SEM can furnish a resolution of 1 nm, relatively simple image interpretation, and large depth of focus, making it possible to directly image the 3D structure of nanomaterials. Transmission electron microscopy (TEM), as a high spatial resolution structure and chemical microanalysis tool, has been proven to be powerful for characterization of nanomaterials.[36] A modern transmission electron microscope can directly image atoms in crystalline specimens at resolutions close to 0.1 nm, smaller than interatomic distance. An electron beam can also be focused to a diameter smaller than 0.3 nm, allowing quantitative chemical analysis from a single nanocrystal. This type of analysis is extremely important for characterizing materials at a length scale from atoms to hundreds of nanometers. Determining the shape of nanocrystals is an important application of TEM. Using a combination of high-resolution lattice imaging and possibly electron diffraction, the crystal structure and facets can be determined.

Photoluminescence spectroscopy is a contactless, nondestructive method of probing the electronic structure of materials. Light is directed onto a sample, where it is absorbed and imparts excess energy into the material in a process called photo-excitation. One way this excess energy can be dissipated by the sample is through the emission of light, or luminescence. In the case of photo-excitation, this luminescence is called photoluminescence. The intensity and spectral content of this photoluminescence is a direct measure of various important material properties. Photo-excitation causes electrons within the material to move into permissible excited states. When these electrons return to their equilibrium states, the excess

energy is released and may include the emission of light (a radiative process) or may not (a nonradiative process). The energy of the emitted light (photoluminescence) relates to the difference in energy levels between the two electron states involved in the transition between the excited state and the ground state. The quantity of the emitted light is related to the relative contribution of the radiative process.

Shape, size and ambient conditions are crucial parameters in understanding the physics and chemistry phenomena of matter at the nanometer scale. The promising technological applications of nanoscience depend on our capacity to control these parameters. In particular, a correct understanding of the optical properties of nanostructures is essential. Optical techniques, such as Raman, differential and anisotropy reflectance spectroscopy, light absorption spectroscopy, surface enhanced Raman scattering (SERS), etc., can be powerful tools for characterizing nanostructures because of their non-destructive and real-time character, together with their *in situ* potentiality. Furthermore, optical spectroscopies provide statistical properties of the whole sample. These attributes have allowed us to control the growth of superlattices,[37] and the growth of nanoparticles, correcting their shape and size during the process. Optical spectroscopies can also be used as complementary tools of the structural characterization techniques such as atomic force microscopy (AFM), scanning tunneling microscopy (STM), transmission electron microscopy (TEM), etc., which provide the image of a small piece of the sample, giving information about local properties and characterizing a few nanoparticles at a time.

1.5 Lanthanides

Lanthanide Metals, traditionally referred to as the rare earth metals, are now widely used in a variety of industries as important luminescent materials. The most common example of Lanthanides application includes light converting molecular devices[38-43] such as luminescent triphosphor materials in fluorescent lights and flat panel displays. The name “rare earth metal” came from the rareness of the minerals in which the rare earth elements are concentrated.

Even though they rarely concentrate into economically exploitable ore deposits due to their geochemical properties, the rare earth elements are found in relatively high concentrations in the Earth's crust.

The Lanthanides (Ln) are the elements with atomic numbers 57-71. They come at a break in the periodicity of the filling of the d-orbitals by the filling of the 4f orbitals. The Lanthanides are also known for the "Lanthanide Contraction" which refers to the decrease in the ionic radius of the Ln(III) ions as their 4f orbitals are filled. Due to the poor shielding among f electrons, the contraction causes an increase in the effective nuclear charge across the lanthanide series.[42,43] Most lanthanide elements are dominated by the +3 oxidation state, relatively stable with electron configuration of $6s^0\ 5d^0\ 4f^n$. A few lanthanides have oxidation states other than +3, for example, Eu and Yb have oxidation states of +2 and Ce has stable +4 state, but these are not stable in aqueous solution.[43] In addition, Sm^{2+} and Tm^{2+} are stabilized with an almost half-filled valence shell and an almost full valence shell.

The energy levels of some of the trivalent lanthanide ions are illustrated in Figure 1.1. It shows that the energy levels for the lanthanide ions series are very well defined and are not greatly affected by the crystal field. The crystal field around the ions will splits each energy levels in sub-levels called Stark levels, which are within only hundreds of wave numbers of each other, so the absorption and emissions for these ions are sharp and their emission position does not change significantly. Photoluminescence is one of the most interesting features of these lanthanide ions. Several lanthanide ions show luminescence in the visible or near-infrared spectral regions upon irradiation with ultraviolet radiation. The color of the emitted light depends on the lanthanide ion. For instance, Eu^{3+} emits red light, Tb^{3+} green light, Sm^{3+} orange light, and Tm^{3+} blue light. Yb^{3+}, Nd^{3+}, and Er^{3+} are well-known for their near-infrared luminescence, but other lanthanide ions (Pr^{3+}, Sm^{3+}, Dy^{3+}, Ho^{3+}, and Tm^{3+}) also show transitions in the near-infrared region. Gd^{3+} emits in the ultraviolet region, but its luminescence can only be observed in the absence of organic ligands with low-lying singlet and triplet levels. In the case of the

lanthanides, the emission is due to transitions inside the 4f shell, thus intraconfigurational f-f transitions. Because the partially filled 4f shell is well shielded from its environment by the closed $5s^2$ and $5p^6$ shells, this shielding is responsible for the specific properties of lanthanide luminescence, more particularly for the narrowband emission and for the long lifetimes of the excited states. Ce^{3+} is a special case because this ion emits intense broadband emission due to allowed f-d transitions.

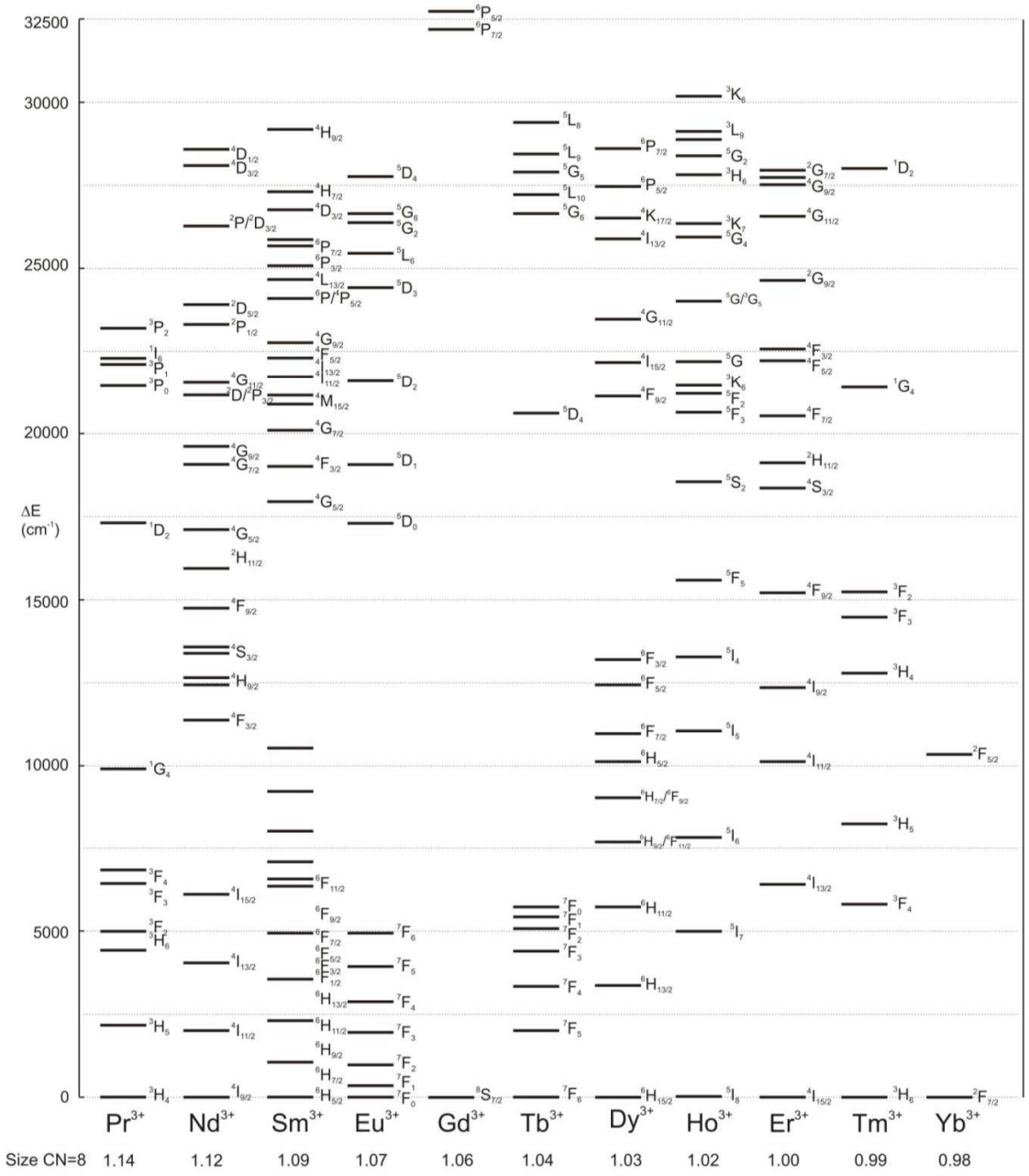

Figure 1.1 Energy level scheme and sizes of a number of the lanthanide ions[44]

The emission from lanthanide ions has been used extensively in biological systems. The applications include luminescent labels of biologically-relevant molecules and detection of

cellular functions in vivo, the elucidation of structure and function of enzymes and proteins.[45-48] The luminescence from lanthanide excited states can be quenched through non-radiative energy transfer to stretching vibrations of nearby or coordinated solvent molecules, especially in aqueous media where there are abundant of O-H oscillators resulting in Frank Condon overlap of energy levels and stretching vibrations.[49-51] The extent of quenching was found to be inversely proportional to the energy gap between the emissive state and the ground state of the metal.[50,52] Terbium is less readily quenched by O-H oscillators due to a less prominent Franck Condon overlap. Both the luminescence lifetimes and intensities were found decreasing linearly with increasing of H_2O's number in the inner coordination sphere of the cation.[53,54] Due to the efficient energy transfer from the excited states of lanthanide ions to the O-H oscillators of bound water molecules, there is a correlation between the luminescence lifetime of the excited state and the hydration number of lanthanide ions, which has been used to identify details of solution phase in aqueous solution.[55-58] On the other hand, the low intensities and quantum efficiencies of lanthanide ions luminescence in solution could be improved by complex formation with organic ligand where there is energy transfer from excited states of organic ligand to emitting state of lanthanide ions. At the same time, ligands that shield the metal from inner sphere solvation prevent the quenching of metal-based luminescence induced by coupling with O-H oscillators, reducing the non-radiative quenching of the metal centered excited state.

1.6 Lanthanide-based Nanoparticles

Lanthanide-based nanoparticles have shown great potential for applications in the general fields of detection and diagnosis as luminescent materials because of their long lifetimes (μs-ms), narrow emission bands and large Stokes shifts. Luminescence is a phenomenon which material emits radiation after the absorption of radiation of higher energy. For most Lanthanide ions, luminescence occurs from transitions of $4f^n$ electron configuration to higher energy states when UV or visible light excites the material. The successful use of highly luminescent rare-earth doped nanoparticles, combining the various properties of doping ions

and the nanoparticle matrix, has ensured the expanded use of nanoparticles. Multifunctional nanoparticles can be tailored for detecting or tracking labeled biomolecules with several complementary techniques,[59] for facilitating the separation and detection of biomolecules,[60] or for performing both diagnosis and therapy.[61] Replacement of organic dyes with inorganic fluorophores, such as lanthanide compounds (Yb, Er),[62] is an interesting strategy for synthesizing efficient luminescent multifunctional nanoprobes, because the lanthanide ions exhibit advantageous optical properties. As they are characterized by high photostability, long luminescence lifetime (1 ms), narrow emission bands, and a broad absorption band, lanthanide ions are indeed very well suited for elaboration of highly luminescent and photostable nanoprobes[63,64] without emission intermittency. Kennedy *et al* demonstrated that Eu_2O_3 nanoparticles can be applied as a fluorescent label in an immunoassay for atrazine with good sensitivity.[65] Biolabeling can also be performed with Eu^{3+} chelates dispersed in silica particles.[66] Moreover, a large palette of colors can be easily obtained by a convenient choice of lanthanide ions.[63] In contrast to quantum dot, the color of the emitted light does not depend on the size of the fluorescent nanoparticles, but only on the nature of the lanthanide ions, therefore avoiding formation of motley particles and a cumbersome purification step. LaF_3 was chosen as the host matrix because this material has very low vibrational energies,[67] thus minimizing the quenching of the excited state of the rare earth ions. This is especially important for the rare-earth ions emitting in the near-infrared part of the spectrum, because they are very sensitive to quenching by high-energy vibrations.[68] Despite their numerous advantages, development of highly luminescent lanthanide-ion-doped nanoparticles was impeded by the lack of efficient synthetic routes.

For doped materials, their properties could be achieved by altering and controlling the doping material, which enables properties that are not innately present in a material.[69,70] However, the doping of bulk materials has been largely exploited, in particular for demands for further miniaturization of components and systems. As a result, nano-sized materials have

received greater attention because of the unique properties resulting from quantum size confinement.[69,70] The natural evolution of these efforts has led to progress in developing practical applications for doped nanomaterials as semiconductors, insulators, energy converters, magnets, and other functionally enhanced materials. One promising application for doped nanomaterials is as a solid-state source of luminescence. Bulk luminescent materials, or phosphors, are employed in a broad range of applications such as cathode ray tubes, projection television screens, fluorescent tubes, X-ray detectors, and biomedical probes. However, luminescence based on bulk materials offers extremely limited opportunities for further reductions in size, complexity, and power consumption. Fortunately, due to the physics of quantum size confinement, nanoscale phosphors provide a convenient route for further advancing solid-state luminescence applications. As compared to bulk materials, nanoparticles may exhibit greater electron-hole overlap, thereby yield greater oscillator strength and enhanced luminescence quantum efficiency. Rare earth-doped insulator nanoparticles such as Y_2O_3: Eu^{3+}, LaF_3:Eu^{3+}, and $LaPO_4$:Tb^{3+} represent a new type of high efficiency luminescent material.[71-78] Quantum size confinement is not as critical for insulator nanoparticles as it is for semiconductor nanoparticles. However, surface effects due to the large surface-to-volume ratios will affect both semiconductor and insulator nanoparticles. Insulator nanoparticles may exhibit some novel properties that make them suitable for numerous applications. For example, as phosphors, nanoparticle insulators can be more efficient and produce less light-scattering than micrometer-sized particles. Also, as a biological labeling agent, insulator nanoparticles are much less toxic than semiconductor nanoparticles.[74-79]

1.7 Properties of Quantum Dots

Quantum dots, the so-called nanocrystals, are nano-sized semiconductor particles composed of II-VI group or III-V main group elements. Since the electrons and holes within are quantumly confined in all three spatial dimentions, in other words, the size of a semiconductor quantum dots is smaller than that of the “free” exciton (electron-hole pair), the continuous

bandgap structures of the bulk material would become discrete when excited to higher energy states. As a result, the concept of bulk energy level of bulk semiconductor can no longer be applied to quantum system. The crystals are essentially too small to form an intrinsic band gap. There will be a series of excited, discrete bound states approaching an ionization limit corresponding to a positively charged crystallite and a free electron in a vacuum, which makes quantum dots have unique properties that are between those of bulk materials and those of discrete molecules.

1.8 Lanthanide-based Nanoparticles Doped ORMOSILS

Lanthanide-based organic-inorganic hybrid materials have drawn a strong interest because these materials have a high potential for different applications such as optical amplifiers, high-power lasers, radiation detection probe, etc.[80-82] In these materials, a molecular lanthanide complex is embedded in an inorganic host matrix (like the sol-gel-derived materials). Generally speaking, these hybrid materials have superior mechanical properties and better processability than the corresponding pure lanthanide complexes. Furthermore, embedding a lanthanide complex in a hybrid matrix enhances luminescence output but remains its thermal stability.[83]

The formation of organically modified silicates (ORMOSIL) is based on the sol-gel process. Sol-gel process is a chemical synthesis technique which is used for the production of glasses, gels, and ceramic powders.[84-86] The advantage of this process is not only that it allows the preparation of glasses at a lower temperature than traditional melt process, but also it is possible to encapsulate organic compounds or metal complexes in sol-gel glasses with different shapes.[87-89] The starting products for the synthesis of silicate sol-gel galsses are tetraethylorthosilicate (TEOS, $Si(OC_2H_5)_4$), which is mixed with water and a mutual solvent to form a homogeneous solution. Another frequently used alkoxide precursor is tetramethylorthosilicate (TMOS, $Si(OCH_3)_4$). Silanol groups (Si-OH) are formed by partial hydrolysis of the alkoxide. Then condensation reactions take place in solution before hydrolysis

is completed to produce silicic acid. As a result, Si-O-Si siloxane bonds are formed from these condensation reactions. A simplified reaction scheme of hydrolysis and condensation of a tetraalkoxysilane $Si(OR)_4$ is as below:

Hydrolysis:

$$Si(OR)_4 + nH_2O \rightarrow Si(OR)_{4-n}(OH)_n + nROH$$

Condensation:

$$(RO)_3Si\text{-}OR + HO\text{-}Si(OR)_3 \rightarrow (RO)_3Si\text{-}O\text{-}Si(OR)_3 + ROH$$

or

$$(RO)_3Si\text{-}OH + HO\text{-}Si(OR)_3 \rightarrow (RO)_3Si\text{-}O\text{-}Si(OR)_3 + H_2O$$

Besides the type of alkoxide used for the hydrolysis, other reaction parameters include: mole ratio of H_2O to Si, solvent, catalyst, PH, temperature, as well as pressure. Oligomers and polymers are formed during the initial phases of the condenstation reaction, which leads to the formation of colloidal particles in the solution, together with the colloidal particles formed by the hydrolysis of the tetraorthosilicate precursor, which are formed *sol*. The interconnecting network is formed when the colloidal particles undergo additional polymerization reactions, then *gel* is formed when the viscosity of the solution increases during the gelation process. Usually the gel needs some time for aging before having a drying process.

The purely inorganic glasses prepared by the controlled hydrolysis of metal alkoxides have some disadvantages especially their brittle mechanics properties. Due to the surface tension of the liquid in the pores, these glasses crack easily. However, the disadvantage can be overcome by incorporation of organic components in the backbone of the xerogel network.[90-93] Different types of hybrid materials such as ORMOSIL can be formed based on different organic modifiers. During the formation of ORMOSIL, the tetraalkoxysilane precursor is partially or totally replaced by trialkoxysilyl compounds with an organic group R', the organotrialkoxysilanes $R'\text{-}Si(OR)_3$. The organic group R' of the organotrialkoxysilane could be an alkyl or aryl group with a functional group such as amino, isocyanate, epoxy and vinyl group. Precursors with

nonreactive R-groups like an alkyl or a phenyl group are acting as network modifiers which make the network less rigid and brittle.

Doping is one of the general methods used to incorporate luminescent complexes into organic hybrid materials such as ORMOSIL.[94] To dope the complex into ORMOSIL, the complex needs to be added into the silica sol prior to gelation. During the gelation, the complex is trapped in the pores of the silica host. It is also possible to dope the complex in silica matrix by adding the metal salt and ligand to the silica gel where the complex is formed in the environment of gel.

1.9 Objective of the Dissertation

In this dissertation, the synthesis of lanthanide fluoride nanoparticles doped with cerium in organic solvent dimethyl sulfoxide (DMSO) is reported, and its applications as an agent in photodynamic therapy for cancer treatment are discussed in Chapter 2. Most lanthanide ions have interactions with DMSO when DMSO is used as solvent, however, the complex of Eu^{3+} with DMSO shows very strong characteristic emissions of Eu ion which becomes supersensitive when water is introduced into Eu-DMSO solution. This phenomenon makes Eu^{3+} in DMSO becoming a new probing for water measurement, the details are presented in Chapter 3. Since for most biological applications, the nanoparticles are required to be water-soluble, lanthanide fluoride nanoparticles doped with Ln^{3+} ions (Ln = Ce^{3+}, Tb^{3+}, Ce^{3+} and Tb^{3+}, Yb^{3+} and Tb^{3+}) are synthesized in water and the application in fluorescence labeling is discussed in Chapter 4. Based on the LaF_3:Ce nanoparticles synthesized in water, the mechanism of possible energy transfer from LaF_3:Ce to CdTe quantum dots is discussed in Chapter 5. This material is particular for application in radiation detection, in this complex, light emitted from Ce^{3+} which is in UV region is transferred to quantum dots CdTe, which results in enhanced emissions of CdTe in visible region. Since hybrid matrix materials have superior mechanical properties and a better processability than the pure molecular lanthanide complexes, moreover, embedding a lanthanide complex in a hybrid matrix enhances its thermal stability and luminescence output,

LaF_3:Ce was embedded into ORMOSIL silica network and the properties of this hybrid material are discussed in Chapter 6. Chapter 7 summarizes the work which has been done in this dissertation and further discusses the future directions of investigation.

CHAPTER 2

LUMINESCENCE PROPERTIES OF CE^{3+} DOPED LAF_3 NANOPARTICLES IN DMSO

2.1 Introduction

Lanthanide-based nanocrystals have shown great potential for use as luminescent materials due to electronic transitions within the 4f shell of the trivalent lanthanide ions.[95,96] In particular, an increasing interest in using Lanthanide-based nanoparticles (NPs) has developed due to their higher photo stability and luminescence compared to organic dyes.[97,98] As a result, they are becoming highly favored for biological applications such as bioconjugation due to their physical and optical properties.[98] Besides the applications in biological system, recent interest in radiation detection has also spurred new interest in Lanthanide-based material such as LaF_3:Ce and LaF_3:Ce,Tb nanoparticles because of the high emission yield and short luminescence lifetime of Ce^{3+}.

The synthesis process and spectroscopic properties of Lanthanide (III)-doped nanoparticles have attracted more considerable interest due to their applications in biological system.[99,100] LaF_3 is an ideal material for various phosphors since this material has very low phonon energy and thus the quenching of the excited state of the lanthanide ions will be minimal. Among many routes taken to impart biological activity to NPs, bioconjugation of proteins to luminescent particles stabilized with polyethylene glycol [$H(OCH_2CH_2)nOH$, PEG] is the most common. The biological advantage of covalently attaching NPs to biological macromolecules, such as peptides and proteins, with PEG chains (commonly referred to as PEGylation) is that it allows for suppression of antigenic and immunogenic epitopes, and prevents recognition and degradation by proteolytic enzymes.[65,101] Furthermore, the hydrophilic nature of PEG is an excellent ligand to render water soluble NPs. The synthesis and photoluminescence of LaF_3:Ce,Tb and LaF_3:Tb nanoparticles have been reported by several

groups.[102,103] Thoma and co-workers[104] have reported the X-ray excited luminescence of solid LaF_3 and CeF_3 at various temperatures. Rodnyi and co-workers[105] have studied the X-ray excited luminescence of LaF_3:Ce crystals and proposed a mechanism for the origin of the fast decay component. Jouda and co-workers[106] have studied the X-ray excited luminescence of rare earth trifluorides. Recently, Liu et al. reported X-ray luminescence of LaF_3:Ce,Tb and LaF_3:Tb water-soluble nanoparticles, and its potential application for radiation detection in water.[107]

In this chapter, we report the investigations on LaF_3 based NPs that are doped with Ce^{3+} in Dimethyl Sulfoxide (DMSO) with PEG as stabilizer. DMSO is a common solvent for many polymers and a vehicle for drug delivery. A unique capability of dimethyl sulfoxide is its ability to penetrate living tissues without causing significant damage. The synthesis of doped nanoparticles from aqueous solution has been investigated and reported extensively.[108] However, little work has been done on the formation of doped nanoparticles in DMSO. DMSO is a clear, colorless to yellowish liquid with a characteristic bitter odor and taste. It is soluble in water, ethanol, acetone, diethyl ether, benzene, and chloroform and is a good solvent for unsaturated, nitrogen-containing, and aromatic compounds.[109-111] DMSO has been used widely as a cryoprotective agent for protection of live cells and tissues against freezing damage as well as a cryopreservative in allogous bone marrow and organ transplants.[111] DMSO itself is also a drug which was approved by the Federal Drug Administration (FDA) in 1970 for the treatment of musculoskeletal disorders in dogs and horses and later in 1978 in humans for the therapy of interstitial cystitis, which is a painful disabling urinary bladder inflammation.[112] DMSO itself has many other clinical properties. It has been used successfully as an adjuvant, for its analgesic properties, in the treatment of pulmonary adenocarcinoma, rheumatologic, and dermatologic diseases and chronic prostatitis, and as a topical analgesic.[109-111] In addition, DMSO is also considered as a magic bullet for cancer by alternative cancer treatment advocates.[113] DMSO readily crosses the blood brain barrier[114] and has anti-inflammatory and reactive oxygen

species scavenger actions.[109-111] DMSO has been used for the local treatment of extravasation in chemotherapy,[115] and it can reduce the ulcer size from Adria extravasation and cure necrosis.[116,117] It has been reported that DMSO increases radioiodination yield for radiopharmaceuticals[118] and it can be used as an adjunct to tissue expansion for breast reconstruction.[119] It has also been used in the treatment of traumatic brain edema and schizophrenia, and it has been suggested as a treatment of Alzheimer's disease.[120]

Of foremost importance to our understanding of the possible functions of DMSO in biological systems is its ability to replace some of the water molecules associated with the cellular constituents or to affect the structure of the surrounding water. It has been reported that DMSO at various concentrations can penetrate the body membranes of both lower animals and man. The process is reversible, and the integrity of most membranes is not affected except at extremely high concentrations of 90-100%.[121] This property has been exploited as an indicator or probe to study changes in the barrier properties of human skin in certain disease states such as atopic dermatitis[122] or damage due to exposure to ultraviolet radiation.[123] In addition, DMSO has the ability to enhance the transport of other drugs through the membranes, and therefore, is a successful drug carrier for disease targeting.[111] DMSO is mutagenic for *Salmonella typhimurium* (*S. typhimurium*) TA1573 and TA2637 and *Escherichia coli* (*E. coli*) WP2uvrA in the Ames mutagenicity assay with a preincubation modification.[124] This property plus its unique membrane penetration makes DMSO potentially useful for bacteria decontamination. These properties indicate that DMSO is worthy of study and the formation of nanoparticles in DMSO may find potential applications such as cell imaging, drug delivery, bacteria, or virus sterilization. However, little attention has been paid to the formation of nanoparticles in DMSO. The formation of CdS nanoparticles in DMSO has been reported by the chemical reaction of cadmium salts with Na_2S[125,126] or elemental sulfur.[127] Actually, DMSO may function as a solvent, stabilizer, or sulfide source for the synthesis of sulfide nanoparticles. For instance, Hodes et al. reported that CdS nanoparticles can be prepared in DMSO without using other sulfide

reagent.[127] Our group has also reported the luminescence properties of sulfide nanoparticles and ZnS:Mn^{2+}doped nanoparticles made in DMSO without other sulfide sources.[128] Here we report the formation and luminescence of LaF_3:Ce^{3+} nanoparticles prepared in DMSO. In addition, luminescent lanthanide-DMSO compounds were also formed along with the nanoparticles, and this provides a new method for formation of nanocomposite materials with multicolor luminescence.

2.2 Experimental Section

2.2.1 Synthesis

Lanthanum(III) nitrate hydrate ($La(NO_3)_3 \cdot XH_2O$, 99.9%), cerium(III) nitrate hexahydrate ($Ce(NO_3)_3 \cdot 6H_2O$, 99.9%), ammonium fluoride (NH_4F, 99.9%), and poly(ethylene glycol) bis(carboxymethyl) ether (PEG) were purchased from Sigma-Aldrich. All of the reagents were used as received, without further purification. LaF_3:Ce^{3+} nanoparticles were synthesized by a wet-chemistry method. Typically, 9 mmol of $La(NO_3)_3$, 1 mmol of $Ce(NO_3)_3$, and 30 mmol of NH_4F were added into 50 mL of dimethyl sulfoxide in a three-necked flask. 1 ml of PEG was added to the mixture as a stabilizer to prevent the particles from aggregating. In this work, $Ce(NO_3)_3$ was used as the dopant at a concentration of 0.1 M. The chemicals were mixed thoroughly with stirring for half an hour at room temperature, and then the mixture was subsequently heated to three different temperatures (70, 150, and 180 °C) under vigorous magnetic stirring and nitrogen protection. A suspension formed gradually upon stirring. The color of the samples changed from white to yellow at 150 °C and to dark yellow at 180 °C; however, the sample at lower temperature (70 °C) remained colorless (see Figure 2.1). The nanocrystals obtained were collected by centrifugation, washed with deionized (DI) water and 0.5% acetic acid solution several times, and stored in DI water.

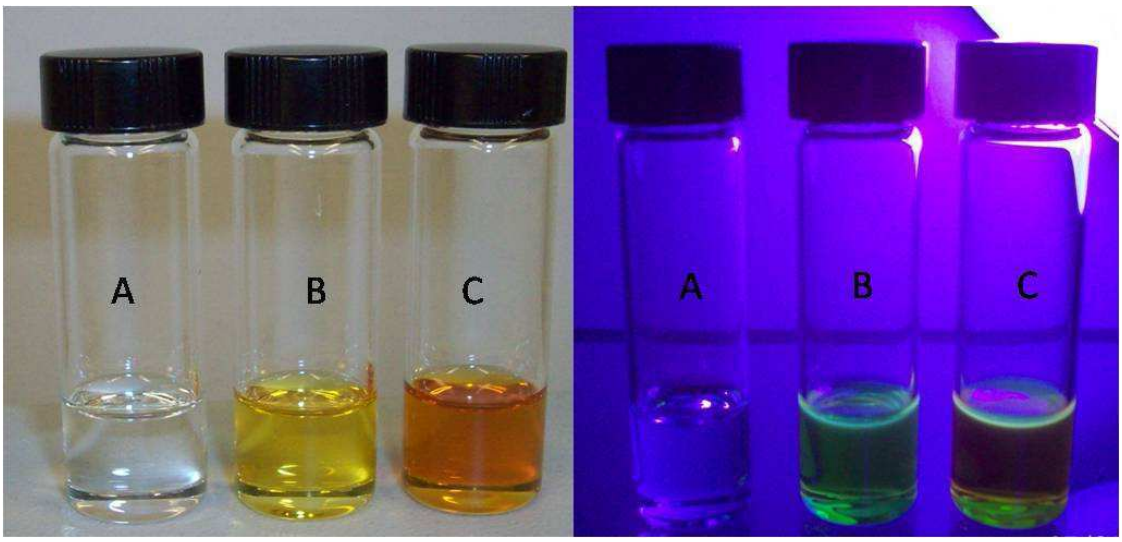

Figure 2.1 Optical (left panel) and fluorescence (right panel) photographs of three samples synthesized under different temperatures (A-70 °C; B-150 °C; C-180 °C)

2.2.2 Characterization

The identity, crystalline structure, size, and shape of the nanoparticles were observed by X-ray diffraction and high resolution transmission electron microscopy (HRTEM). The X-ray powder diffraction (XRD) patterns of $LaF_3:Ce^{3+}$ nanoparticles were recorded in the range of $20° \leq 2\theta \leq 80°$ using a Siemens Kristalloflex 810 D-500 X-ray diffractometer operating at 40 kV and 30 mA with a radiation beam of λ = 1.5406 Å. The nanoparticles in solution were brought onto holey carbon covered copper grids for HRTEM observations. The HRTEM images of the particles were obtained with a JEOL JEM-2100 electron microscope with accelerating voltage of 200 kV. The excitation and emission spectra were measured using a Shimadzu RF-5301PC fluorescence spectrophotometer. Luminescence lifetimes were collected using the frequency-doubled output of a synchronously pumped picosecond dye laser operating at 610 nm. The doubled output was focused onto the samples and emission collected at right angle to the input. The emission was spectrally filtered and the lifetime measured using time-correlated single-photon counting. The instrument resolution was determined to be about 50 ps full width at halfmaximum (fwhm) using a standard scattering material.

2.3 Results and Discussion

2.3.1 XRD

Figure 2.2 shows the XRD patterns of LaF_3: Ce^{3+} nanoparticles synthesized at 70, 150, and 180 °C, respectively. The XRD results are in good agreement with the trigonal tysonite LaF_3 structure as described in the reports[129,130] and from bulk LaF_3 and CeF_3 crystals (JCPDS cards 32-0483 and 08-0045). The broadening of the XRD diffraction lines is the result of the small particle size. The particle size can be estimated from the Scherrer equation, $D = 0.90\lambda/\beta \cos \theta$, where D is the average crystallite size, λ is the X-ray wavelength (0.15405 nm), and θ and β are the diffraction angle and fwhm of an observed peak, respectively. The strongest peak (111) at $2\theta = 27.8°$ was used to calculate the average crystallite size (D) of the nanoparticles.[129,130] Based on the calculation, the estimated average crystallite sizes of LaF_3:Ce nanoparticles prepared at 70, 150 and 180°C are about 15 nm, 10 nm and 8nm, respectively. No XRD signals were observed for impurity phases, indicating that Ce^{3+} is likely doped into LaF_3 crystal lattice. The ionic radius of Ce^{3+} (1.034 Å) is very close to that of La^{3+} (1.061 Å), therefore, Ce^{3+} can easily substitute for La^{3+} ions in LaF_3 crystals.

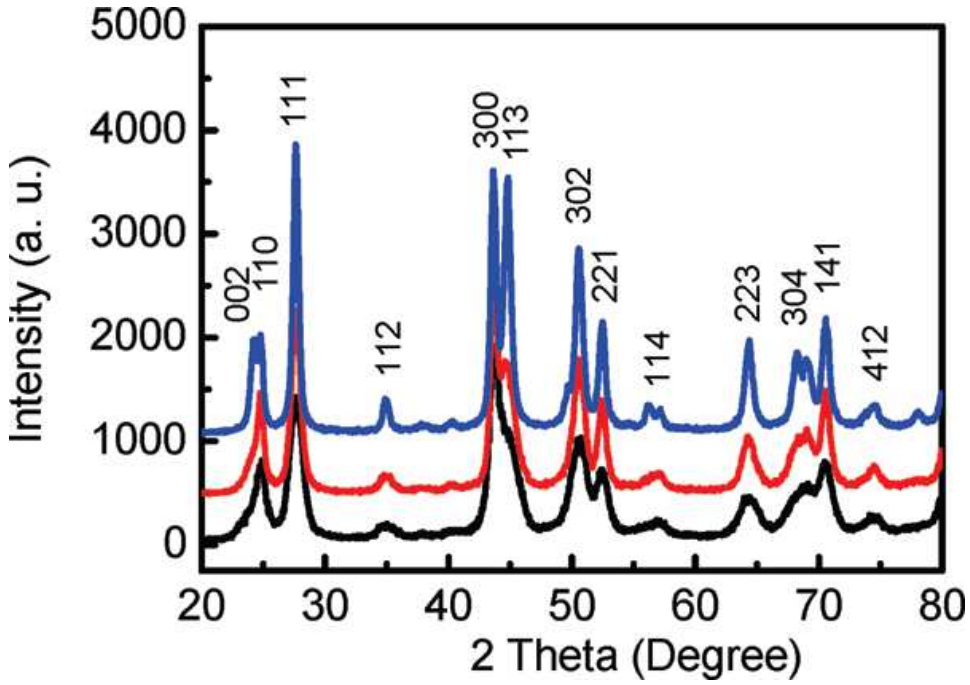

Figure 2.2 XRD patterns of $LaF_3:Ce^{3+}$ nanoparticles synthesized at 70 (upper), 150 (middle), and 180 °C (lower).

2.3.2 TEM

Figure 2.3 a shows high-resolution TEM images of $LaF_3:Ce^{3+}$ nanocrystals synthesized at 70 °C. As observed in the images, most of the nanoparticles are nanorods of about 20 nm long and 5 nm wide. There are also some nanoparticles with spherical shape with diameter of 10 nm. Image b and c in Figure 2.3 display high-resolution TEM images of $LaF_3:Ce^{3+}$ nanocrystals synthesized at 150 and 180 °C. Most nanoparticles formed are in spherical shape, and the average sizes are around 12 nm for 150 °C sample and 10 nm for 180 °C sample, which are consistent with the sizes obtained with XRD. The HRTEM images of the $LaF_3:Ce^{3+}$ nanoparticles indicate high crystalline quality as evidenced by the clear lattice fringes in the inset images. The interplanar spacings shown in Figure 2.3 a-c are about 3.5 Å along the $[1\bar{2}10]$ and $[\bar{2}110]$ directions. These values are very close to the plane distance of 3.4 Å measured by X-ray diffraction. The result is also in agreement with the results observed in LaF_3 nanoplates.[131]

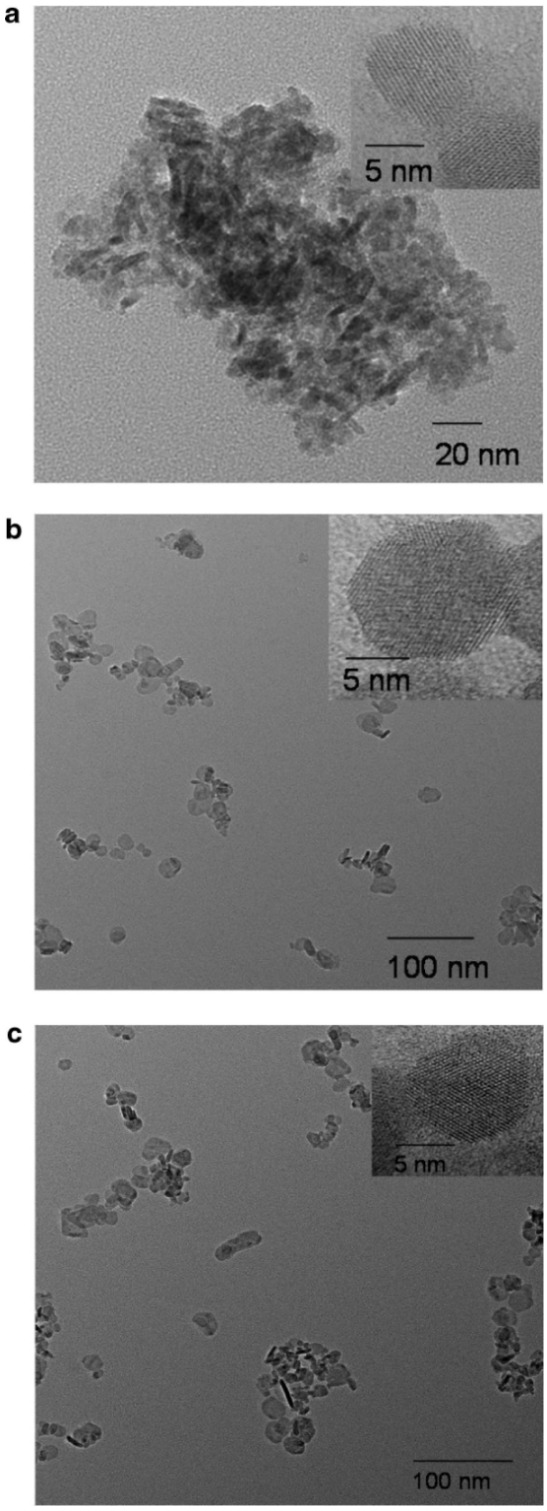

Figure 2.3 HRTEM images of $LaF_3:Ce^{3+}$ nanoparticles synthesized at (a) 70, (b) 150, and (c) 180 °C.

2. 3.3. Luminescence Properties.

A. Powder Samples.

The luminescence of $LaF_3:Ce^{3+}$ has been studied extensively.[102-106] Ce^{3+} is a strong emitter with nanosecond luminescence lifetimes which makes it very attractive for applications in radiation detection.[132] Spin-orbit interaction splits the ground-state configuration of Ce^{3+} with about 2000 cm^{-1} apart between $^2F_{7/2}$ and $^2F_{5/2}$ ground levels. The first excited state is also spin-orbit split into $^2D_{3/2}$ and $^2D_{5/2}$ levels.[133] The fluorescence excitation and emission spectra of the powder samples prepared at 70, 150, and 180 °C are shown in Figure 2.4. All three samples display emission peaks around 311 nm, which is attributed to transitions from the lowest 5d excited state to the spin-orbit split ground f state.[133,134] The peaks from excitation spectra of the three samples are attributed to the f to d transitions of Ce^{3+} ion, as the LaF_3 absorption onset is significantly higher in energy.

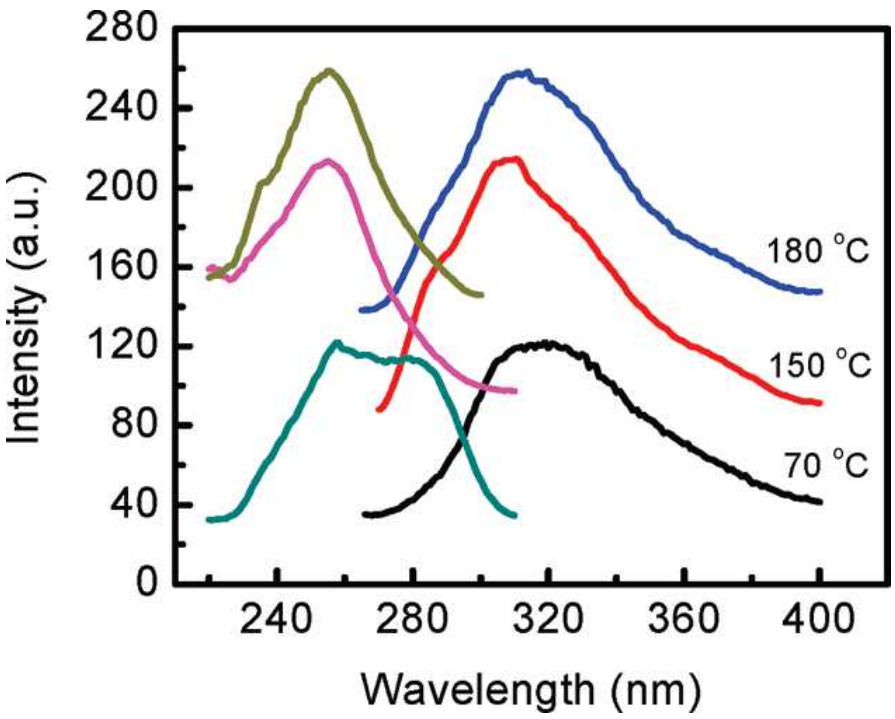

Figure 2.4 Excitation and emission spectra of three powder samples prepared at 70, 150, and 180 °C (emission at 320 nm, excitation at 255 nm).

B. Solution Samples.

The luminescence properties of solution samples are much more complicated than those of solid samples as shown in Figure 2.4. The excitation and emission spectra of the solution samples prepared at 70, 150, and 180 °C are displayed in Figure 2.5. Obviously, the excitation and emission spectra of solution samples are different from those of solid samples which were precipitated from the solutions; the peaks shift from 311 nm in powder samples to longer wavelengths greater than 375 nm as the chemical reaction temperature increases. In addition, the excitation and emission wavelengths are dependent on the reaction time as shown in Figure 2.6. For the solution sample prepared at 180 °C, the emission peak shifts from 483 to 645 nm when the reaction time increases from 0.5 to 3 h (see Table 2.1). Furthermore, the emission intensity increases with increasing reaction time. Obviously, there are two emission peaks when the reaction time is longer than 1.5 h, and the relative change in the intensity of the two peaks is responsible for the emission shift. It is also observed that the emission peaks shift to longer wavelengths at longer wavelengths of excitation (Figure 2.7a,b). This is a typical phenomenon of selective excitation when the material has multiple luminescence centers or emitting states.[135-138]

Table 2.1 Emissions of solution sample at 180 ^{o}C with different reaction times

Reaction Time (hour)	Emission peak (nm)
0.5	483
1.0	523
1.5	554, 635
2.0	601, 635
2.5	614, 645
3.0	616, 649

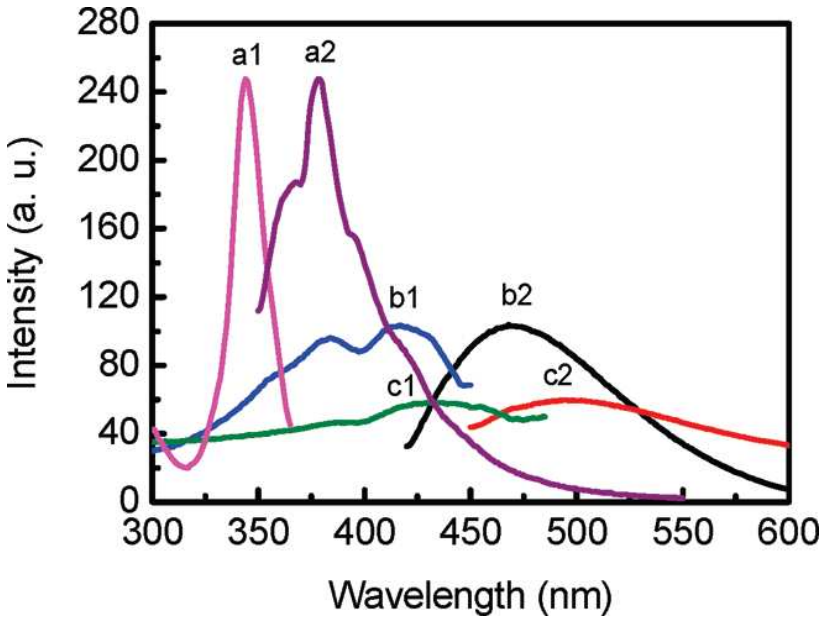

Figure 2.5 Excitation and emission spectra of solution samples prepared at 70, 150, and 180 °C. Spectra a1 and a2 are excitation and emission spectra for the sample prepared at 70 °C (emission, 375 nm; excitation, 340 nm); b1 and b2 are excitation and emission spectra for the sample prepared at 150 °C (emission, 468 nm; excitation, 400 nm); c1 and c2 are the excitation and emission spectra for the sample prepared at 180 °C (emission, 497 nm; excitation, 430 nm).

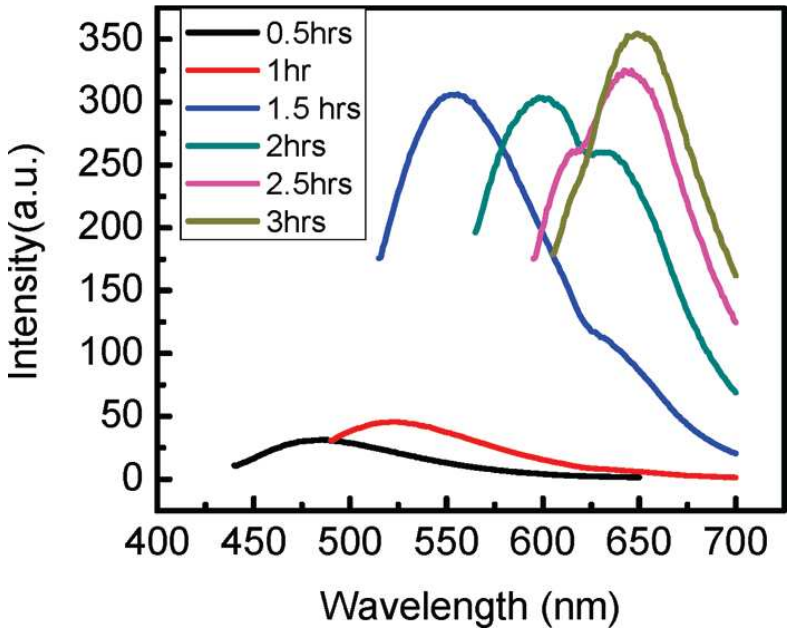

Figure 2.6 Luminescence of $LaF_3:Ce^{3+}$ solution prepared at 180 °C with reaction time of 0.5, 1.0, 1.5, 2.0, 2.5, and 3.0 h.

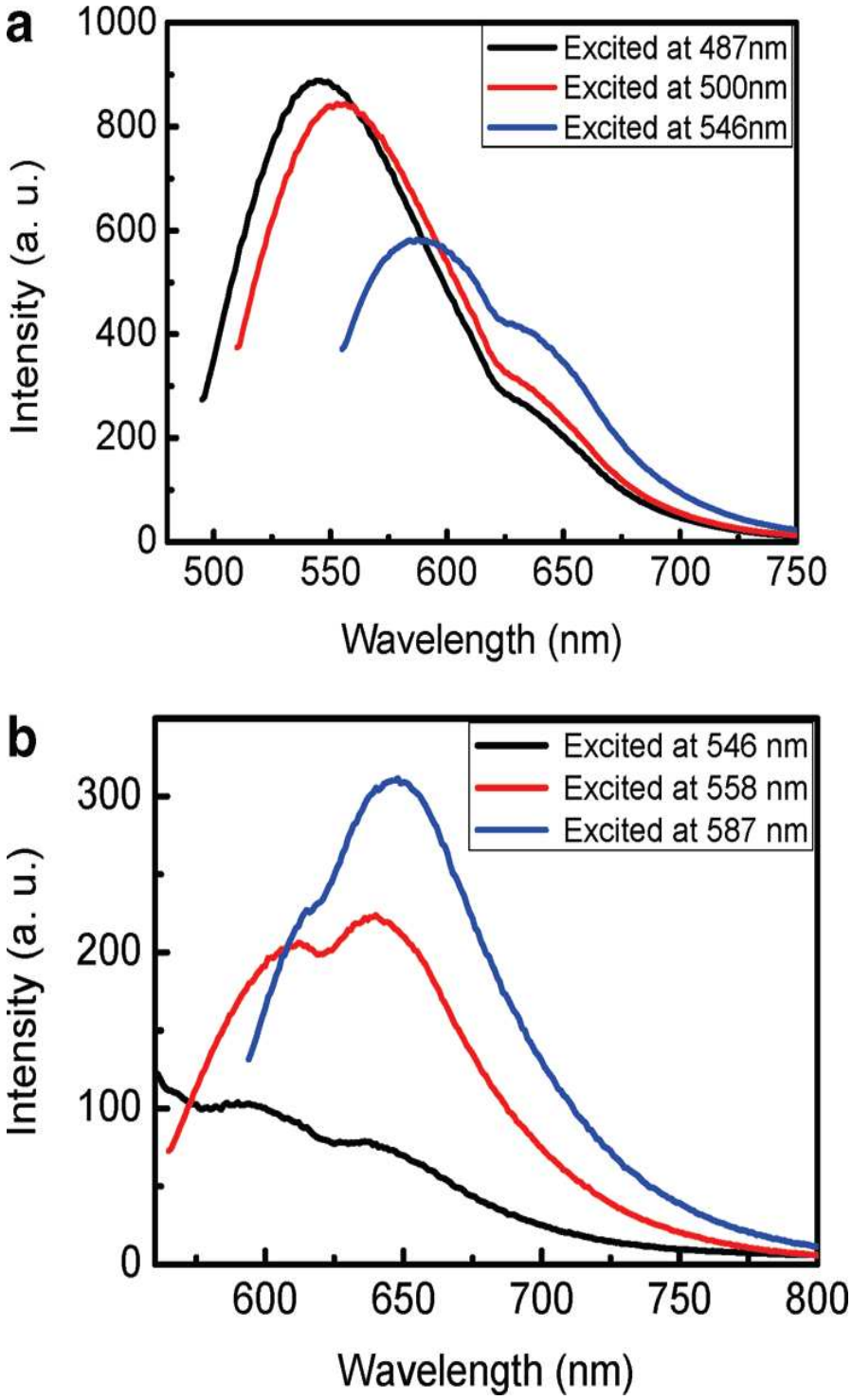

Figure 2.7 Emission spectra of the sample prepared at (a) 150 °C and (b) 180 °C excited with different excitation wavelengths.

C. Luminescence Mechanism.

Nanoparticle powders can be precipitated from the solution samples by adding dioxane, and the luminescence spectra of the nanoparticle powders are almost the same as that of LaF_3:Ce^{3+} nanoparticles reported in the literature.[107,132,134] Both XRD and TEM measurements demonstrated that the nanoparticle powder obtained from the solutions is LaF_3: Ce^{3+} nanoparticles; therefore the solutions do contain LaF_3:Ce^{3+} nanoparticles. However, the luminescence properties (excitation and emission wavelengths as well as intensity) of the solutions are almost the same before and after the nanoparticle powders were precipitated from the solutions. This indicates that LaF_3:Ce^{3+} nanoparticles are not responsible for the luminescence from the solution samples. To uncover the origin of the luminescence from the solution samples, lanthanum(III) nitrate hydrate and cerium(III) nitrate hexahydrate were refluxed in DMSO at the same temperatures as used for the nanoparticle syntheses. Surprisingly, the DMSO solutions boiled with lanthanum(III) nitrate hydrate (La^{3+}/DMSO) or cerium(III) nitrate hexahydrate (Ce^{3+}/DMSO) exhibit intense luminescence as shown in Figure 2.8 for the solution prepared at 150 °C, The emission of Ce^{3+}/ DMSO solution peaks at 460 nm, while the La^{3+}/DMSO solution emission peaks at 640 nm. When DMSO was refluxed with both lanthanum(III) nitrate hydrate and cerium(III) nitrate hexahydrate, the excitation and emission spectra are very similar to the DMSO solution in which LaF_3:Ce^{3+} nanoparticles were prepared. Therefore, it is likely that metalorganic compounds of Ce^{3+} with DMSO and La^{3+} with DMSO are responsible for the luminescence from DMSO solution samples in which LaF_3:Ce^{3+} nanoparticles were synthesized.

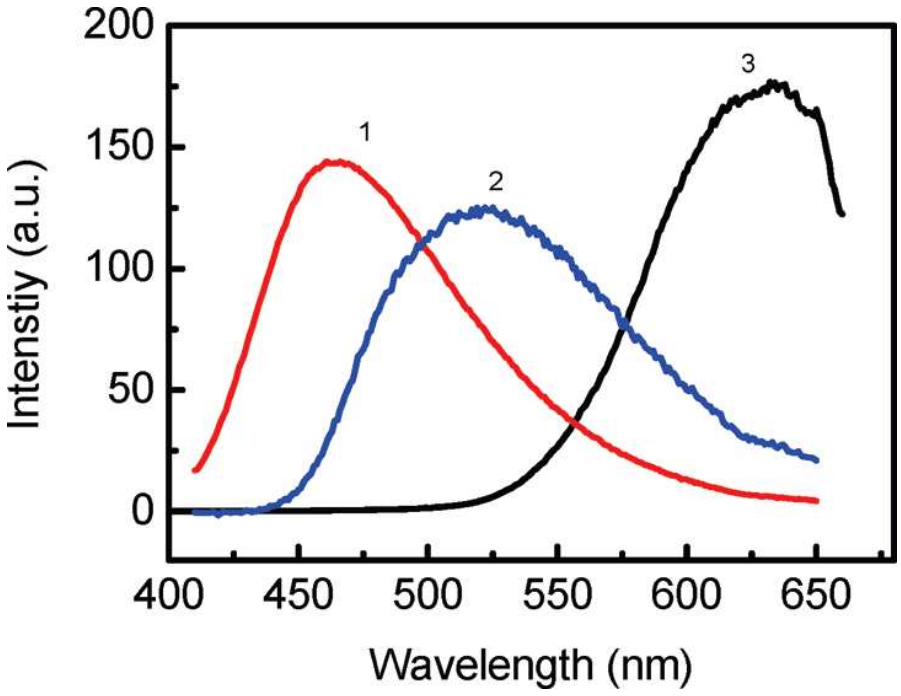

Figure 2.8 Comparison of emission spectra of solution samples prepared at 150 °C with a excitation wavelength of 400 nm: (1) Ce^{3+}-DMSO; (2) LaF_3:Ce nanoparticle solution; (3) La^{3+}-DMSO.

The details about the structures and luminescence origin of the metalorganic compounds of Ce^{3+} and La^{3+} with DMSO are still under investigation. However, it is clear that the luminescence of solution is not from intrinsic emission of intra ion transitions of La^{3+} or Ce^{3+} ions. It is well-known that La^{3+}, Y^{3+}, Lu^{3+}, and Sc^{3+} ions have no 4f electrons, therefore they have no electronic energy levels that can induce excitation and luminescence processes in or near the visible region.[139] The luminescence lifetimes of d-f transitions of Ce^{3+} are typically about 20-25 ns. However, the luminescence lifetimes of the solution samples are much shorter (0.36 and 2.8 ns; see Figure 2.9). This is strong evidence that the luminescence of the solution samples is not from the intra ion transitions of La^{3+} or Ce^{3+} ions. Most likely, the emissions of the solution samples originate from metal-to-ligand charge-transfer (MLCT) excited states as reported in similar metal organic compounds.[140] It is interesting to observe that the emission of the solution samples shifts to longer wavelengths at higher reaction temperatures and longer

reaction times. At short reaction times, the luminescence of solution appears more similar to the Ce^{3+}-DMSO spectrum, but as the reaction time and temperature increase, more La^{3+}-DMSO metal organic compounds are formed. La^{3+}-DMSO metal organic compounds have longer emission wavelengths; therefore as more La^{3+}-DMSO metal organic compounds are formed, the overall emission shifts to longer wavelengths. Increases in luminescence self-absorption at higher concentrations could also contribute to this shift.[138]

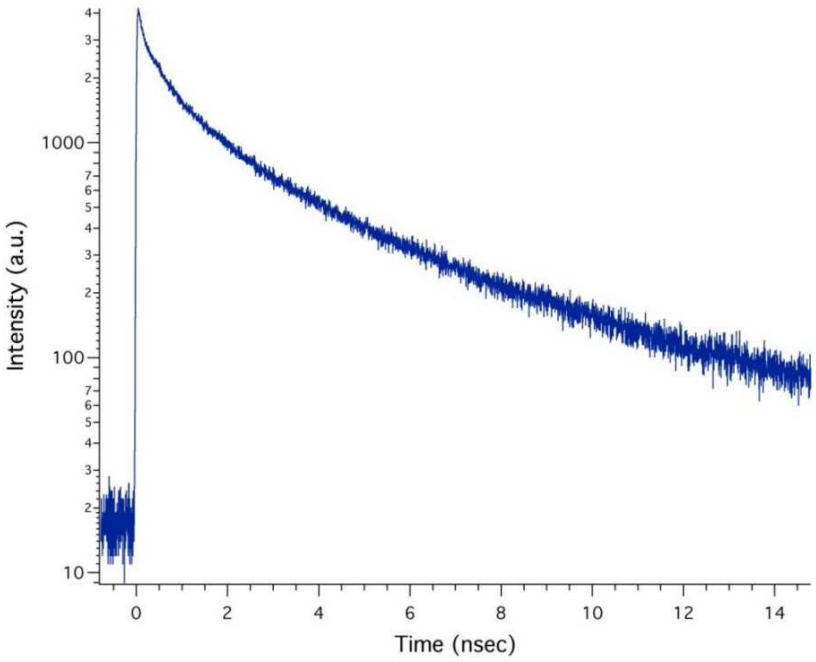

Figure 2.9 LaF_3:Ce solution sample luminescence lifetime following 305 nm excitation. The bi-exponential decay can be fit to components of 0.3 and 2.8 nsec.

In solid samples, the emission from d to f transition of Ce^{3+} in LaF_3:Ce nanoparticles is very strong, while no such emission is observed from LaF_3:Ce nanoparticles in the solution samples. This is most likely due to quenching by energy transfer from Ce^{3+} ions to Ce^{3+}-DMSO and La^{3+}-DMSO compounds because the emission of Ce^{3+} overlaps with the absorption of the compounds. It is also interesting to observe that LaF_3:Ce nanoparticles are smaller in size when

prepared at higher reaction temperature, as shown in Figure 2.2. This is contrary to results when making nanoparticles in water or inert organic solvents: usually the higher the reaction temperature, the larger the particle size.[141,142] The likely reason for this behavior is that the formation of the metal organic compounds between Ce^{3+} or La^{3+} with DMSO competes with the formation of LaF_3:Ce nanoparticles. Increases in reaction temperature or time favor La^{3+}-DMSO metal organic formation at the expense of nanoparticle LaF_3 formation. Consequently, the nanoparticles are smaller in size at higher temperatures since the amount of La^{3+} metal organic compounds increases. Furthermore, this competition not only affects the particle size, but also the shapes as shown in Figure 2.3.

Due to the unique penetration of DMSO to cell membranes, DMSO with luminescence as reported in this chapter may be used for cell imaging and probing. In our pilot studies, we have applied nanoparticles in DMSO for cell imaging in comparison with CdTe quantum dots. As observed by fluorescence and confocal microscopy, the CdTe quantum dots diffuse into the porcine and human lens capsule and into human cortical lens fibers, but they do not pass through the intact lens capsule.[143] However, nanoparticles in DMSO can pass through the intact lens capsule and penetrate into the lens cells. Therefore, this type of new luminescent agent may be used for cell imaging. The luminescence properties are more like organic dyes (such as Rodamine B) rather than nanoparticles in aqueous solution. However, attention should be paid to the sample dose as DMSO indeed can damage some cells. DMSO is miscible with water; therefore the luminescent DMSO-lanthanide complex should be diluted with water or buffer solution for cell imaging. The application of luminescent DMSO-lanthanide complexes for biological imaging and detection is currently being investigated in our group.

2.4 Applications in Biomedical Imaging and Cancer Treatment

2.4.1 Introduction

Due to the emissions induced by MLCT excited states, LaF_3:Ce in DMSO exhibits special luminescence properties which are quite different from its characteristic emissions of

LaF_3:Ce in aqueous solution or other solid phosphors. In order to explore some potential applications in biomedical system, we conjugated LaF_3:Ce in DMSO with protoporphyrin IX (shortened as PpIX), then coated the complex with Poly(Lactic-Co-Glycolic Acid) (shortened as PLGA). PpIX is an efficient photosensitizer which has been applied as a clinically useful photo sensitizer for photodynamic theraphy[144]; PLGA is a copolymer which is used in a host of Food and Drug Administration (FDA) approved therapeutic devices due to its superior biocompatibility and biodegradability, It has been successfully used as a biodegradable polymer because it undergoes hydrolysis in the body to produce the original monomers, lactic acid and glycolic acid. These two monomers under normal physiological condition are by-products of various metabolic pathways in the body. Since the body effectively deals with these two monomers, there is very minimal systemic toxicity associated with using PLGA for drug delivery or biomaterial applications. Also, the possibility to tailor the polymer degradation time by altering the ratio of the monomers used during synthesis has made PLGA a common choice in the production of a variety of biomedical devices such as: grafts, sutures, implants, prosthetic devices, micro and nanoparticles. It has also been used successfully in delivery Amoxicillin in treating listeriosis (treatment of Listeria monocytogenes infection). Based on these applications, we synthesized PLGA encapsulated LaF_3:Ce/PpIX and studied the cytotoxicity effect of PLGA encapsulated particles regarding their ability in generating oxidant injury within PC3 cells by using confocal microscopy. The results show this material has a potentially promising application in photodynamic therapy.

2.4.2 Synthesis of PLGA Encapsulated LaF_3:Ce/PpIX

Firstly, 9 mg of PpIX was added into a mixed solution of 1 ml of DI water and 10 ml of acetonitrile, in another container 14.11 mg of PLGA was added into 10 ml of DMSO. Under vigorous magnetic stirring, the chemicals were dissolved thoroughly after being stirred for about three hours under room temperature. Secondly, different amounts of PpIV solution were added dropwisely into 2 ml of LaF_3:Ce in DMSO (the same sample as the one in section 2.2 with a

reaction temperature of 150˚C). Based on luminescence measurements, select the one with optimal energy transfer between LaF_3:Ce and PpIX for encapsulation within PLGA by using the solution prepared in the first step, The mixture was stirred for two more hours to allow encapsulation to complete.

2.4.3 Luminescence Property of Encapsulated LaF_3:Ce/PpIV

Figure 2.10 shows emissions of LaF_3:Ce conjugated with different concentrations of PpIX compared with pure LaF_3:Ce. Due to the emissions induced by MLCT excited states as discussed in section 2.3, LaF_3:Ce in DMSO emits light at 519 nm when excited at 468 nm. When LaF_3:Ce is conjugated with PpIX, being affected by the crystal field of PpIX, the emissions from MLCT excited states are split into two peaks at 524 nm and 556 nm with a lower amount of PpIX, then two more peaks are shown at 487 nm and 594 nm as concentration of PpIX increases. At the same time, the emissions from LaF_3:Ce decrease while increase from PpIX with increasing concentration of PpIX. In order to find out if there is energy transfer from LaF_3:Ce to PpIX, Figure 2.11 compares emission changes of LaF_3:Ce dilutions with DMSO, LaF_3:Ce conjugated with increasing amount of PpIX and increased concentrations of PpIX solutions. It is clearly seen that the decreasing emissions of LaF_3:Ce in LaF_3:Ce condjugated PpIX is not just because of the decreasing concentration of LaF_3:Ce caused by adding more PpIX, similarly, the increasing emissions of PpIX in LaF_3:Ce conjugated PpIX is not simply caused by increasing concentration of PpIX compared with the emissions from pure PpIX solutions. One possibility for the luminescence quenching in one accompanied by luminescence enhancement in another is energy transfer between the two materials. In order to find out the optimal amount of PpIX used for conjugation with LaF_3:Ce to achieve efficient energy transfer, we recorded the emission intensity changes with increasing concentration of PpIX as shown in Figure 2.12. It is clearly seen that emissions from PpIX starts quenching after reaching one certain concentration (say 9 drops) as a result of concentration quenching. Correspondingly, after this specific point, the 633 nm emissions from conjugate complex of LaF_3:Ce/PpIX stop

increasing and tend to stay in similar intensities. Therefore, we concluded that the conjugate complex formed from 2 ml of LaF_3:Ce and 9 drops (9/30 ml) of PpIX has the most efficient energy transfer from LaF_3:Ce to PpIX. Based on this ratio, we encapsulate the conjugate complex into PLGA for further biomedical studies.

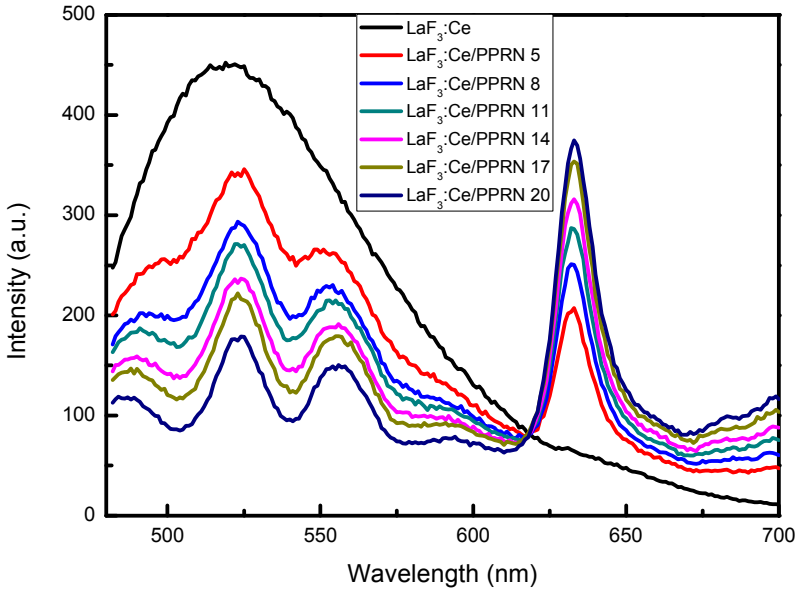

Figure 2.10 Emissions of LaF_3:Ce conjugated with different concentration of PpIX compared with pure LaF_3:Ce (excited at 468 nm)

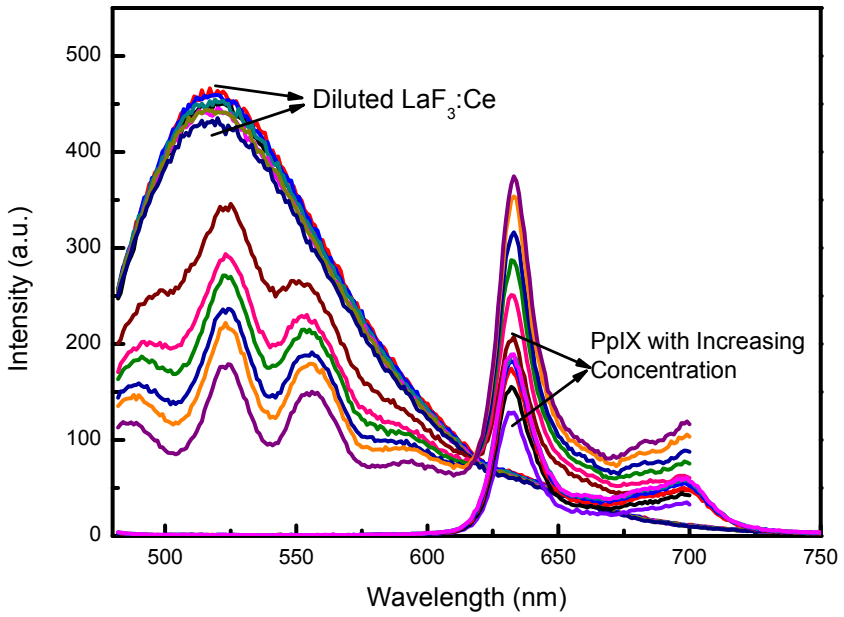

Figure 2.11 Emission comparisons among diluted LaF_3:Ce, LaF_3:Ce/PpIX and PpIX with increasing concentrations

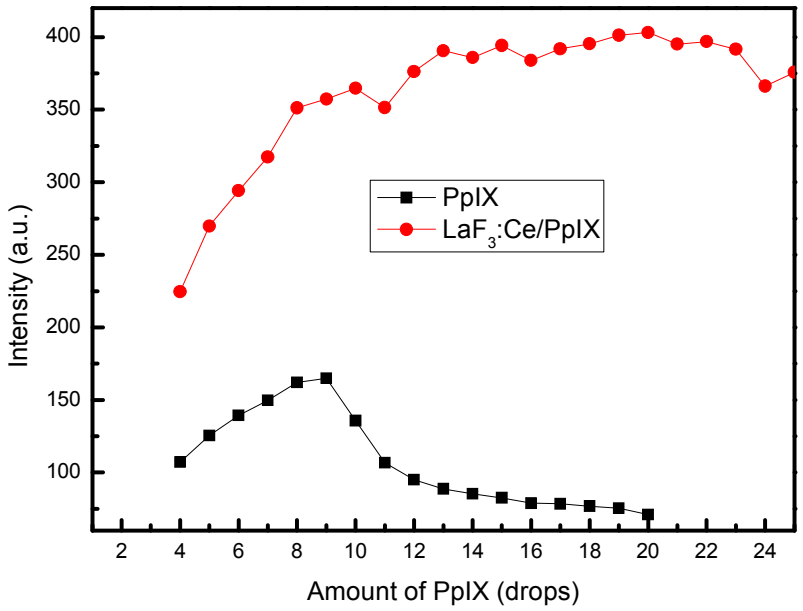

Figure 2.12 The dependence of 633 emissions in both PpIX and LaF_3:Ce/PpIX on amount of PpIX

2.4.4 Morphology and Cytotoxicity Study on PLGA Encapsulated LaF_3:Ce/PpIV to Cancer Cells

The shape and size distribution of PLGA encapsulated LaF_3:Ce/PpIX were studied with a confocal laser scanning microscopy (Zeiss LSM 510 Meta) and LM 20 (Nanosight, USA). Left figure in Figure 2.13 shows particle size distribution of PLGA encapsulated LaF_3:Ce/PpIX. The sizes of the particles are in a range of less than 50 nm and the sharp peaks show very narrow size distributions in upper figure, which indicates the particles have uniform sizes. The peaks at 37 nm and 45 nm show a large amount of particles have sizes around 37nm and 45 nm. The right figure is scattered intensity and particle size distribution, which shows clearly the particle size distribution of the population, with an average diameter of 41 nm.

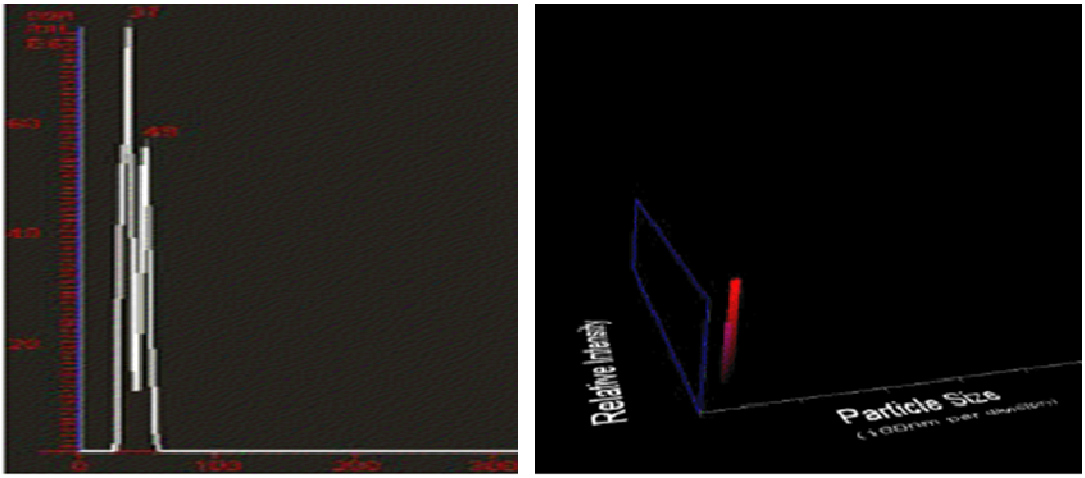

Figure 2.13 Particle size distribution of PLGA encapsulated LaF_3:Ce/PpIV

The tumor cellular uptake capability and cytotoxicity of PLGA encapsulated LaF_3:Ce/PpIX were studied with human prostate cancer cell line (PC_3). Figure 2.14 shows fluorescence microscopic images of PLGA encapsulated LaF_3:Ce/PpIX. The dark dots in figure A are complexes of LaF_3:Ce conjugated with PpIX, which are encapsulated within thick cells of PLGA. The bright green area shown in figure B indicates the uptake of the encapsulated

particles in cytoplasm of PC_3 is very efficient, the dark nuclear area shows that the particles did not penetrate into the nuclear. Figure C shows cancer cells after the incubation of 24 hrs, where blue nuclei and red cytoplasm show healthy mitochondria. Mitochondria with decreased membrane potentially cause the monomer formation of JC1 molecules which yield green fluorescence as shown in large area of cells, this indicates that LaF_3:Ce/PpIX encapsulated PLGA causes large percentage of cells with mitochondrial perturbation. With efficient uptake by cancer cells and large mitochondrial perturbation to cancer cells, PLGA encapsulated LaF_3:Ce/PpIX may find application as a promising agent in photodynamic therapy for cancer treatment.

.

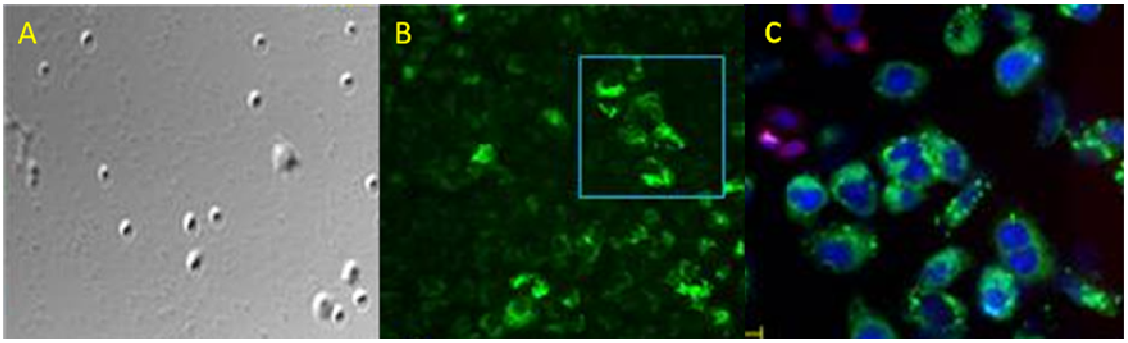

Figure 2.14 A. Fluorescence microscopic image; B. Confocal microscopy shows efficient uptake of encapsulated particles in cytoplasm of PC_3 cells in 24 hrs; C. Cytotoxicity study on particles under confocal microscopy after incubation of 24 hrs. Healthy cells show blue nuclei and red cytoplasm, while green fluorescence shows monomer caused by decreased membrane.

2.5 Conclusion

$LaF_3:Ce^{3+}$ nanoparticles were successfully synthesized in dimethyl sulfoxide by chemical reactions of lanthanum nitrate hydrate and cerium nitrate hexahydrate with ammonium fluoride at different temperatures. However, the luminescence of the $LaF_3:Ce^{3+}$ nanoparticle powders precipitated from the DMSO solution is markedly different from that of the solution samples. UV emission at around 310 nm attributed to Ce^{3+} d-f transitions was observed in the solid samples; however, this emission was absent in the solution samples. The solution

samples show emissions from UV to blue and red depending on the reaction temperature and duration. The luminescence lifetimes of the solution samples are much shorter than the decay lifetime of Ce^{3+} emission. When lanthanum(III) nitrate hydrate and/or cerium(III) nitrate hexahydrate were heated in DMSO, similar emissions were observed. This indicates that Ce^{3+}-DMSO and La^{3+}-DMSO compounds formed in solution are likely responsible for the luminescence of the solution samples. The formation of these metal organic compounds may compete with the formation of the LaF_3:Ce nanoparticles, and this competition likely influences the shapes and the sizes of the nanoparticles. Thus, at higher temperatures, the nanoparticles are smaller in size, a result that is contrary to nanoparticle formation in water or inert solvents. The LaF_3:Ce in DMSO has found a potential application as an agent in photodynamic therapy for cancer treatment when the conjugation of LaF_3:Ce in DMSO with PpIX is encapsulated within PLGA. The efficient uptake and great damages to cancer cells make this nanomaterial promising in photodynamic therapy for cancer treatment.

CHAPTER 3
THE APPLICATION OF HYPERSENSITIVE LUMINESCENCE OF EU^{3+} IN DIMETHYL SULFOXIDE AS A NEW PROBING FOR WATER MEASUREMENT

3.1 Introduction

The emission from lanthanide ions has been studied extensively in these years because of their wide applications in various areas such as luminescence imaging,[45,46] luminescent labels and the detection of cellular functions[47,145] etc. Luminescence of Ln(III) ions, characterized by sharp, narrow emission spectroscopy bands corresponding to the ff transitions of the metal ion, has proven useful as a sensitive detection method in biological systems. The luminescence from lanthanide excited states can be quenched through non-radiative energy transfer to stretching vibrations of nearby or coordinated solvent molecules, especially in aqueous media where there are abundant of O-H oscillators resulting in Frank Condon overlap of energy levels and stretching vibrations.[49-51,146] Europium was the first lanthanide that has been studied in solution due to its more efficient luminescence compared with other lanthanide ions.[55] Back in 1939, Freed et al. found that the intensities of the spectral emission lines of europium (III) were affected by the solvent in which it was studied.[147] Furthermore, the changes in the intensity of the Eu (III) luminescence upon binding to proteins and enzymes have been utilized to examine the ligation sphere within the active site,[55,148-150] therefore, the luminescence quenching rates have become valuable data in evaluating hydration in the primary coordination sphere of complexes of Eu ion.[54,149,151,152]

Lanthanide-DMSO compounds may find some new and interesting applications due to their unique properties. The properties and applications of DMSO in biomedical systems have been described in Chapter 2. Moreover, DMSO is miscible with water and it is very common that the two solvents are mixed for some specific applications. In a sense, it is important to

detect water in DMSO and this has been done using the luminescence decay lifetimes from Eu^{3+} ions.[9] Barthelemy et al calculated the degree of hydration of Eu(III) from the luminescence decay rate constants to determine water amount in DMSO,[148] Stefan and Gregory measured the lifetimes of Eu(III) and found the linearity of response to water concentration in DMSO solution.[153] Here we report the strong emissions of Eu (III) in DMSO which becomes supersensitive when water was introduced, the dependence of emission changes on water provides a new and convenient method for water measurement in DMSO.

3.2 Experimental Details

Europium (III) nitrate pentahydrate, ($Eu(NO_3)_3 \cdot 5H_2O$, 99.9%) and Dimethyl Sulfoxide (DMSO) were both purchased from Sigma-Aldrich. The reagents were used as received, without further purification. The synthesis of Europium-DMSO compounds is straightforward. 2.14 g $Eu(NO_3)_3 \cdot 5H_2O$ were firstly dissolved into 25 ml DMSO and then boiled at 150 ^oC with vigorously stirring for 2 hours under the protection of nitrogen. In order to find out the luminescence quenching effect of Eu-DMSO on coordinating solvent containing OH group, the sample was diluted with same calculated amount of DMSO and DI water respectively with different sets of concentrations for comparison. The excitation and emission spectra were measured on a Shimadzu RF-5301PC fluorometer. All measurements were conducted at room temperature.

3.3 Results and Discussion

Our previous research found that some of the lanthanide-DMSO compounds such as Ce-DMSO and La-DMSO show very strong emissions in longer wavelength area other than their characteristic emissions, which have been considered as the emissions induced by metal to ligand charge transfer (MLCT),[154] however, the situation is totally different for Eu-DMSO. Eu-DMSO compounds show the typical luminescence of Eu^{3+} which is similar to that of Eu(III) ions in aqueous solution or other solid phosphors, no obvious MLCT emissions were observed. However, unlike the weak luminescence from aqueous solution of Eu(III) due to the low

absorption cross section of the ions in the UV-visible region, Eu-DMSO has very strong luminescence as displayed in Figure 3.1. The excitation and emission spectra of Eu-DMSO are shown in Figure 3.2. The sharp and narrow bands in excitation and emission spectra are corresponding to the f - f transitions of the Eu ion, the emissions within the range of 575-725 nm are due to $^5D_0 \rightarrow {}^7F_{1\text{-}4}$ transitions of Eu^{3+}.[155,156] The two weak emission peaks at 536 and 555 nm are originated from transitions of $^5D_1 \rightarrow {}^7F_1$ and $^5D_1 \rightarrow {}^7F_2$ of Eu^{3+}.[157] The absorption peaks in the excitation spectrum are from the ground state of $^7F_0$ to the high energy levels of Eu^{3+} and their assignments are labeled in the spectrum in Figure 3.2.

Figure 3.1 Pictures of Eu-DMSO solution in room light (left) and under a UV lamp excitation (right).

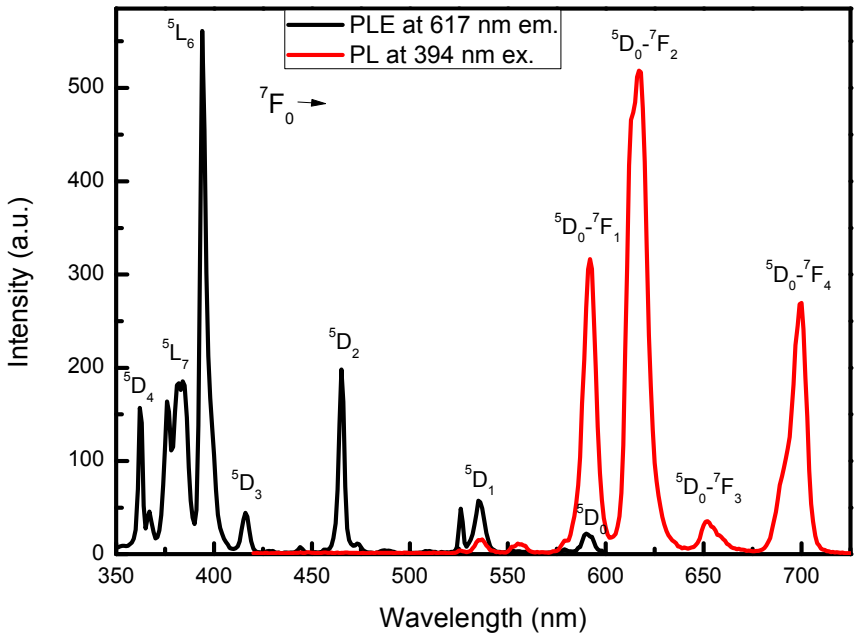

Figure 3.2 Excitation and emission spectra of Eu-DMSO solution. The excitation spectrum was recorded by monitoring the emission at 617 nm and the emission spectrum was taken by excitation at 394 nm.

Figures 3.3 and 3.4 show excitation and emission spectra of Eu-DMSO solution in comparison with the spectra when different amounts of water and DMSO were dropped into the compound. Clearly, the excitation and emission intensities of Eu^{3+} in DMSO are decreased when water or DMSO is added into the solution. However, the intensity decreases caused by adding water are almost five times greater than that by the same amount of DMSO. Figures 3.5 compares the emission intensity changing trends corresponding to all emission peaks in water and DMSO dilutions. The emission intensity decreases gradually with increasing concentration of DMSO added, but drops sharply at first, and then decreases gradually with increasing concentration of water added, which indicates that the quenching rate induced by DMSO and water are quite different. It is even more interesting to see that the emission of $^5D_0 \rightarrow {}^7F_2$ of Eu^{3+} in Eu-DMSO is hypersensitive when encountering with water. The $^5D_0 \rightarrow {}^7F_2$ emission band is

split into two peaks at 613 and 617 nm as a result of J-mixing in crystal field expansion and spin-orbit interaction.[158] In original Eu-DMSO compound, the peak at 617 nm is stronger than that at 613 nm. After different amount of DMSO being added into the compound, the emission intensity of $^5D_0 \rightarrow {}^7F_2$ transition is decreased gradually but the relative intensities of the two peaks at 613 and 617 nm are not varied. However, when the same amount of water is dropped into the Eu-DMSO compound, not only the emissions are decreased but the relative intensities of the two peaks at 613 and 617 nm are changed remarkably. That is the emission peak at 617 nm becomes weaker than that at 613 nm as water concentration increases, which is opposite to that in Eu-DMSO compound. This indicates that the quenching mechanisms by water and DMSO are different. By adding water, the quenching on the peak at 617 nm is much faster than that on the peak at 613 nm. While the quenching on two peaks at 613 and 617 nm by adding DMSO is at the same step and obviously this quenching is simply due to the decrease of the Eu^{3+} concentration. However, the quenching mechanism by water is more complicated. The quenching of emission intensities is due to coupling of the Eu excited state to O-H oscillators of water molecules where some of the energy from Eu excited state has been transferred to the O-H oscillators of bound water molecules.[53,54]

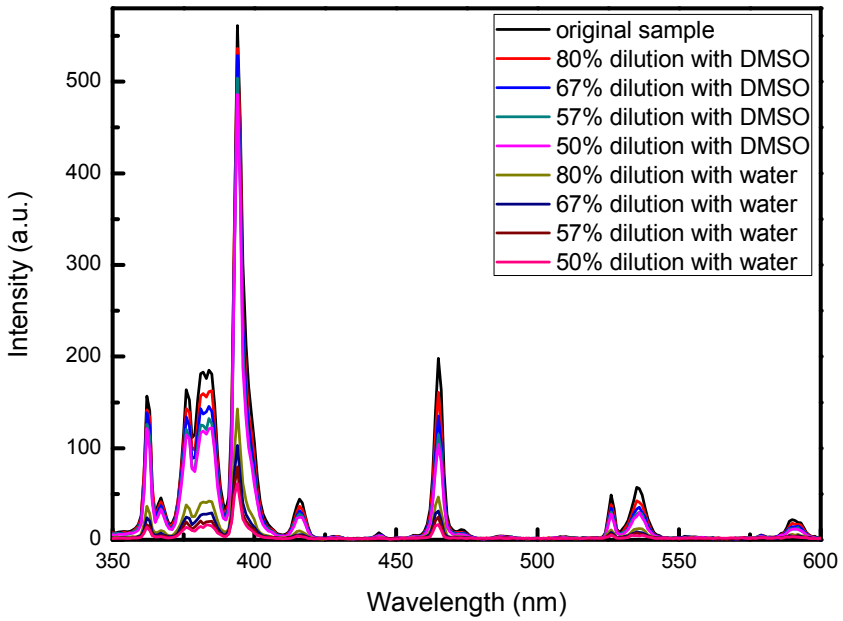

Figure 3.3 Excitation spectra of Eu-DMSO original and solution and dilutions (emission monitored at 617 nm)

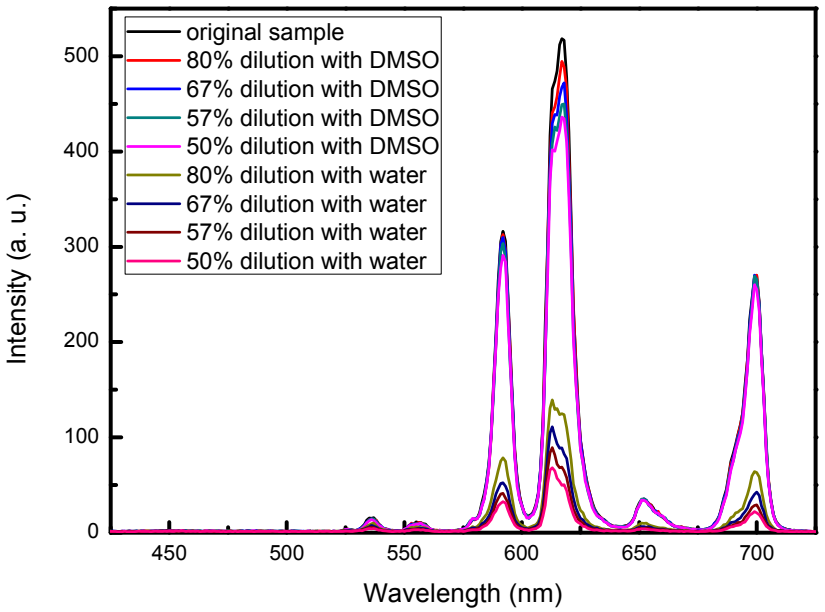

Figure 3.4 Emission spectra of original Eu-DMSO solution and dilutions (v/v) with water and DMSO. The excitation is at 394 nm.

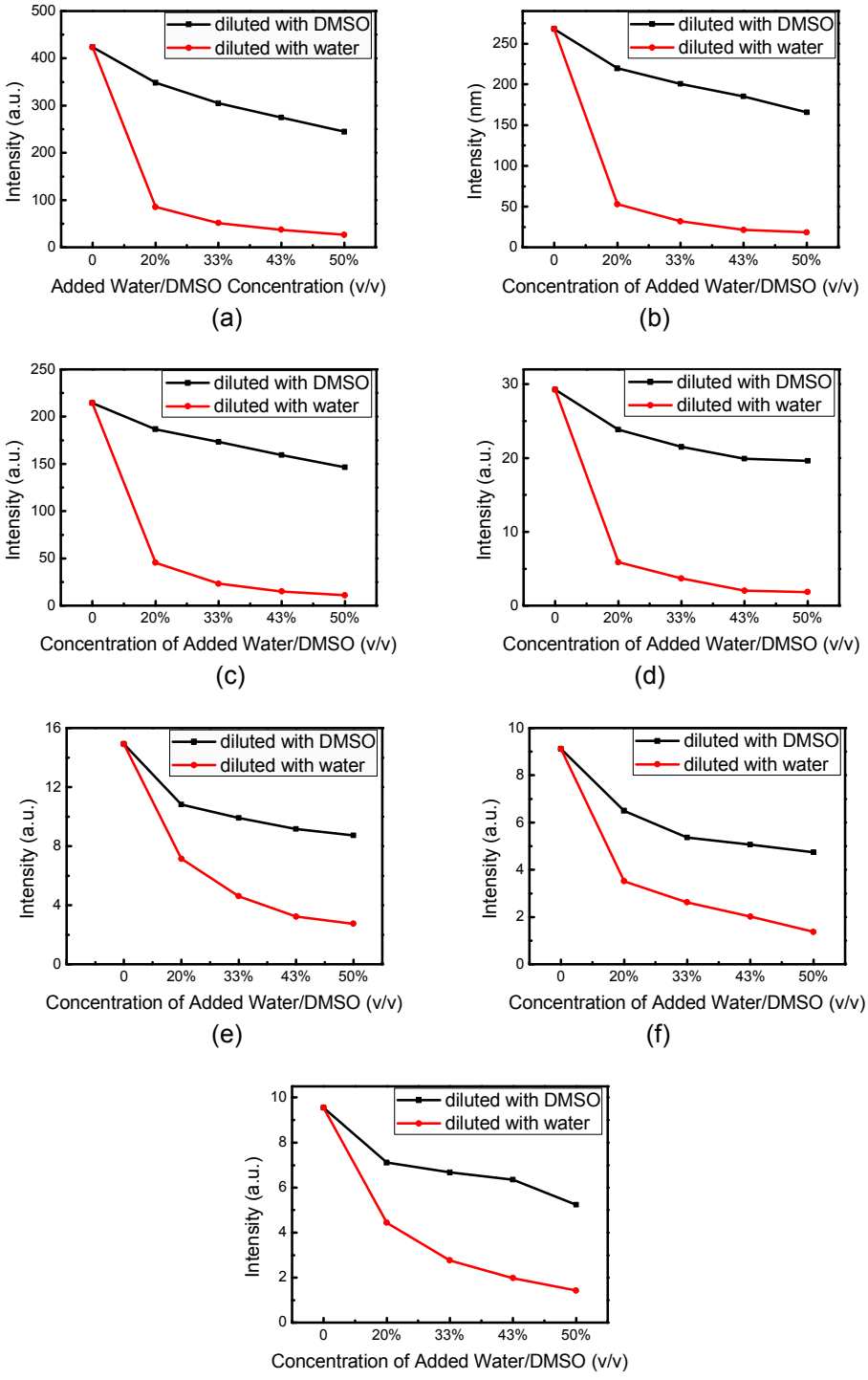

Figure 3.5 Comparisons on intensity changes of emissions at (a) 617 nm (b) 592 nm (c) 700 nm (d) 651 nm (e) 536 nm (f) 553 nm (g) 557 nm in Eu-DMSO dilutions with DMSO and water, respectively

In order to observe the gradual variation in the two peaks at 613 and 617 nm, reduced amounts of water were added into Eu-DMSO compound, Figure 3.6 and 3.7 show the changes in the excitation and emission spectra with water concentration changes from 0.5 % to 14.3 %. It shows that as water concentration reaches to 6.2%, the two peaks have almost equal intensity, and then as water concentration is increased, the 617 nm peak is gradually quenched and becomes weaker than the peak at 613 nm. The intensity changing trends of two peaks at 613 and 617 nm corresponding to the concentration of water added are displayed in Figure 3.8 and the dependence of intensity ratio of 613 nm to 617 nm emissions on water concentration is shown in Figure 3.9. A linear fitting shows that the intensity ratio is changed linearly with the water concentrations added to the Eu-DMSO solution as

$$R_I = 0.769P_V + 0.916$$

or

$$P_V = (R_I - 0.916)/0.769.$$

Where P_v stands for the volume concentration of water in Eu-DMSO in percentage, R_I stands for the intensity ratio of two emission peaks at 613 nm to 617 nm. This relationship provides a new method for the measurement of water in DMSO and this method is much easier and more convenient than the lifetime measurement because the measurement of the emission spectra is much easier than the lifetime measurement. In addition, the cost by using the method described here is much cheaper than that by lifetime methods. It is believed that the reported method can be used for other solvent detection in DMSO such as ethanol, acetone, diethyl ether, benzene, chloroform, phosphate buffered saline (PBS) buffer solutions, and cell culture media which are under investigation. However, we need to point out that when the concentration of water is higher than 50%, the emission peak at 617 nm disappears, so the method of using the ratio of the 613 and 617 nm peaks is limited to the concentrations from 0 to

50%. For water concentrations higher than 50%, the intensities of Eu^{3+} emission are still decreased gradually with the increasing of water, so the intensity change is still reliable for determination of water in DMSO.

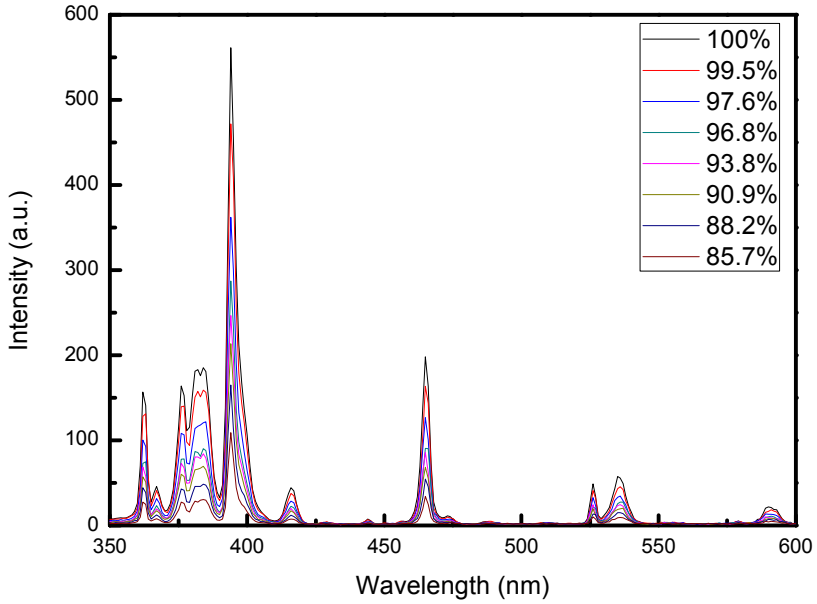

Figure 3.6 Excitation Spectra of original Eu-DMSO and dilutions with small amount of water (v/v)

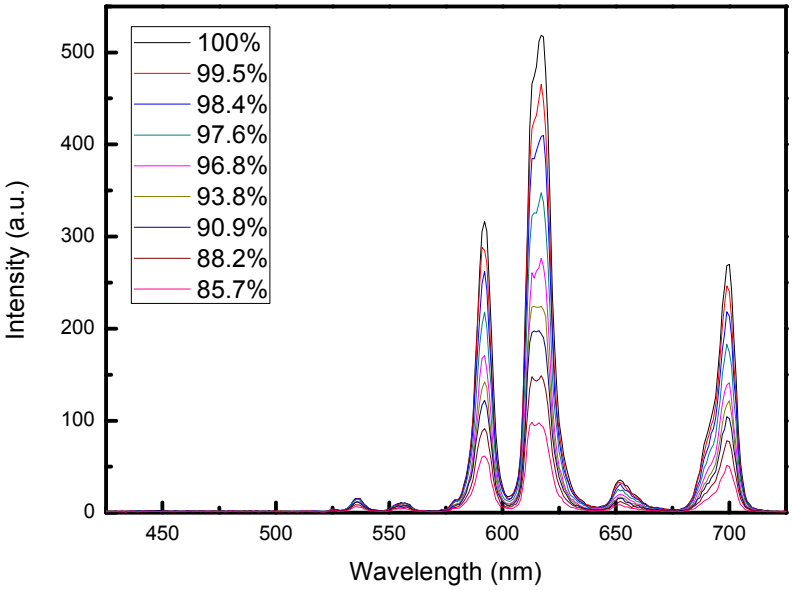

Figure 3.7 Emission spectra of original Eu-DMSO and dilutions (v/v) with small amount of water. The excitation is at 394 nm.

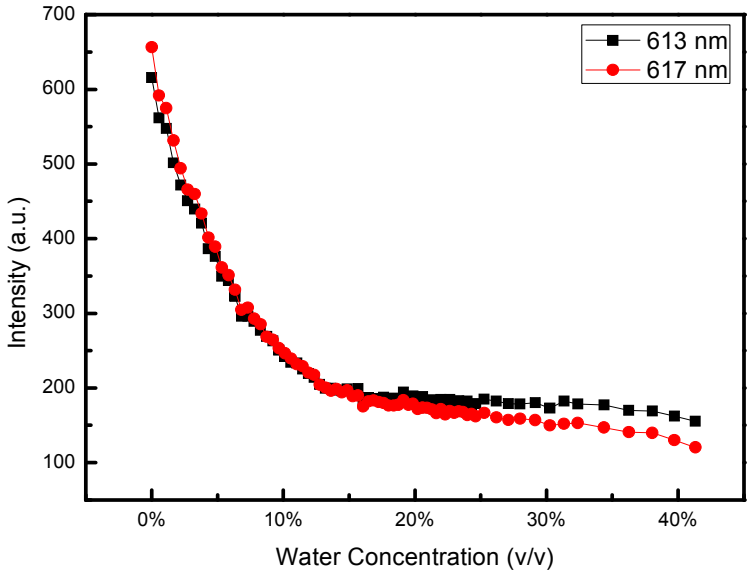

Figure 3.8 The intensity changing trends of emission peaks at 613 nm and 617 nm from water-diluted Eu-DMSO compound

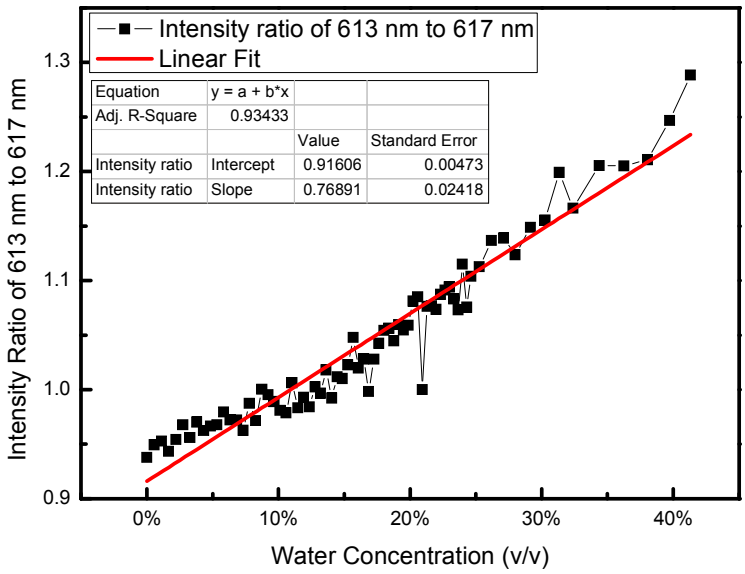

Figure 3.9 The dependence of ratio of emission intensities of 613 nm to 617 nm in water-diluted Eu-DMSO compound on water concentration.

3.4 Conclusion

Unlike the other Lanthanide-DMSO compounds, Eu-DMSO emits very strong characteristic emissions of Eu^{3+} as observed in the luminescence spectra and X-ray luminescence measurements. Luminescence quenching behavior of Eu in DMSO was investigated with great details. Four main emission peaks of Eu^{3+} at 593, 617, 656 and 700nm are corresponding to transitions of $^5D_0 \rightarrow {}^7F_1$, $^5D_0 \rightarrow {}^7F_2$, $^5D_0 \rightarrow {}^7F_3$ and $^5D_0 \rightarrow {}^7F_4$, respectively. It is interesting to be found that the 617 nm emission peak had a shoulder at 613 nm, the coupling of Eu ion with O-H oscillators had a great effect on relative emission intensities between these two peaks when Eu-DMSO encountered with water, which resulted in different quenching rates on these two peaks. The ratio of emission intensity of 613 nm to 617 nm has a nearly perfect linear dependence on increasing water concentration in Eu-DMSO. This linear

relationship provides a very convenient and valuable method for water determination in DMSO.

CHAPTER 4

LUMINESCENCE PROPERTIES OF LN^{3+} DOPED LAF_3 NANOPARTICLES IN WATER

4.1 Introduction

Fluorescent labeling of molecules is a common and very useful technique in biological science. LnF_3-based nanoparticles could have a number of advantages for use as probes in bioconjugation applications over other biolabels, since emissions from lanthanide ions involve f-orbital electrons and are much narrower than those observed from organic molecules. The quantum yield of lanthanide emission is high in the absence of quenching and photobleaching effects which are commonly observed in fluorescent dye molecules, but not observed in lanthanide ions. In addition, LnF_3-based nanoparticles have a number of advantages as probes used in bioconjugation applications over other biolabels, such as inherent long-lived luminescent lifetimes and long-term stability of the nanoparticle signal. In recent years, some research in this area confirmed that Ln^{3+} doped LnF_3 can be turned into biolabels with some specific binding to proteins.[159-161] Most reaction processes of labeling compounds with target biomaterials require the presence of water,[162] therefore, site-specific, photostable and water-soluble nanoparticles are needed for achieving ultrasensitive labeling and detection of biomaterials. Different methods have been used to synthesize LnF_3-based nanoparticles.[163-169] However, most LnF_3 nanoparticles that are synthesized so far are not water soluble or biocompatible, which greatly limits their application in biological systems. Here we report the synthesis of LaF_3: Ce nanopowder and Ln^{3+} doped LaF_3 nanoparticles (Ln^{3+} refers to Tb^{3+}, Tb^{3+}+Yb^{3+} and Tb^{3+}+Ce^{3}) with surface functionalized with poly(ethylene glycol) bis(carboxymethyl) ether (COOH-PEG-COOH), they are all water-soluble and have surface-reactive carboxylic (-COOH) functional group capable of labeling amide group of target

biomaterials. The investigation of luminescent properties and potential application as labeling agents for ultrasensitive and time-gate imaging is detailed in sections 4.2 and 4.3.

4.2 Synthesis and Characterization of $LaF_3:Ce^{3+}$ Nanopowder

4.2.1 Synthesis of $LaF_3:Ce^{3+}$ Nanopowder

Lanthanum (III) nitrate hydrate ($La(NO_3)_3 \cdot X\ H_2O$, 99.9%), Cerium (III) nitrate hexahydrate ($Ce(NO_3)_3\ 6H_2O$,99.9%), ammonium fluoride (NH_4F, 99.9%), Poly(ethylene glycol) bis(carboxymethyl) ether were purchased from Sigma-Aldrich. All reagents were used as received, without further purification. $LaF_3:Ce^{3+}$ nanoparticles were synthesized using the wet-chemistry method. Typically, 9 mmol of $La(NO_3)_3$, 1 mmol of $Ce(NO_3)_3$ and 30 mmol of NH_4F were added to 50 ml water in a three-necked flask, 1 ml of Poly (ethylene glycol) PEG was added dropwise to the mixed chemical solution. PEG is a water soluble polymer composed of repeating ethylene oxide units flanked by alcohols with a formula of $HO\text{-}CH_2\text{–}(CH_2\text{-}O\text{-}CH_2)n\text{-}CH_2\text{-}OH$. Structurally, the polar and uncharged nature of PEG renders itself hydrophilic characters, which has been approved to be used as hydrophilic neutral surface coating ligand. Thus, the material coated with PEG allows to be synthesized and analyzed under aqueous conditions. In this work, $Ce(NO_3)_3$ was used as dopant at the concentration of 0.1 M. The chemicals were mixed thoroughly with stirring for half an hour at room temperature; the mixture was subsequently heated to 100°C under vigorous magnetic stirring and nitrogen protection. A white suspension was formed gradually upon stirring. The nanoparticles obtained were collected by centrifugation, washed with DI water several times, then stored in DI water.

4.2.2 Characterization of $LaF_3:Ce^{3+}$ nanopowder

The $LaF_3:Ce^{3+}$ nanoparticles were characterized with high-resolution transmission electron microscopy (TEM). Images were taken with a JEOL JEM-2100 instrument, with accelerating voltage of 200 kV. Samples for TEM were prepared by depositing a drop of a colloidal aqueous solution of the powder sample onto a carbon-coated copper grid. The excess liquid was wiped away with filter paper, and the grid was dried in air. The X-ray powder

diffraction (XRD) patterns of $LaF_3:Ce^{3+}$ nanoparticles were recorded in the range of 20° ≤2θ ≤80° from a Siemens Kristalloflex 810 D-500 X-ray diffractometer under an operating mode of 40 kV and 30 mA with λ=1.5406 Angstrom radiation. The emission and excitation spectra of the samples were measured using a Shimadzu fluorescence spectrometer (RF-5301PC) with a 400W monochromatized xenon lamp.

Figure 4.1 shows the XRD patterns of the $LaF_3:Ce^{3+}$ nanoparticles synthesized in water. The peak positions and intensities are consistent with the data reported in the JCPDS standard card (32-0483) of pure hexagonal lanthanum fluoride crystals. The sizes of the nanocrystals were calculated from the XRD pattern based on the Debye–Scherrer formula, assuming that all the particles are spherical in shape. The results show that the size of the nanoparticles produced is about 16 nm.

Figures 4.2 and 4.3 show the high-resolution TEM images of the $LaF_3:Ce^{3+}$ nanocrystals. It can be seen in Figure 4.2, with 40K magnification, that the nanocrystals are well dispersed and the shape of the $LaF_3:Ce^{3+}$ nanoparticles is spherical. Figure 4.3 shows an 800K-magnified TEM image of $LaF_3:Ce^{3+}$ nanocrystals, in which clear lattice fringes are evidence of crystalline quality. The size of the nanoparticles is about 15 nm, which is consistent with the size obtained from XRD measurement.

Figure 4.4 shows the excitation and emission spectra of $LaF_3:Ce^{3+}$ nanocrystals at different reaction time from 1 hr to 11 hrs. These samples all have the same emission peak at 343 nm, which was attributed to 5d-4f transitions of the Ce ion. The intensity of emission decreases as reaction time is increased; the sample with reaction time of 1 hr has the strongest emission.

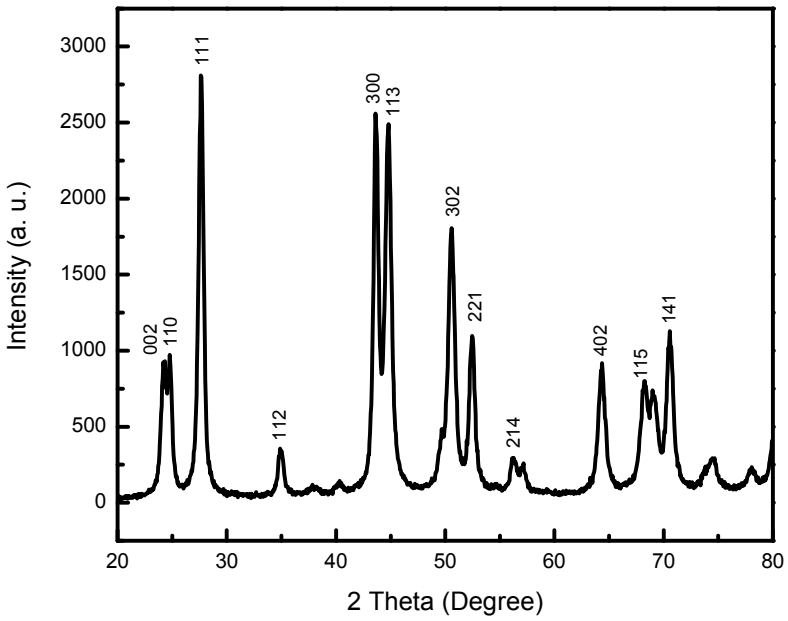

Figure 4.1 XRD pattern of $LaF_3:Ce^{3+}$ nanoparticles synthesized in water

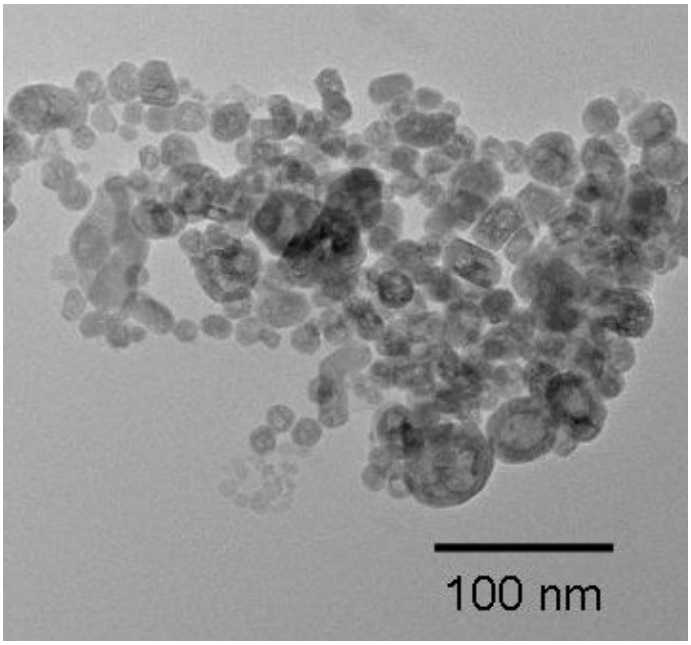

Figure 4.2 HRTEM images of $LaF_3:Ce^{3+}$ nanoparticles synthesized in water (40K)

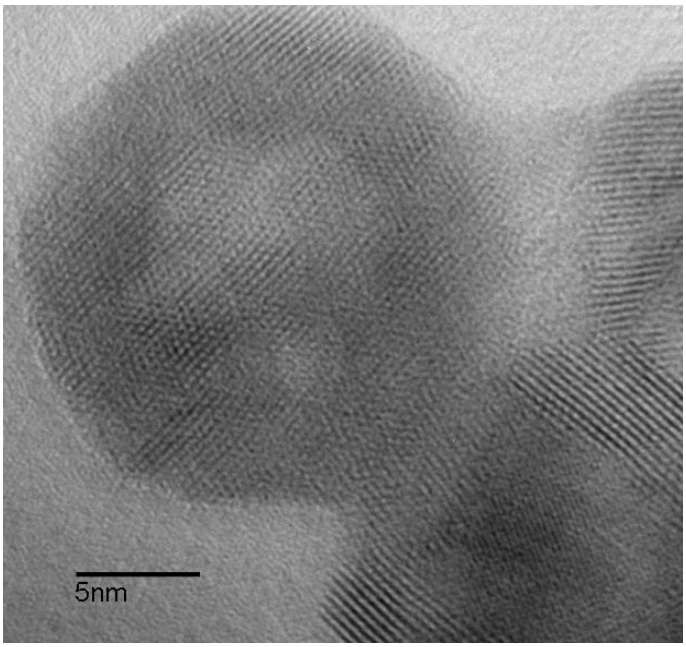

Figure 4.3 HRTEM images of $LaF_3:Ce^{3+}$ nanoparticles synthesized in water (800K)

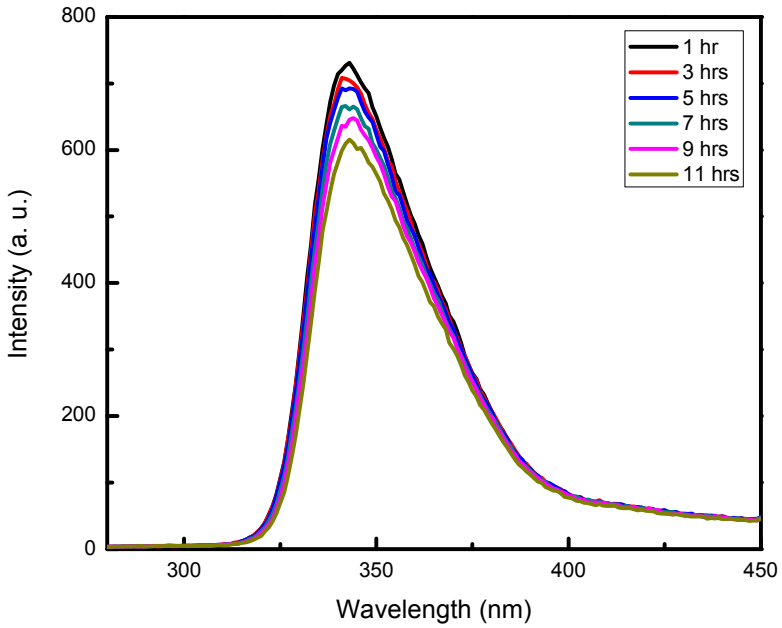

Figure 4.4 Excitation and emission spectra of LaF_3: Ce^{3+} nanoparticles at different reaction time

4.3 Synthesis and Characterization of Water-soluble $LaF_3:Ln^{3+}$ Nanoparticles

4.3.1 Synthesis of Water-soluble $LaF_3:Ln^{3+}$ Nanoparticles

Lanthanum (III) nitrate hydrate ($La(NO_3)_3 \cdot XH_2O$, 99.9%), Cerium (III) nitrate hexahydrate($Ce(NO_3)_3$ $6H_2O$,99.9%), Terbium (III) nitrate pentahydrate($Tb(NO_3)_3 \cdot 5H_2O$, 99.9%), Ytterbium (III) nitrate pentahydrate($Yb(NO_3)_3 \cdot 5H_2O$, 99.9%), Ammonium fluoride (NH_4F, 99.9%), poly(ethylene glycol) bis(carboxymethyl) ether were purchased from Sigma-Aldrich. All of the reagents were used directly, without further purification.

$LaF_3:Tb^{3+}$ nanoparticles were synthesized using the wet-chemistry method with different dopant concentrations as shown in the molecular formulas: $La_{0.7}Tb_{0.3}F_3$ and $La_{0.8}Tb_{0.2}F_3$. Typically, the $La_{0.7}Tb_{0.3}F_3$ nanoparticle was synthesized according to the following protocol: 2.8 mmol of $La(NO_3)_3 \cdot XH_2O$, 1.2 mmol of $Tb(NO_3)_3 \cdot 5H_2O$ and 10.5 mmol of NH_4F in 10 ml water solution were added to 90 ml water in a three-necked flask, 1 ml of PEG was added dropwise to the mixed chemical solution as stabilizer to prevent the particles from aggregation. The $La_{0.8}Tb_{0.2}F_3$ nanoparticle was synthesized following the same protocol as the former except that 3.2 mmol of $La(NO_3)_3 \cdot XH_2O$ and 0.8 mmol of $Tb(NO_3)_3 \cdot 5H_2O$ was used instead of 2.8 mmol of $La(NO_3)_3 \cdot XH_2O$ and 1.2 mmol of $Tb(NO_3)_3 \cdot 5H_2O$. The chemicals were mixed thoroughly by stirring for half an hour at room temperature; the mixture was subsequently heated to 100° C under vigorous magnetic stirring and nitrogen protection. A white suspension was formed gradually upon stirring. The nanoparticles obtained were collected by centrifugation, washed with DI water several times, and then re-dissolved in DI water.

$LaF_3:Yb^{3+}Tb^{3+}$ nanoparticles ($La_{0.4}Yb_{0.45}Tb_{0.15}F_3$) were synthesized as follows: 1.6 mmol of $La(NO_3)_3 \cdot XH_2O$, 0.6 mmol of $Tb(NO_3)_3 \cdot 5H_2O$, 1.8 mmol of $Yb(NO_3)_3 \cdot 5H_2O$ and 10.5 mmol of NH_4F in 10 ml of water solution were added to 90 ml of water in a three-necked flask, 1 ml of PEG was added dropwise to the mixed chemical solution as stabilizer to prevent the particles from aggregation. The chemicals were mixed thoroughly by stirring for half an hour at room temperature; the mixture was subsequently heated to 100° C under vigorous magnetic stirring

and nitrogen protection. A white suspension formed gradually upon stirring. The nanoparticles obtained were collected by centrifugation, washed with DI water several times, then re-dissolved in DI water.

$LaF_3:Ce^{3+}Tb^{3+}$ nanoparticles ($La_{0.4}Ce_{0.45}Tb_{0.15}F_3$) were prepared as follows: 1.6 mmol of $La(NO_3)_3{\cdot}XH_2O$, 0.6 mmol of $Tb(NO_3)_3 \cdot 5H_2O$, 1.8 mmol of $Ce(NO_3)_3 \cdot 6H_2O$ and 10.5 mmol of NH_4F in 10 ml water solution were added to 90 ml of water in a three-necked flask, 1 ml of PEG was added dropwise to the mixed chemical solution as stabilizer to prevent the particles from aggregation. The chemicals were mixed thoroughly by stirring for half an hour at room temperature; the mixture was subsequently heated to 100° C for 2 hours under vigorous magnetic stirring and nitrogen protection. A white cloudy solution formed homogeneously upon stirring. The nanoparticles were formed directly as water-soluble particles.

4.3.2 Characterization of Water-soluble $LaF_3:Ln^{3+}$ Nanoparticles

The fluorescence spectra of the samples were measured using a fluorescence spectrometer (RF-5301PC) with a 400W monochromatized xenon lamp and 3/3 slit widths. Figures 4.5 and 4.6 show the excitation and emission spectra of $La_{0.7}Tb_{0.3}F_3$ and $La_{0.8}Tb_{0.2}F_3$ nanoparticles. Both Figure 4.5 and Figure 4.6 show four sharp emission peaks, at 490 nm, 543 nm, 584 nm and 621 nm, although the intensity of emissions in Figure 4.5 is stronger than that in Figure 4.6. The emission peaks are generally assigned to $^5D_4 \rightarrow {}^7F_j$ (j=3-6) transitions of Tb^{3+}. We conclude that $La_{0.7}Tb_{0.3}F_3$ water-soluble nanoparticles have stronger luminescence than $La_{0.8}Tb_{0.2}F_3$ nanoparticles. Figures 4.7 and 4.8 show excitation and emission spectra of $La_{0.4}Yb_{0.45}Tb_{0.15}F_3$ and $La_{0.4}Ce_{0.45}Tb_{0.15}F_3$ water-soluble nanoparticles, respectively. The four emission peaks at 487, 540, 584 and 622 nm in both kinds of nanoparticles are corresponding to the strong and typical $^5D_4 \rightarrow {}^7F_J$ (J=3-6) transitions of doped Tb^{3+}. In LaF_3:CeTb nanoparticles, very weak emission peaks at 334 and 363 nm are likely originated from the doped Ce^{3+} (compared with figure 4.4) and self-trapped exciton emission from LaF_3 host,[73] the decreased Ce^{3+} emission under the same excitation wavelength as used to excite LaF_3:Ce nanoparticles

and enhanced Tb^{3+} (compared with other Tb^{3+} doped LaF_3) indicate an efficient energy transfer happening from Ce^{3+} (donor) to Tb^{3+} within the lattice host of LaF_3,[73,170] which is the direct reason that emission of $La_{0.4}Ce_{0.45}Tb_{0.15}F_3$ is significantly stronger than that of $La_{0.4}Yb_{0.45}Tb_{0.15}F_3$ since no energy transfer was observed in the case of $La_{0.4}Yb_{0.45}Tb_{0.15}F_3$.

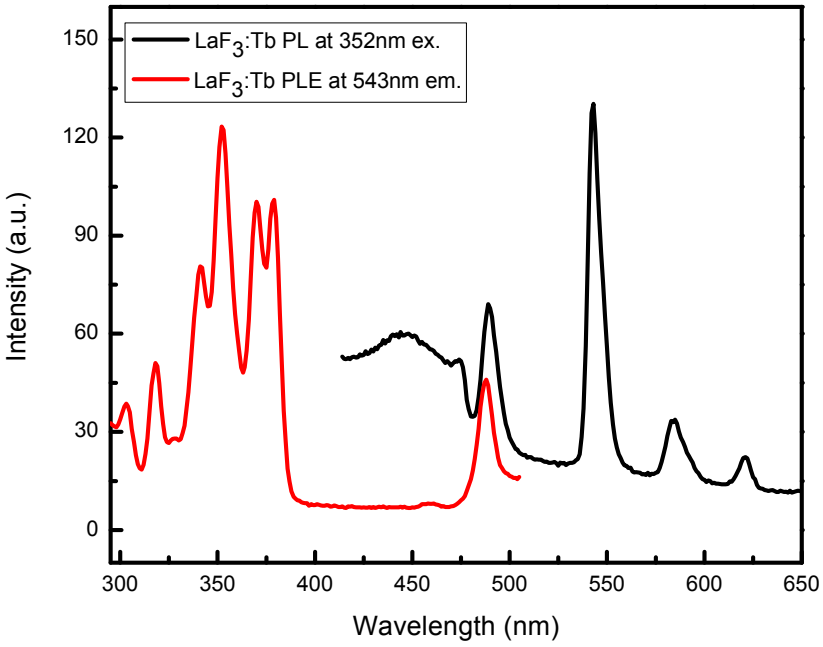

Figure 4.5 Excitation and emission spectra of LaF_3: Tb ($La_{0.7}Tb_{0.3}F_3$) nanoparticles

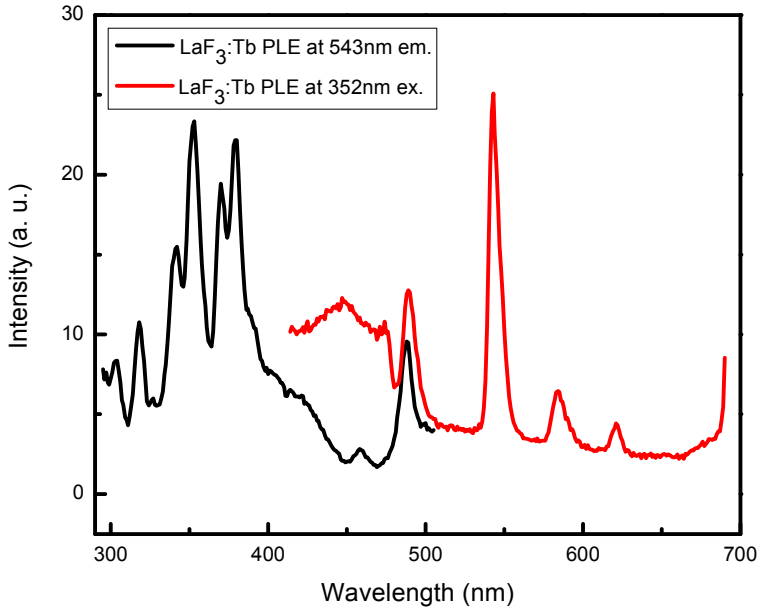

Figure 4.6 Excitation and emission spectra of LaF_3: Tb ($La_{0.8}Tb_{0.2}F_3$) nanoparticles

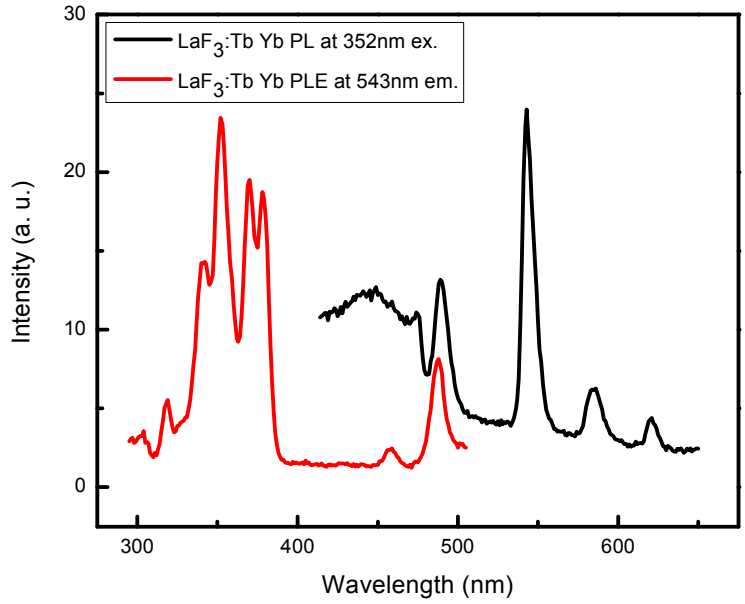

Figure 4.7 Excitation and emission spectra of LaF_3: TbYb ($La_{0.4}Yb_{0.45}Tb_{0.15}F_3$) nanoparticles

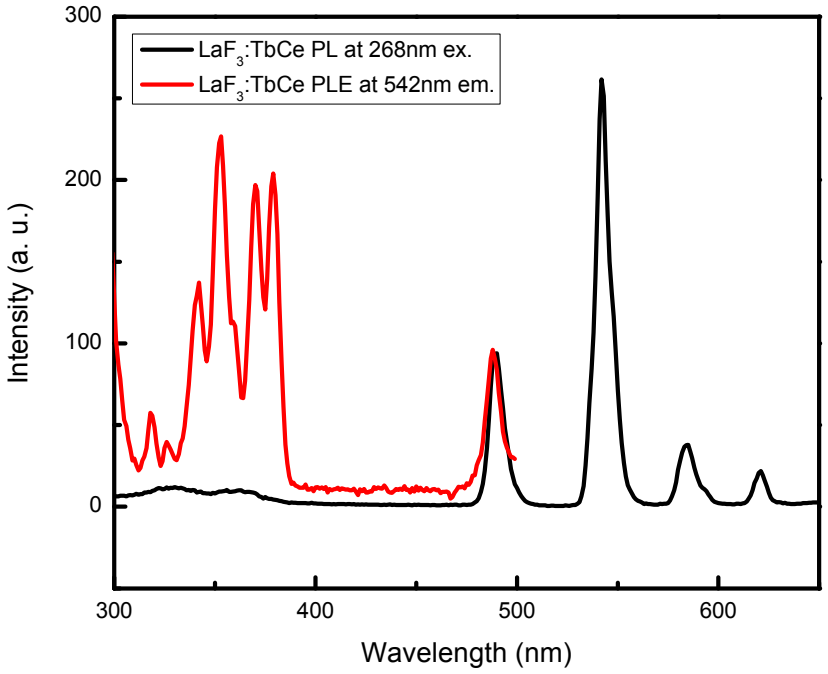

Figure 4.8 Excitation and emission spectra of LaF_3: CeTb nanoparticles

4.3.3 The application of $La_{0.4}Ce_{0.45}Tb_{0.15}F_3$ as fluorescence labeling

Among all the above water-soluble nanoparticles, we further studied the potential application of $La_{0.4}Ce_{0.45}Tb_{0.15}F_3$ (will be shortened as LaF_3:CeTb) in labeling because of its high fluorescence efficiency. The representative HRTEM image of LaF_3:Ce, Tb as shown in figure 4.9 indicates most of the particles are spherical with a diameter around 20 nm, and a few are nano-rods. The particles are highly crystalline as evidenced by the clear lattice fringes from [121] and [211] planes. From these fringes, the atomic plane distance was measured and found to be around 0.33 nm, which is very close to the plane distance of 0.32 nm reported by Yanes et al.[171]

Latent fingerprint residues were employed as a testing platform to assess the fluorescence labeling efficiency of LaF_3:CeTb nanoparticles to trace biomaterials deposited on

nonporous fingerprints on different substrates such as thin aluminum foil, micro glass slide and polymethylpentene plastic Petri Dish. After a certain reaction time, the nanoparticles were removed. After being rinsed with DI water, the surface was allowed to dry before imaging. The LaF_3:CeTb nanoparticles labeled fingerprint images as shown in figure 4.10 were captured by our collaborator Dr. Kwan H. Cheng at the Texas Tech University.[172] Bright dots showing in the images are representing sweat pores within friction ridges of fingermarks, which were clearly evidenced on aluminum and plastic surfaces. However, only labeled friction ridges were observed on glass surface. Overall, LaF_3:CeTb possesses excellent potential for trace biomaterials detections on a surface.

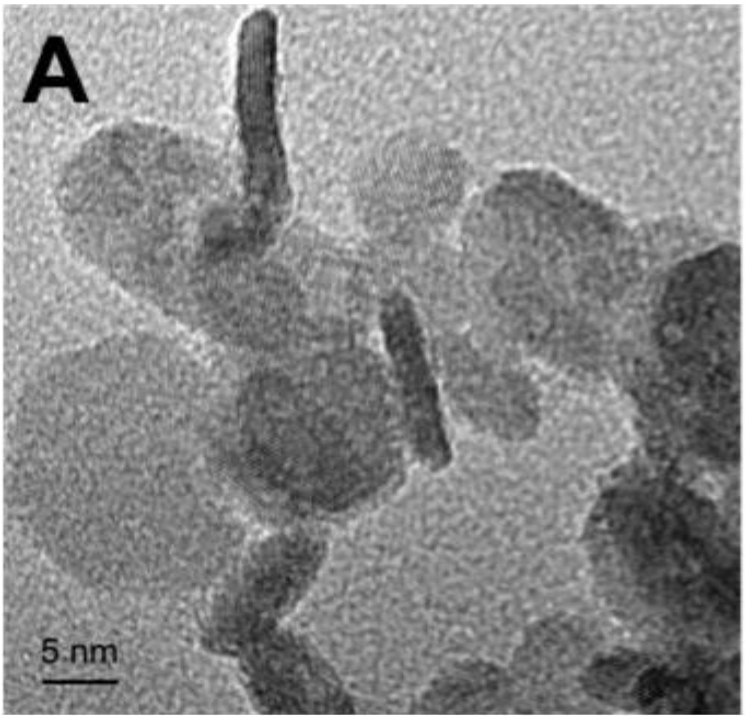

Figure 4.9 Representative HRTEM image of LaF_3:CeTb nanoparticles

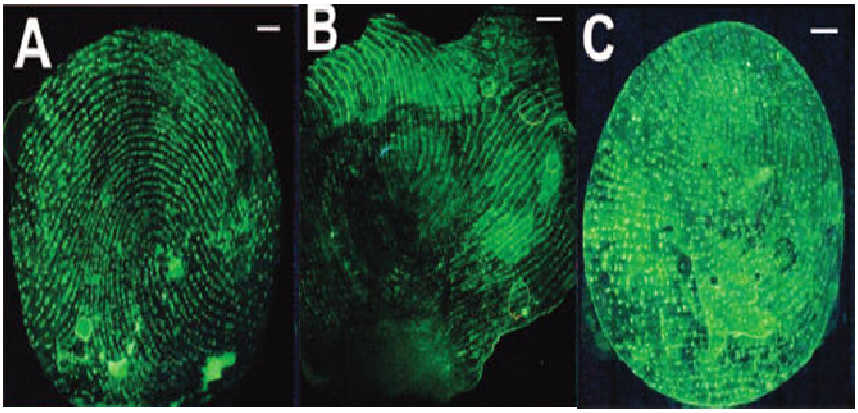

Figure 4.10 Representative fluorescence images of latent fingerprints labeled by LaF_3:CeTb on aluminum (A), glass (B) and polymethylpentene plastic (C) surfaces in the air-dried state and at room temperature.

4.4 Conclusion

We synthesized Ln^{3+} doped LaF_3 nanoparticles in water using the wet-chemistry method. The X-ray diffraction (XRD) pattern shows that LaF_3:Ce was synthesized. Transmission electron microscopy (TEM) clearly shows the nanocrystal's lattice fringes. Also, the average size of these nanoparticles is about 15 nm, which is consistent with the size obtained from XRD measurement. The nanoparticles have an emission peak at 343 nm, which was attributed to the 5d→4f transitions of the Ce ion. Intensity of emission decreases as reaction time is increased; the sample with a reaction time of 1 hr has the strongest emission. Water-soluble LaF_3 nanoparticles doped with Tb^{3+} and coped with other Ln^{3+} are synthesized with strong emissions at 490 nm, 543 nm, 584 nm and 621 nm. These emissions are attributed to $^5D_4 \rightarrow {}^7F_j$ (j=3-6) transitions of Tb^{3+}. The further fluorescence imaging shows LaF_3:CeTb nanoparticles could be targeted to trace biomaterials in fingerprints, which indicates LaF_3:CeTb nanoparticles could be potentially useful as labeling agents for ultrasensitive and time-gate imaging.

CHAPTER 5

LUMINESCENCE ENHANCEMENT OF CDTE NANOSTRUCTURES IN LAF_3:CE/CDTE NANOCOMPOSITES

5.1. Introduction

Luminescent nanoparticles have many potential applications including medical labeling, imaging, photodynamic activation and radiation detection.[108,173-175] For radiation detection, the sensitivity, response time and energy resolution are important.[176,177] To meet these requirements, a scintillator must have a high luminescence quantum efficiency, a short luminescence lifetime, high stopping power, as well as high carrier mobility-lifetime.[177] Ce^{3+} is a great activator exhibiting a very fast response in radiation detectors of medical imaging systems employed in diagnostic radiology.[178-181] Currently, Ce^{3+} doped scintillators meet most of the requirements and have become popular scintillators for radiation detection and dosimetry.[178-181] However, Ce^{3+} doped scintillators have their own shortcomings. For example, some Ce^{3+} doped scintillators such as $LaBr_3$:Ce^{3+} have very high quantum efficiency and energy resolution, but their hygroscopic property makes them impractical for many applications. In addition, most Ce^{3+} doped scintillators have emission within the ultraviolet (UV) range. This is an issue as UV light is often limited in detection systems and many materials are not transparent in the UV range. Quantum dots such as CdTe and CdSe have very high quantum efficiencies as a consequence of quantum size confinement.[182, 108,183] Indeed, quantum dots have very high luminescence quantum efficiency up to 98%[184] and short luminescence lifetimes in the nanosecond range.[185-187] Therefore, in principle, semiconductor quantum dots could be promising for the application of radiation detection because of their short lifetimes and high sensitivities. However, the stopping power of most II-VI quantum dots is low and their scintillation luminescence is very weak.[188] Nanocomposites composed of CdTe quantum dots and LaF_3:Ce^{3+} nanoparticles may overcome

the shortcomings of Ce^{3+} doped scintillators and semiconductor quantum dots, therefore, they can provide improved properties for radiation detection. This combination may solve these problems because Ce^{3+} doped scintillators have high stopping power and high scintillation efficiency. The possible energy transfer from Ce^{3+} doped scintillation nanoparticles to semiconductor quantum dots may be very high since the emission of Ce^{3+} ions and the absorption of the quantum dots can be adjusted to be largely overlapped by simply changing the size of the quantum dots. In this chapter, we report the synthesis and luminescence enhancement of CdTe nanostructures in LaF_3:Ce/CdTe nanocomposites, and explore their potential application as a new kind of phosphor for radiation detection and solid state lighting.

5.2. Experimental Details

CdTe/LaF_3:Ce nanocomposites were prepared by a wet-chemistry method in two steps. In the first step, CdTe quantum dots coated with thioglycolic acid (TGA) surfactant were synthesized. In the second step, LaF_3:Ce nanopartilces were attached to CdTe quantum dots to form LaF_3:Ce/CdTe nanocomposites. To synthesize CdTe quantum dots, Cd^{2+}-containing solution was prepared by dissolving 0.7311 g of $Cd(ClO_4)_2 \cdot 6H_2O$ in 125 ml of water. Then, TGA (0.396 mole) was added to the solution and the pH value adjusted to ~11 by the addition of 0.1M NaOH. The solution was then purged with nitrogen for at least 30 min. H_2Te gas was generated by the chemical reaction of excess aluminum telluride with 0.5M sulfuric acid in an inert atmosphere (nitrogen) and was combined with the above solution containing Cd^{2+} ions using the setup as described.[189] After the completion of the reaction a yellow solution of CdTe nanocrystal nuclei was obtained. This solution was then refluxed at 100 °C to promote crystal growth with the particle size controlled by the reaction time.

To form LaF_3:Ce/CdTe nanocomposites, 6.3 mmol of $La(NO_3)_3 \cdot 6H_2O$ and 0.7 mmol of $Ce(NO_3)_3 \cdot 6H_2O$ were first dissolved in 15 ml of deionized water and then mixed with 10 ml of the CdTe nanoparticle solution prepared in step-1, 1 ml diethylene glycol (DEG) was added to the mixture solution as a surfactant. $Ce(NO_3)_3$ was used to provide the Ce^{3+} dopant with doping

concentration of 0.1M. The chemicals were mixed thoroughly, and then 20.1 mmol of NH_4F water solution with a volume of 5 ml was added drop wise to the mixture solution under stirring at room temperature. The reaction solution was stirred at room temperature for 0.5 hours and subsequently was heated to 50 °C for different reaction times up to 3.5 hours under protection of nitrogen. The product was centrifuged, washed with de-ionized water three times and dried at 40 °C in a vacuum atmosphere. Similarly, LaF_3/CdTe nanocomposites (undoped with Ce^{3+}) were prepared and their structures as well as luminescence properties were investigated for comparison with those of the LaF_3:Ce/CdTe nanocomposites.

The identity, crystalline structure, size and shape of the nanoparticles were observed by X-ray diffraction and high-resolution transmission electron microscopy (HRTEM). The X-ray powder diffraction (XRD) patterns of LaF_3:Ce/CdTe nanocomposites were recorded in the range of $20° \leq 2\theta \leq 80°$ using a Siemens Kristalloflex 810 D-500 X-ray diffractometer operating at 40 kV and 30 mA with a radiation beam of λ=1.5406 Angstrom. The nanocomposites in solution were brought onto holey carbon covered copper grids for HRTEM observations. The HRTEM images of the particles were obtained with a JEOL JEM-2100 electron microscope with accelerating voltage of 200 kV. The excitation and emission spectra were measured using a Shimadzu RF-5301PC fluorescence spectrophotometer. Luminescence lifetimes were collected using the frequency-doubled output of a synchronously-pumped psec dye laser operating at 610 nm. The doubled output was focused onto the samples and emission collected at right angle to the input. The emission was spectrally filtered and the lifetime measured using time-correlated single photon counting. The instrument resolution was determined to be about 50 picoseconds FWHM using a standard scattering material.

5.3. Results and Discussion

5.3.1 XRD

Figure 5.1 shows the XRD patterns of LaF_3:Ce/CdTe and LaF_3:Ce. The results of the XRD are in good agreement with the trigonal tysonite LaF_3 structure as described in the reports[188,189] and from bulk LaF_3 and CeF_3 crystals (JCPDS Card 32-0483 and 08-0045). No XRD signals were observed for CdTe in LaF_3:Ce/CdTe nanocomposites which is most likely due to its low concentration. The particle size can be estimated from the Scherrer equation, $D = 0.90\lambda/\beta\cos\theta$, where D is the average crystallite size, λ is the X-ray wavelength (0.15405 nm), and ɵ and β are the diffraction angle and full-width at half maximum (FWHM) of an observed peak, respectively. The strongest peak (111) at $2\theta = 27.8°$ was used to calculate the average crystallite size (D) of the nanoparticles, [188,189] which produces an estimation on particle size to be about 15 nm. No XRD signals were observed for impurity phases indicating that Ce^{3+} is likely doped into the LaF_3 crystal lattice. The ionic radius of Ce^{3+} (1.034 Å) is very close to that of La^{3+} (1.061 Å), therefore, Ce^{3+} can easily substitute the occupation of La^{3+} ions in LaF_3 crystal lattices.

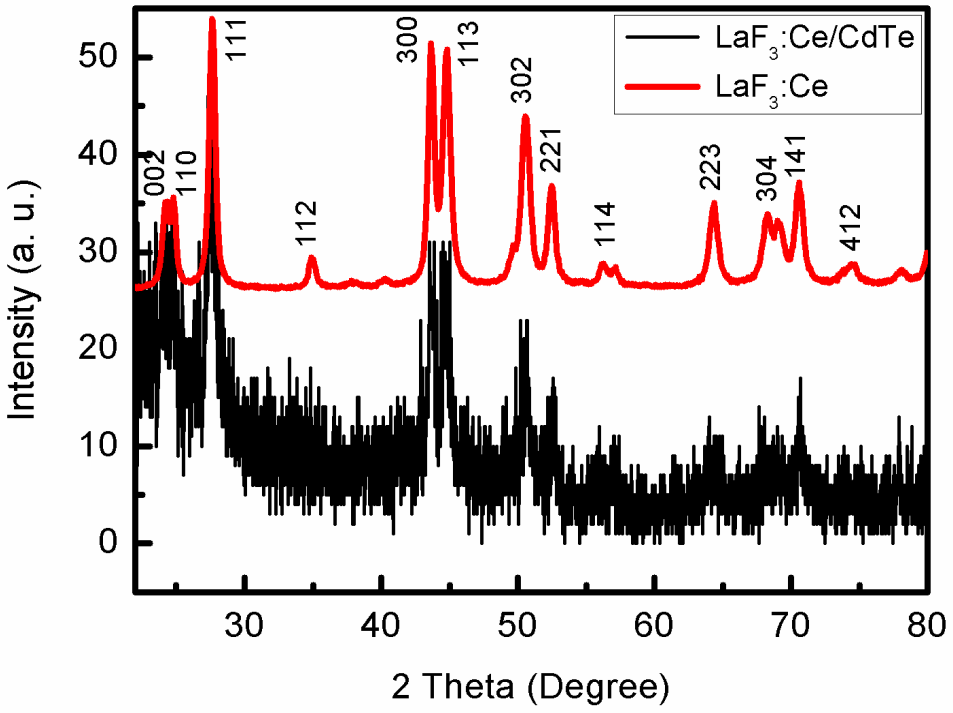

Figure 5.1 XRD patterns of LaF_3:Ce/CdTe composites (black, lower) and LaF_3:Ce (red, upper).

5.3.2 TEM

Figure 5.2 displays the HRTEM images of LaF_3:Ce/CdTe nanocomposites. Oval shaped nanostructures are observed with an average dimension of about 22 nm long and 10 nm wide, which is consistent with the XRD results. In the nanocomposites, there are two kinds of nanostructures in the HRTEM images, nanowires and nanoparticles. The spacing between adjacent lattice planes is about 0.39 nm shown in figure 5.2, which corresponds to the (110) plane of the wurtzite CdTe lattice. In the nanoparticles, the interplanar spacing is about 0.36 nm which is corresponding to the interplanar spacing of (0001) planes in the hexagonal LaF_3 structure.[190] The HRTEM observations demonstrate that CdTe and LaF_3:Ce nanostructures are in close proximity in the composites. During the synthesis, CdTe quantum dots have been

converted to nanowires shown in figure 5.2 (b) from oval-shaped nanocomposites shown in figure 5.2 (a).

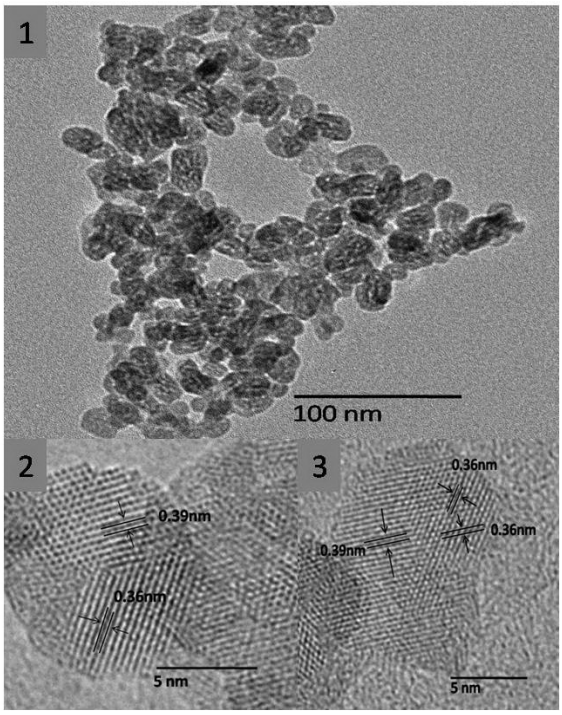

(a)

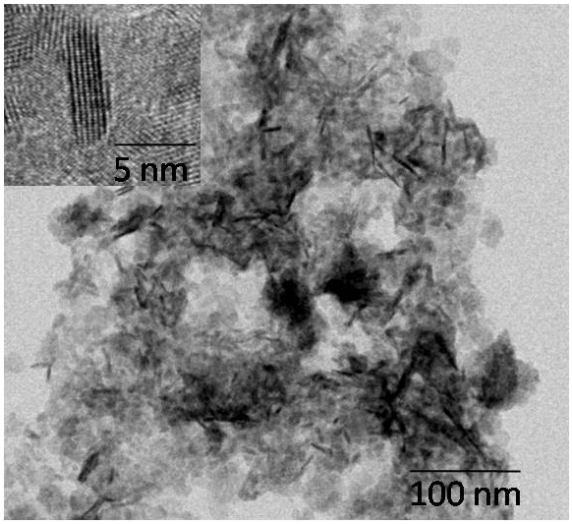

(b)

Figure 5.2 HRTEM images of LaF_3:Ce/CdTe nanocompotistes heated for (a) 1 hr and (b) 3.5 hrs

5.3.3 Optical Properties

Figure 5.3 displays the optical absorption spectra of LaF_3:Ce nanoparticles, CdTe quantum dots, and LaF_3:Ce/CdTe nanocomposites. In the measurement, the concentration of CdTe quantum dots is kept constant between the CdTe quantum dots and LaF_3:Ce/CdTe nanocomposites samples. Similarly, the concentration of LaF_3:Ce nanoparticles is the same in LaF_3:Ce and LaF_3:Ce/CdTe nanocomposites samples. The absorption spectrum of CdTe quantum dots is similar to those reported in literatures.[141,185] The absorption spectrum of LaF_3:Ce is similar to that of the LaF_3:Ce/CdTe nanocomposites with the main absorption band attributed to the LaF_3:Ce nanoparticles. The absorption from CdTe quantum dots is very weak and barely observed. This may be due to the conversion of the quantum dots to nanowires as observed by TEM as shown in figure 5.2 (b). The change of three dimensionally quantified quantum dots to two dimensionally quantified nanowires reduces the nanostructure absorption coefficient.[183] Figure 5.4 shows emission spectra of LaF_3:Ce nanoparticles, CdTe quantum dots, and LaF_3:Ce/CdTe nanocomposites. The CdTe quantum dots have a green emission at 547 nm. The emission peak at around 342 nm in LaF_3:Ce is attributed to the 5d→4f transition of Ce^{3+} from the lowest 5d excited state to the spin-orbit split ground f state.[133,134] Two emissions peaking at 368 and 541 nm are observed from LaF_3:Ce/CdTe nanocomposites, they are attributed to the LaF_3:Ce nanoparticles and CdTe quantum dots, respectively. Compared with the emissions in pure CdTe quantum dots and LaF_3:Ce nanoparticles, in LaF_3:Ce/CdTe nanocomposites, the emission originated from CdTe quantum dots shifts to shorter wavelength and the emission from Ce^{3+} shifts to longer wavelength. As compared to pure CdTe quantum dots and LaF_3:Ce nanoparticles, the emission from LaF_3:Ce nanoparticles decreases in intensity while the emission from CdTe quantum dots increases in intensity in the nanocomposites. The excitation wavelength is 265 nm for the luminescence measurement in Figure 5.4, and the absorbance at 265 nm is almost identical for both LaF_3:Ce and LaF_3:Ce/CdTe samples. This

indicates that the luminescence quantum efficiency of CdTe in LaF_3:Ce/CdTe nanocomposites is much higher than in pure CdTe nanoparticles.

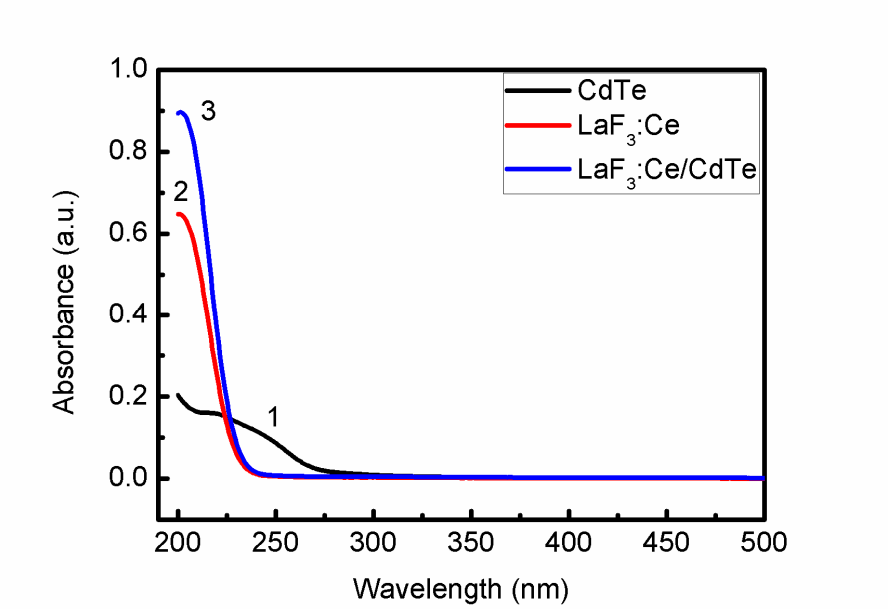

Figure 5.3 Optical absorption spectra of (1) CdTe quantum dots, (2) LaF_3:Ce nanoparticles, and (3) LaF_3:Ce/CdTe nanocomposites

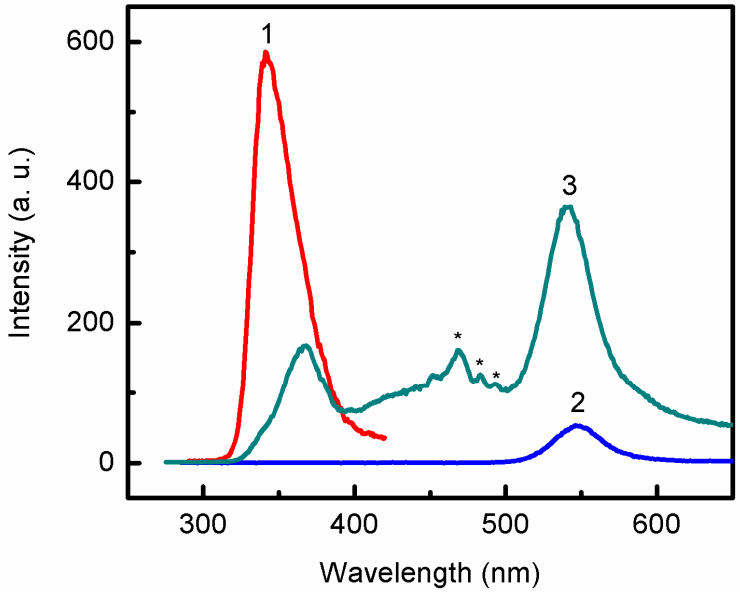

Figure 5.4 Emission spectra following excitation at 265 nm of (1) LaF_3:Ce nanoparticles, (2) CdTe quantum dots, and (3) LaF_3:Ce/CdTe nanocomposites. The peaks labeled with * are due to the xenon lamp used for excitation.

Figure 5.5 shows LaF_3:Ce/CdTe nanocomposite emission spectra prepared at room temperature and followed by heating at 50 °C for 1, 2.5 and 3.5 hours, respectively. As the annealing time increases, the LaF_3:Ce nanoparticle emission decreases but the CdTe quantum dot emission increases gradually. We note that the CdTe quantum dot emission shifts to longer wavelengths at longer reaction time while the Ce^{3+} emission in LaF_3:Ce nanoparticles remains at the same position. This emission color change is visible to even the naked eyes as shown in Figure 5.6. It is clearly observed that the nanocomposites are significantly brighter than the quantum dots. As observed by TEM, CdTe nanoparticles are converted to nanowires during the heating process during the formation of the nanocomposites. The mechanism of the conversion from quantum dots to nanowires is not yet clear, but it is likely that the red shift in emission wavelength is due to the formation of nanowires as previously reported in the literature.[191] As the heating time increases, more and more nanowires are formed. This is perhaps also the reason of the increase in CdTe emission with increasing reaction time.

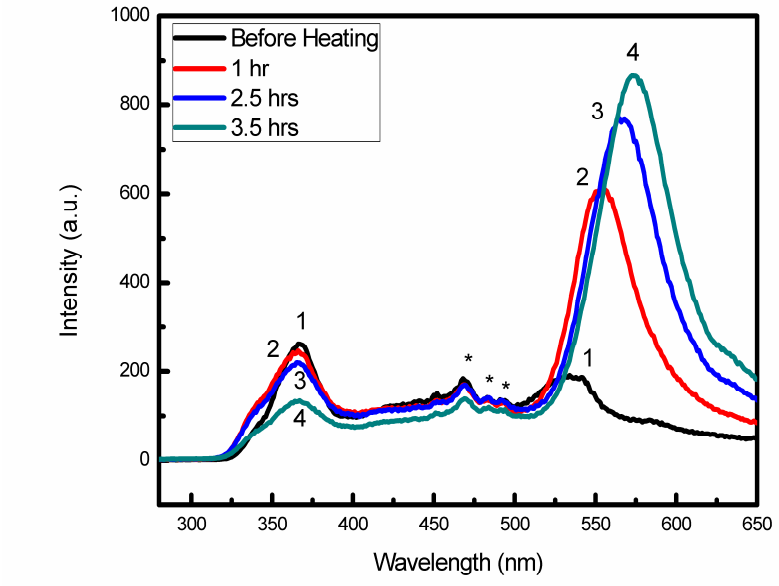

Figure 5.5 Emission spectra of LaF_3:Ce/CdTe nanocomposites prepared at room temperature and annealing at 50 oC for 1, 2.5 and 3.5 hours respectively. The excitation wavelength is at 265 nm. The peaks labeled with * are artifacts from the instrumentation.

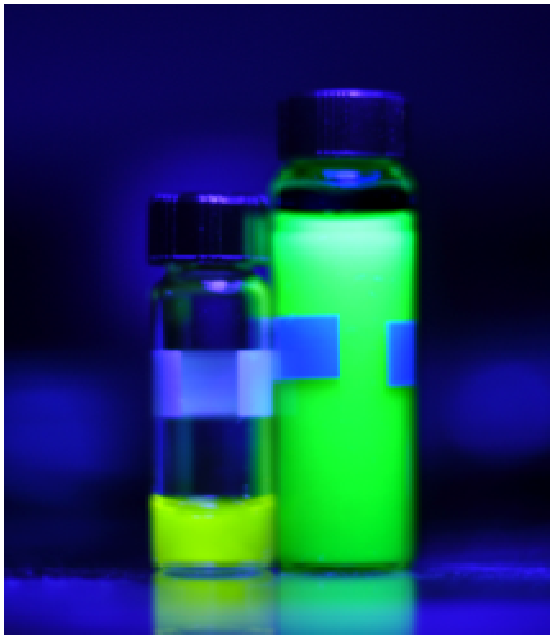

Figure 5.6 Photograph of CdTe quantum dot (left) and LaF_3:Ce/CdTe nanocomposite (right) aqueous solutions under a UV lamp.

5.3.4 Lifetime Measurement

One possible mechanism for the CdTe luminescence enhancement in LaF_3:Ce/CdTe nanocomposites is considered as energy transfer from LaF_3:Ce nanoparticles to CdTe nanowires. The decrease of the Ce^{3+} emission along with the increase of CdTe emission in intensity is a good indication that energy transfer from Ce^{3+} to CdTe may take place in the nanocomposites. To reveal if there is energy transfer between them, the Ce^{3+} luminescence lifetimes in LaF_3:Ce and LaF_3:Ce/CdTe as well as the CdTe lifetime in LaF_3:Ce/CdTe were measured as shown in Figure 5.7, the data were collected in table 1. For the fast component, the lifetime of Ce decreases from 3.2 ns in LaF_3:Ce to 1.5 ns in LaF_3:Ce/CdTe, and for the slow component, the lifetime of Ce decreases from 24.5 ns in LaF_3:Ce to 12.5 ns in LaF_3:Ce/CdTe (Table 1). The reduction of the Ce^{3+} lifetime is consistent with energy transfer from Ce^{3+} to CdTe which would lead to an observed luminescence enhancement in LaF_3:Ce/CdTe composites.

According to the Förster resonance energy transfer (FRET) theory, FRET efficiency is related to the quantum yield and the fluorescence lifetime of the donor molecule as following:

$$E = 1 - \tau'_{\mathrm{D}}/\tau_{\mathrm{D}}$$

where $\Gamma_D^{'}$ and Γ_D are donor fluorescence lifetimes in the presence and absence of an acceptor, respectively. Based on this formula, the energy transfer efficiency from LaF_3:Ce to CdTe were calculated as 53% for the fast component and 49% for the slow component, respectively. However, energy transfer may also change the lifetime of the acceptor if the lifetimes of the donor and acceptor are different. For example, if the donor lifetime is significantly longer than the acceptor lifetime, in the energy transfer system, the lifetime of the acceptor should be the same or similar to that of the donor as found in BaFBr:Eu^{2+}/CdTe nanocomposites.[188] Here in the LaF_3:Ce/CdTe nanocomposites, it is noted that the CdTe nanowire lifetime is almost the same as in pure CdTe quantum dots[185] and is about a factor of two shorter than the donor (Ce^{3+}) lifetime. This cannot exclude that energy transfer from Ce^{3+} to CdTe in LaF_3:Ce/CdTe nanocomposites but indicates that the energy transfer rate is not high and energy transfer is not the only reason for the enhancement. In addition, as the Ce^{3+} emission peak effectively overlaps the CdTe nanowires absorption, emitted light from Ce^{3+} can be reabsorbed by the CdTe nanowires in the nanocomposites. This could also be another factor responsible for the luminescence enhancement.

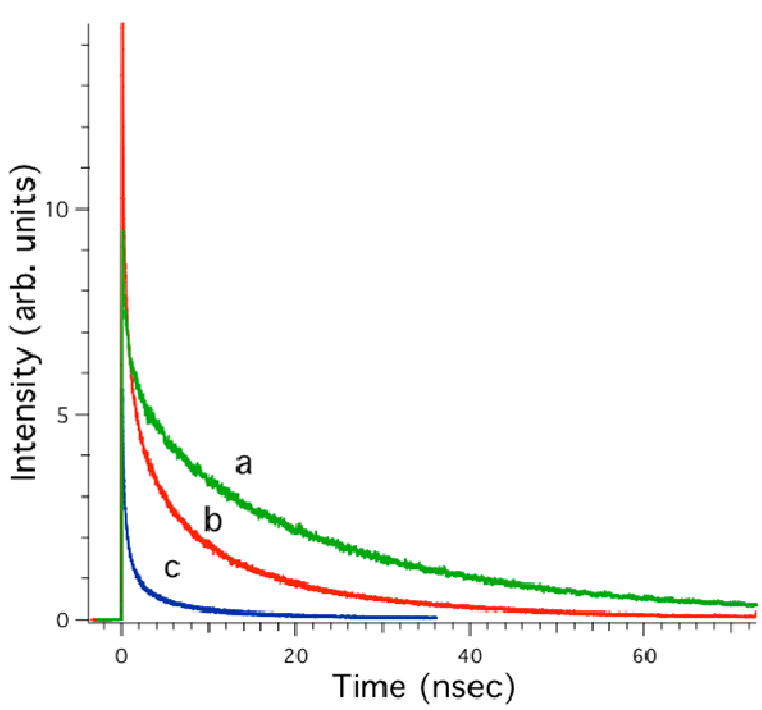

Figure 5.7 Lifetime measurements following 285 nm excitation of (a) LaF_3:Ce nanoparticles (emission 350 nm); (b) LaF_3:Ce/CdTe nanocomposites (375 nm emission); and (c) LaF_3:Ce/CdTe nanocomposites (emission 520 nm).

Table 5.1 Lifetime comparisons of LaF_3:Ce with LaF_3:Ce/CdTe

Sample	Excitation/ emission	Lifetime T1	Lifetime T2	curve
LaF_3:Ce	285 nm/350 nm	3.2 ns	24.5 ns	a (Ce^{3+})
LaF_3:Ce/CdTe	285 nm/375 nm	1.5 ns	12.5 ns	b (Ce^{3+})
	285 nm/520 nm	0.6 ns	5.2 ns	c (CdTe)

5.3.5 Possible Mechanism for Luminescence Enhancement

Energy transfer is one possibility for the luminescence enhancement observed. In addition to energy transfer, there might be other factors such as surface modification by annealing that increases the CdTe luminescence efficiency. LaF_3 coating and the configuration conversion from quantum dots to nanowires could also have an effect. To determine whether annealing is responsible for the enhancement, pure CdTe quantum dots were annealed at 50 ˚C for 1, 2 and 3.5 hours under the same conditions as for LaF_3:Ce/CdTe nanocomposites. The

results indicate that the CdTe quantum dot emission increases about 5% in intensity for 1 hour annealing, and then decreases in intensity with 2.5 and 3.5 hour annealing. Therefore, enhancement by annealing could be excluded. To determine if coupling with pure LaF_3 nanoparticles is the reason for the luminescence enhancement, LaF_3 nanoparticles and LaF_3/CdTe nanocomposites were prepared for comparison with both LaF_3:Ce nanoparticles and LaF_3:Ce/CdTe nanocomposites. Surprisingly, Ce^{3+} emission was detected in pure LaF_3 nanoparticles but its intensity is nine times weaker than in LaF_3:Ce nanoparticles (Figure 5.8). The Ce^{3+} emission is likely due to Ce^{3+} contamination in the $La(NO_3)_3$ precursor. In the LaF_3/CdTe nanocomposites, the emissions of Ce^{3+} and CdTe quantum dots are five times weaker than those in LaF_3:Ce/CdTe nanocomposites (Figure 5.9). After annealing at 50 °C for 1 hour, the Ce^{3+} emission in LaF_3/CdTe nanocomposites increased slightly but the CdTe emission was almost the same. After annealing for 2 hours, both the Ce^{3+} and CdTe quantum dot emissions are quenched in intensity (Figure 5.10). These observations exclude the contributions of annealing as well as LaF_3 coating to the CdTe luminescence enhancement in the LaF_3:Ce/CdTe nanocomposites.

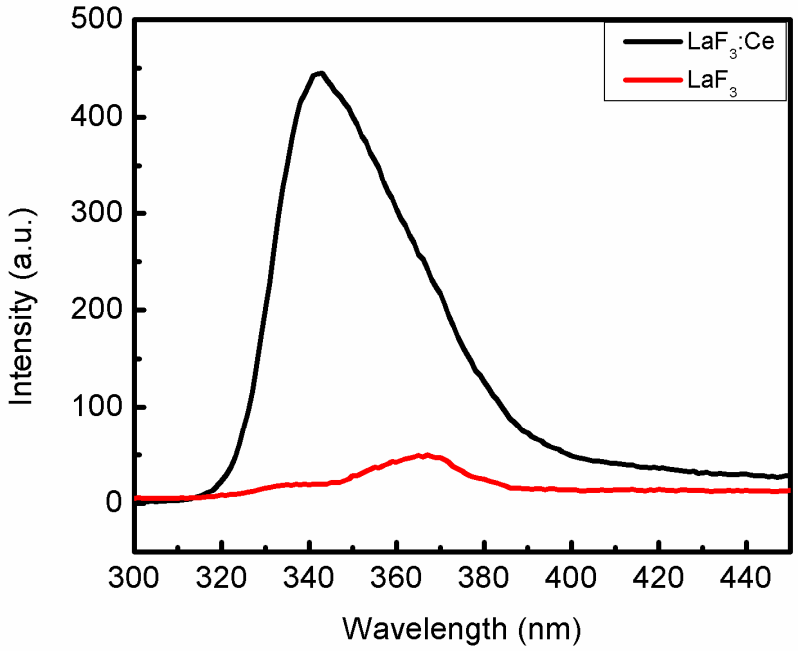

Figure 5.8 Emission spectra of LaF_3:Ce and LaF_3 excited at 265 nm.

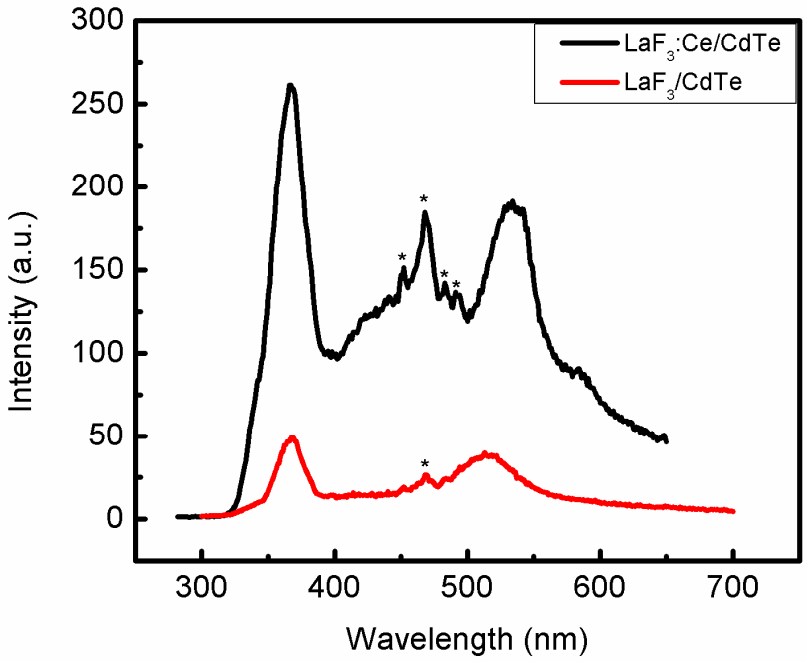

Figure 5.9 Emission spectra of LaF_3:Ce/CdTe and LaF_3/CdTe nanocomposites. The peaks labeled with * are artifacts from the instrumentation.

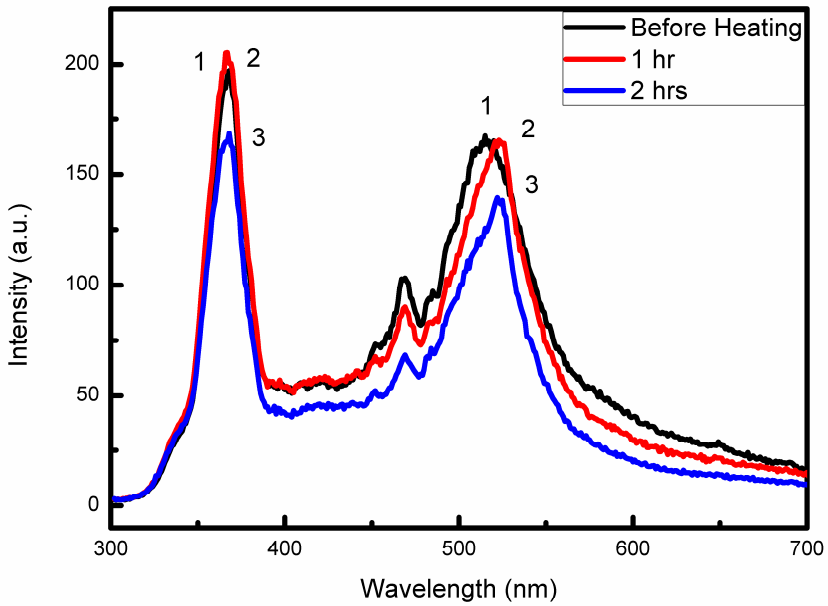

Figure 5.10 Emission spectra of LaF_3/CdTe (1- before heating; 2- heating for 1 hr; 3-heating for 2 hrs). The peaks labeled with * are artifacts from the instrumentation.

The HRTEM images of LaF_3/CdTe nanocomposites with no Ce^{3+} doping annealed for 3.5 hrs are shown in Figure 5.11. By comparing the TEM results between LaF_3:Ce/CdTe (Figure 5.2b) and LaF_3/CdTe (figure 5.11), it is noted that in LaF_3:Ce/CdTe, the CdTe quantum dots are converted to nanowires, while this conversion does not occur in LaF_3/CdTe nanocomposites. The CdTe lifetime in LaF_3/CdTe nanocomposites before heating and after heating for one hour are shown in Figure 5.12. The two samples show very similar emission spectra and lifetimes. This also indicates there is no conversion of the quantum dots into nanowires in LaF_3/CdTe nanocomposites. The conversion of CdTe quantum dots to nanowires is most likely the reason for the red shift of the CdTe emission observed in LaF_3:Ce/CdTe since the increase of the dimensionality results in narrowing energy gap.[191-194] However, the conversion of general quantum dots to nanowires does not cause luminescence enhancement because the increase of the dimensionality reduces luminescence yield.[191-195] It is interesting that the luminescence

enhancement of quantum dots CdTe in LaF_3:Ce/CdTe nanocomposites seems correlated with the formation of nanowires. Rare earth ions such as Ce^{3+} can have unique properties and have been used as catalysts for crystal growth.[196-198] It has been reported that several rare-earth elements, including Y, Ce, Tb, La, Ho, Gd, and Pr, together with Ni form bimetallic catalysts during carbon nanotube synthesis. The addition of rare-earth elements can improve the nanotube yield and as a result affects the structure of the material.[197] In our experiments, we observe that when Ce^{3+} ions are added to the nanoparticle synthesis, the nanoparticle solubility and luminescence efficiency are enhanced. There is a possibility that Ce^{3+} ions catalyze CdTe nanowire formation and also passivate defect sites. This would result in both luminescence enhancement and formation of nanowire.

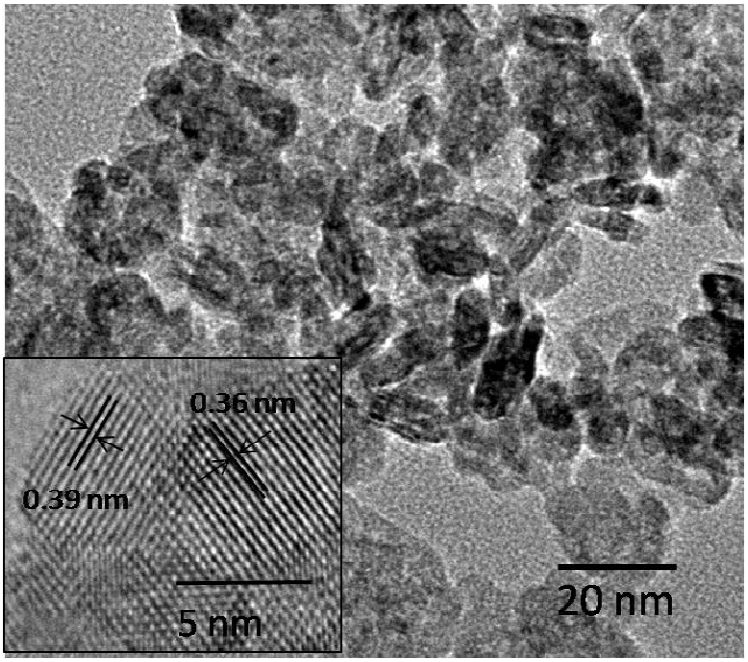

Figure 5.11 HRTEM images of LaF_3/CdTe nanocomposites annealed for 3.5 hrs. TEM observations show that CdTe quantum dots were not converted to nanowires during the synthesis of LaF_3/CdTe nanocomposites.

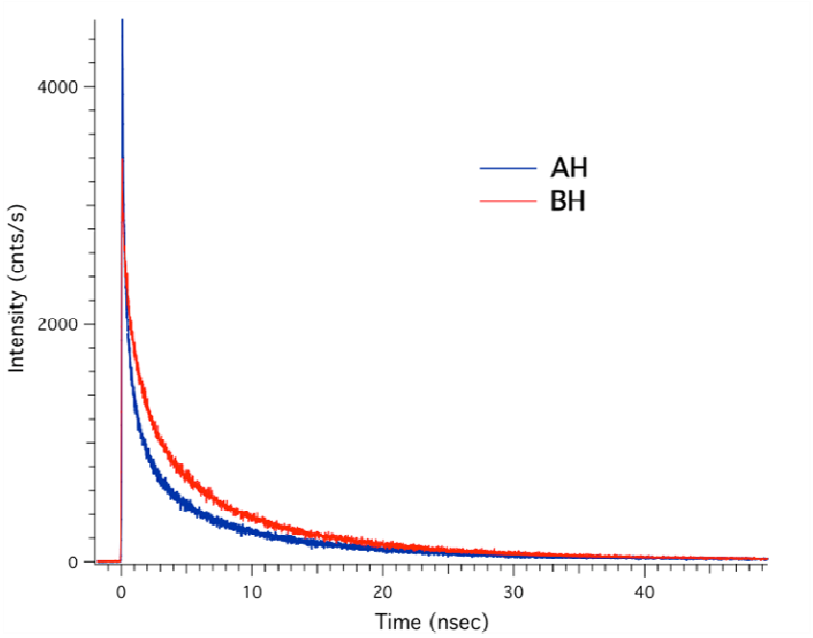

Figure 5.12 Luminescence lifetimes of LaF_3:CdTe samples excited at 280 nm before (BH, upper) and after (AH, lower) heating.

5.4. Conclusion

In summary, LaF_3:Ce/CdTe nanocomposites were successfully synthesized using a two-step wet chemistry method. CdTe quantum dots were converted into nanowires during the synthesis of LaF_3:Ce/CdTe nanocomposites, while in LaF_3/CdTe nanocomposites no such conversion was observed. As a result, The luminescence of CdTe in LaF_3:Ce/CdTe nanocomposites is about five times stronger than pure CdTe quantum dots while no enhancement was observed from undoped LaF_3/CdTe nanocomposites. Energy transfer, light-re-absorption and defect passivation are considered as possible reasons for the luminescence enhancement. The LaF_3:Ce/CdTe nanocomposites with enhanced luminescence may find their applications in radiation detection and solid state lighting.

CHAPTER 6

SYNTHESIS AND CHARACTERIZATION OF LAF_3:CE DOPED ORMOSIL

6.1. Introduction

In the past two decades, research on sol-gel science has been concentrated primarily on inorganic oxides. Generally, the sol-gel process consists of hydrolysis and condensation reactions, in which alkoxysilanes are mixed with a low molecular mass, such as tetramethoxysilance (TMOS) or tetraethoxysilane (TEOS), with water in a mutual solvent like methanol or ethanol.[94,199-201] Doping of silica xergels by nano sized particles[202-207] has trigged the interest of scientist since the sol-gel method starts from a homogeneous solution, which gives a better control over distribution and property of the nanoparticles embedded silica matrix. However, Silica xerogels produced by conventional sol-gel process are generally brittle and stiff since capillary pressure collapses the nano-porous structure to a dense structure during normal drying.[208] Organically modified silicates (ORMOSIL) have been considered as a better solid matrix due to their flexibility, permeability and porosity by incorporating organics into gel-derived silica.[94,209,210] ORMOSIL bulk and powder materials as incorporated with nanoparticles have been found to be good phosphors with high relative emission intensity.[211-213] As a great activator in exhibiting a very fast response in radiation detectors of medical imaging systems employed in diagnostic radiology, Ce^{3+} doped nanoparticles has been found a great deal of applications in radiation detection and dosimetry.[214-217] The synthesis and photoluminescence of LaF_3:Ce,Tb and LaF_3:Tb nanoparticles have been reported by several groups.[75,76] In this chapter, we investigate the physical and luminescence properties of LaF_3:Ce doped ORMOSIL, as well as the potential applications of the material in radiation detection.

6.2. Experimental Section

Lanthanum (III) nitrate hydrate ($La(NO_3)_3 \cdot X\ H_2O$, 99.9%), Cerium (III) nitrate hexahydrate ($Ce(NO_3)_3 \cdot 6\ H_2O$,99.9%), ammonium fluoride (NH_4F, 99.9%), poly(ethylene glycol) bis(carboxymethyl), ethanol, tetramethylorthorilicate (TMOS), 3-aminopropyltriethoxysilane, and nitric acid (HNO_3) were all purchased from Sigma Aldrich and used as received, without further purification.

6.2.1 Synthesis of Water and Ethanol Soluble LaF_3:Ce

Firstly, LaF_3:Ce nanoparticles were synthesized in two different formations: water-soluble and ethanol-soluble nanoparticles. To form LaF_3:Ce water-soluble solution, 3.52 mmol of $La(NO_3)_3$ and 0.88 mmol of $Ce(NO_3)_3.6H_2O$ were first dissolved in 15 ml of de-ionized water, $Ce(NO_3)_3$ was used as a doping material providing Ce^{3+} to form LaF_3:Ce. 1 ml polyethyleneglycol (PEG) was added to the above solution as a stabilizer. After the chemicals were mixed and dissolved in water thoroughly, 14 mmol of NH_4F water solution with a volume of 5 ml was added drop wise to the mixture solution under stirring at room temperature. The reaction solution was stirred at room temperature for 0.5 hours and subsequently heated to 50˚C for 2 hours under the protection of nitrogen. The product was centrifuged, washed with de-ionized water for three times and dried at 40˚C in a vacuum atmosphere and re-dispersed into 20 ml de-ionized water. Similarly, ethanol-soluble LaF_3:Ce nanoparticle solution was synthesized by following the above procedure except using ethanol as solvent in each steps instead of water. Due to the solubility difference of LaF_3:Ce nanoparticles in water and ethanol, the concentrations of solutions are 0.22 M for water-soluble nanoparticles and 0.16 M for ethanol-soluble nanoparticles.

6.2.2 Synthesis of Amine Modified ORMOSIL

The synthesis of ORMOSIL was based on sol-gel process. Sol–gel process is a method of-material preparation by room temperature reaction of organic precursor. The particles in the colloidal sol are linked to form a gel, which is subsequently dried to form a porous material. The

hydrolysis and polycondensation associated with sol–gel process are reactions of metal-organic compounds, such as silicon alkoxide (tetramethyl orthosilicate – TMOS or tetraethyl orthosilicate – TEOS) mixed with water, catalyst (acid or base) and a solvent (such as methanol or ethanol) to achieve homogeneity of the material. In the case of inorganic–organic hybrid system of ORMOSILs, the silicate network may be modified by organic substitute groups, such as alkyl (*e.g.*, methyl or ethyl) groups or other functional groups (*e.g.*, 3-glycidoxypropyl or 3-isocyanatopropyl) which may form organic copolymers by crosslinking process. In our experiments, we used amine-functionalized 3-aminopropyltriethoxylsilane (APTES) combined with tetramethylorthosilicate (TEOS) to produce ormosils with surface modification of amines. Typically, two solutions were prepared separately, one is the mixture of 11 ml of TMOS, 2 ml of de-iodized water, 25 ml of Ethanol and 0.155 ml of HNO_3 (solution 1), another one is the mixture of 2 ml of APTES and 10 ml of ethanol (solution 2). De-iodized water was used to promote hydrolysis process and HNO_3 was used as a catalyst.

The detailed procedures for synthesizing ORMOSIL are as follows: firstly solution 1 was thoroughly stirred in a beaker for 30 minutes to initialize the hydrolysis process, then solution 2 was added and mixed rapidly, the resulting sol was consequently casted into molds made of 5 ml volume polyethylene syringes, open ends of the molds were covered by three layers of Parafilm. Gelation takes place about 3 seconds to 5 minutes after these steps, varying with different doping materials. After 5 hours of aging, samples removed from molds were becoming wet gels. To obtain the dry gel, we used a convenient and simple way by punching 1 small pinhole in the covered parafilm every two days for slowing down the drying process to prevent the gel from cracking. The drying process usually takes 15 days by this way.

6.2.3 Synthesis of LaF_3:Ce Doped ORMOSIL

To dope LaF_3:Ce nanoparticles into ORMOSIL, we used two different sources of nanoparticles: water-soluble LaF_3:Ce and ethanol-soluble LaF_3:Ce. The first set of samples were using LaF_3:Ce water-soluble nanoparticles substitute the corresponding same amount of

de-iodized water of solution 1 in the process of synthesis of ORMOSILS, from which four LaF_3:Ce doped ORMOSILs were synthesized with different doping concentrations of 0.001964 M, 0.0039 M, 0.0059 M and 0.0078 M. The second set of samples were using LaF_3:Ce ethanol-soluble nanoparticles as doping source, similarly, portion of ethanol of solution 1 in ORMOSIL synthesis was substituted by ethanol-soluble LaF_3:Ce nanoparticles solution. Accordingly, another set of four LaF_3:Ce doped ORMOSILs were synthesized with different doping concentrations of 0.0145 M, 0.029M, 0.0435M and 0.058M.

6.3. Characterization of Nanoparticle Doped ORMOSIL

The X-ray powder diffraction (XRD) patterns of LaF_3:Ce^{3+} nanoparticles were recorded in the range of $20^\circ \leq 2\theta \leq 80^\circ$ from a Siemens Kristalloflex 810 D-500 X-ray diffractometer under an operating mode of 40 kV and 30 mA with λ=1.5406 Angstrom radiation. Scanning Electron Microscope (SEM) image was taken with a scanning electron microscope operation Zeiss Supra-40. The emission and excitation spectra of the samples were measured using a Shimadzu fluorescence spectrometer (RF-5301PC) with a 400W monochromatized xenon lamp. Excitation and emission spectra were measured using a Shimadzu RF-5301PC fluorescence spectrophotometer.

6.4. Results and Discussion

The synthesis of ORMOSIL is very sensitive to the ratio of reaction agents in each solution. Change of ratio of reaction agents may cause ORMOSIL intend to crack or become opaque. By using our protocol, we synthesized ORMOSIL with and without doping with LaF_3:Ce water-soluble nanoparticles. Figure 6.1 and 6.2 shows wet and dried ORMOSIL samples without doping and doped with LaF_3:Ce with the doping mole concentration of 0.001964 M. All wet and dried samples are transparent which meet one of the most important requirements for application of radiation detection since transparent ORMOSILs allow making imaging arrays with better spatial resolution and gamma selectivity. The shapes of wet ORMOSIL samples are columns with diameter of 1 cm and length of 6 cm, however, the dried sample shrinked a lot

with diameter of 0.35 cm and length of 2 cm. According to the volume change of the ORMOSIL after dried, we estimated that the nanoparticle mole concentration in dried samples should be 24.5 times as much as in wet samples.

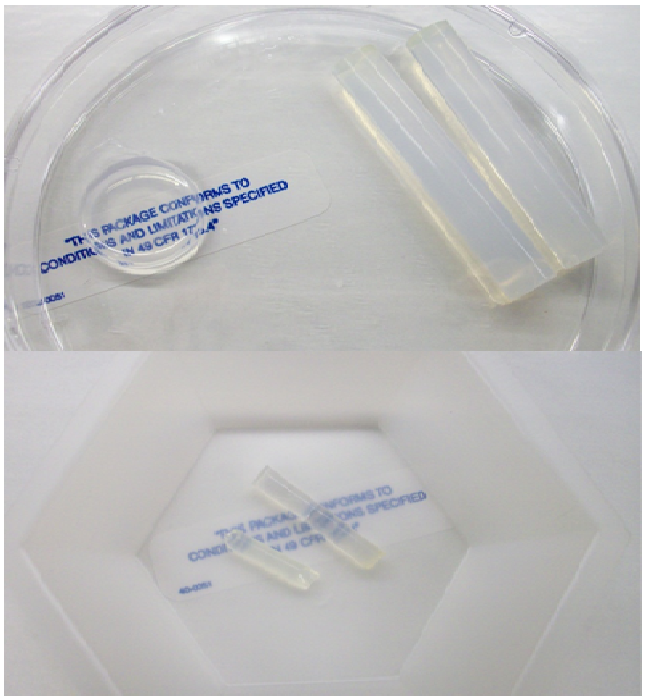

Figure 6.1 Wet (upper) and dried (lower) ORMOSIL samples

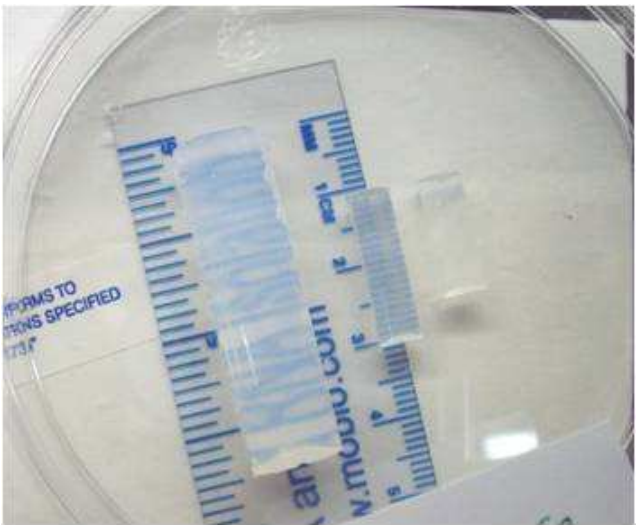

Figure 6.2 Wet (left) and dried (right two) ORMOSIL samples

Based on the results we obtained, we varied the nanoparticles loading by using two different formations of nanoparticles: water-soluble and ethanol-soluble LaF_3:Ce nanoparticles. The original mole doping concentration of ORMOSIL: LaF_3:Ce were 0.001964 M, 0.0039 M, 0.0059 M and 0.0078 M when using water-soluble LaF_3:Ce nanoparticles, 0.0145 M, 0.029M, 0.0435M and 0.058M when using ethanol-soluble LaF_3:Ce nanoparticles. Transferring the mole concentration of the nanoparticle loading in wet ORMOSILs into weight percentage loading in dried ORMOSILs, we obtained the LaF_3:Ce nanoparticle loading of ORMOSIL samples by using LaF_3:Ce water-soluble solution are 3.63%, 7.01%, 10.17% and 13.11%, while nanoparticle loading of ORMOSIL samples by using LaF_3:Ce ethanol-soluble solution are 15.66%, 27.09%, 35.78% and 42.63%. Figure 6.3 shows water-soluble LaF_3:Ce doped ORMOSIL with nanoparticle loading increased from 3.63% on the left to 13.11% on the right. They are all showing transparent except the very right sample with the highest loading concentration of 13.11%, this indicates nanoparticle loading by using water-soluble LaF_3:Ce can reach up to somewhere between 10.17 % and 13.11% to show transparent for radiation detection application, while it became opaque beyond 13.11%. Ethanol-soluble LaF_3:Ce doped ORMOSIL samples are shown in figure 6.4, within four samples, only the left one with the lowest loading percentage of 15.66% in this set of sample was transparent, the rest three all became opaque with increasing loading nanoparticles. It indicates that using ethanol-soluble LaF_3:Ce as doping material can increase the nanoparticle loading in ORMOSIL effectively, the nanoparticle loading percentage reached a point between 15.66% and 27.09% where LaF_3:Ce doped ORMOSIL started changing from transparent to opaque. Comparing these two sets of samples, even though the solubility of LaF_3:Ce in ethanol is lower than in water, due to the large ratio of ethanol to water in the process of ORMOSIL synthesis, using LaF_3:Ce ethanol-soluble nanoparticles is an effective way to increase the nanoparticle loading in ORMOSIL. The samples shown in Figure 6.3 and 6.4 displayed homogenous color distribution within the entire samples. During the synthesis of ORMOSIL, the metal clusters were incorporated into the

ORMOSIL matrices by dissolving metal salts into the precursor solution prior to gelation. We used APTES as organic source which also helped anchor the dopant to the silica network of the ORMOSIL, thereby avoiding precipitation of the salt, besides being a reagent, APTES was also acting as the (base) catalyst.

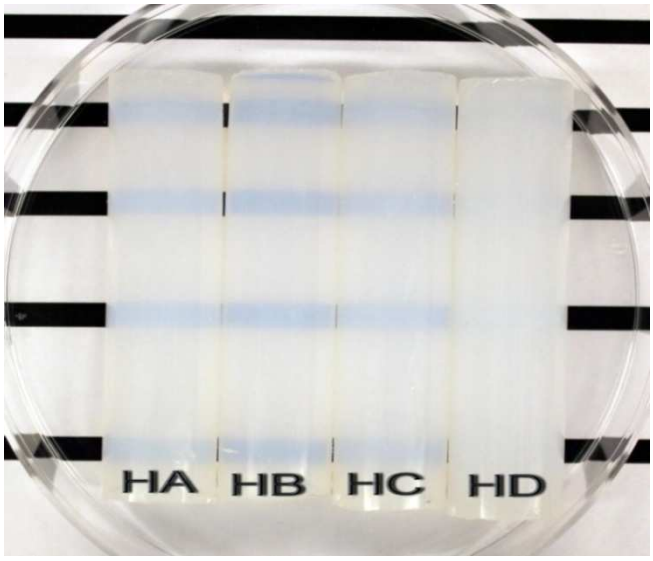

Figure 6.3 Water –soluble LaF_3:Ce doped ORMOSILS with different doping concentrations (WNP-0%; HA-3.63%; HB-7.01%; HC-10.17% ; HD-13.11%)

Figure 6.4 Ethanol–soluble LaF_3:Ce doped ORMOSILS with different doping concentrations (WNP-0%; EA-15.66%; EB-27.09%; EC-35.78% ; ED-42.63%)

Figure 6.5 shows XRD pattern of ORMOSIL doped with ethanol-soluble LaF_3:Ce nanoparticles compared with that of pure LaF_3:Ce crystals. The results of the XRD are in good agreement with the trigonal tysonite LaF_3 structure as described in the reports[188,189] and from bulk LaF_3 and CeF_3 crystals (JCPDS Card 32-0483 and 08-0045). No XRD signals were observed for impurity phases, indicating that Ce^{3+} is likely doped into the LaF_3 crystal lattice. The ionic radius of Ce^{3+} (1.034 Á) is very close to that of La^{3+} (1.061 Á), therefore, Ce^{3+} can easily substitute the occupation of La^{3+} ions in LaF_3 crystal lattices. This result indicates that nanomaterial remains its crystal structure even after it is doped into ORMOSIL, which ensures LaF_3:Ce doped ORMOSIL can be used for application in radiation detection without losing any radiation detection capability of nanomaterial. SEM image as shown in figure 6.6 provides information visually on morphology of LaF_3:Ce doped ORMOSIL bulk material. It shows the material has open porous structure which allows the radiation detection capability of LaF_3:Ce remains high efficiency.

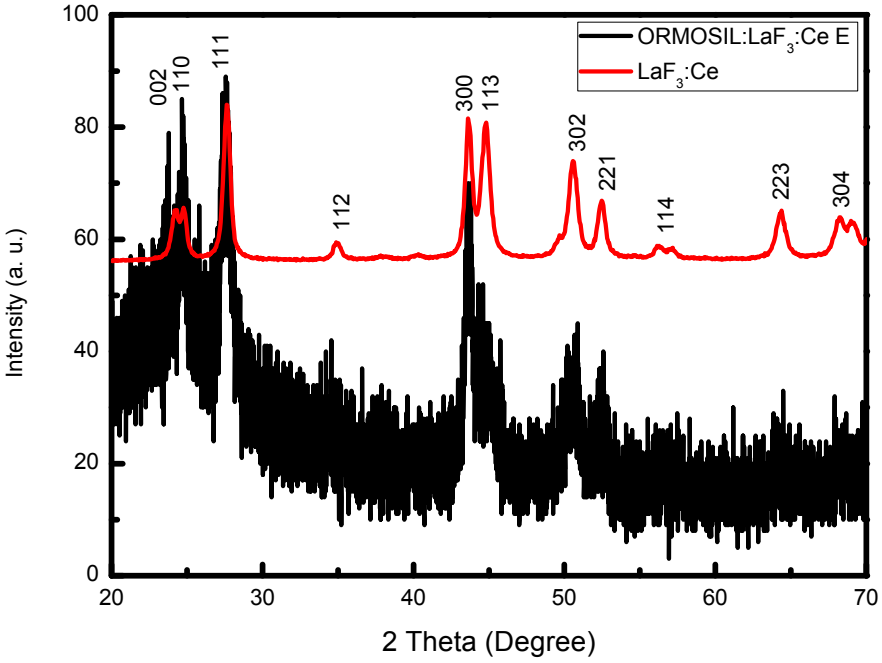

Figure 6.5 XRD pattern of LaF_3:Ce doped ORMOSIL showing LaF_3:Ce crystal structure within ORMOSIL (compared with standard LaF3:Ce crystal)

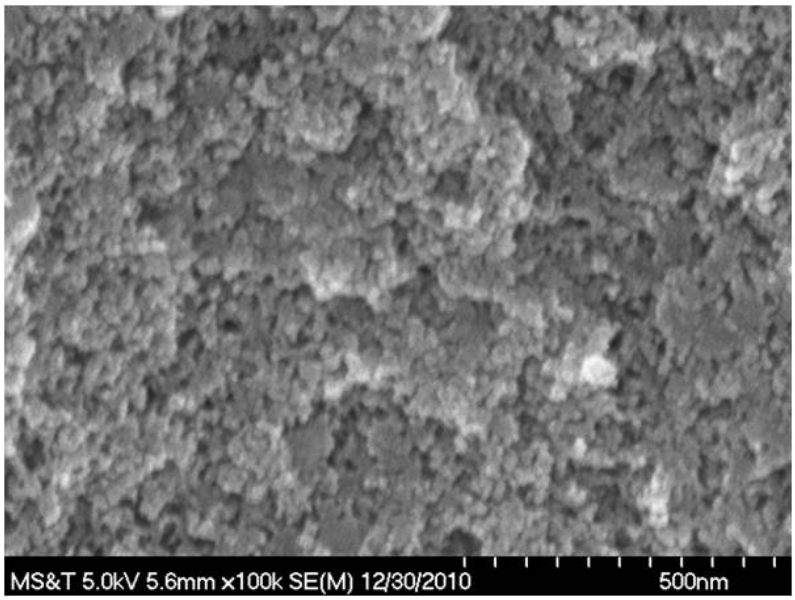

Figure 6.6 SEM image of ORMOSIL showing open porous structure

Figure 6.7 shows emission spectra of LaF_3:Ce water-soluble nanoparticles doped ORMOSIL with different doping concentrations (WNP-0%; HA-3.63%; HB-7.01%; HC-10.17% ; HD-13.11%). The ORMOSIL without doping has very weak emissions peaked at 363 nm, this phenomena is similar to that reported by Kang,[218] during the sol-gel process, the silicate framework Si-O-Si was synthesized from the reaction of tetraethoxysilane (TEOS) with nitric acid by eliminating methyl formate instead of water under an anhydrous condition,[219] where decomposed formate could create C substitutional defects which are considered as the reason for the 363 emission. After doped with LaF_3:Ce nanoparticles, due to the emission induced by 5d→4f transition of Ce^{3+} , the emissions are all blue-shift. The intensity of emissions increased as doping concentration increased and then reached to the maximum with doping concentration of 10.17%, the further increased doping concentration of 13.11% has not lead to a stronger emission. This could be the result that ORMOSILS pores formed from the silicate networking have been saturated with nanoparticles under this situation, therefore, the emission of extra doping nanoparticles was quenched as scattering light which shown opaque rather than transparent in figure 6.3.

Figure 6.8 shows emission spectra of LaF_3:Ce ethanol-soluble nanoparticles doped ORMOSIL with different doping concentrations (EA-15.66%; EB-27.09%; EC-35.78% ; ED-42.63%). Similar to the emissions of those doped with water-soluable nanoparticles, all the emissions of ethanol-soluble LaF_3:Ce doped ORMOSIL have been blue shifted compared with the defect emission of ORMOISL without any doping. The emissions of the samples were increased first then decreased with a maximum at doping concentration of 27.09%. The reason for the decreased emissions is similar to the previous water-soluble doped ORMOSIL. When the doping concentration was increased beyond the capability of silicate networking, the emission of Ce^{3+} started to quench until the defect emission of ORMOSIL dominated, which also made sample lose their transparency. Based on the observation of transparency of the samples shown in figure 6.4, we conclude that there must be a maximum doping concentration

with a value between 15.66% and 27.09% at which point sample start to transform from transparency to opaque.

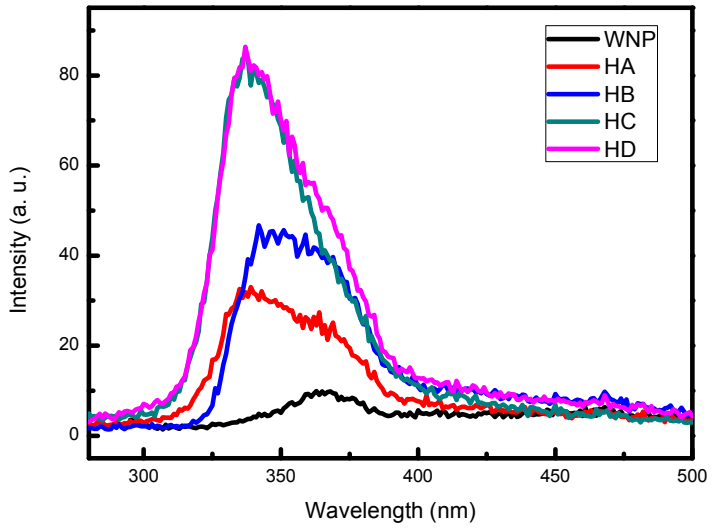

Figure 6.7 Emissions of LaF_3:Ce water-soluble nanoparticles doped ORMOSIL with different doping concentrations

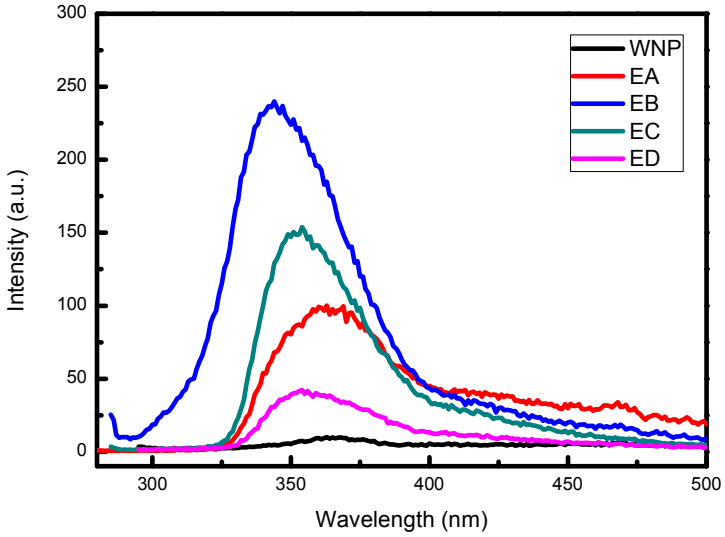

Figure 6.8 Emissions of LaF_3:Ce ethanol-soluble nanoparticles doped ORMOSIL with different doping concentrations

6.5 Conclusion

Even through ORMOSIL have a better flexible solid matrix than typical silica xerogels, due to the large portion of ethanol content, rapid evaporation makes producing crack-free ORMOSIL is still a challenging issue. LaF_3:Ce doped Crack-free ORMOSILs were synthesized by controlling the drying speed. Water-soluble and ethanol-soluble LaF_3:Ce nanoparticles were doped into ORMOSIL with different doping concentrations. By using water-soluble LaF_3:Ce, the doping concentrations can reach up to 10.17% to remain transparent and strong luminescent of the material, while due to the larger content of ethanol reagent compared with water, ethanol-soluble LaF_3:Ce can be doped into ORMOSIL with doping concentration above 15.66% to maintain transparent and luminescent properties. As LaF_3:Ce has been widely used as radiation detection material due to the fast response of Ce^{3+}, using ORMOSIL as carrier, this material may find promising applications in radiation detection.

CHAPTER 7

SUMMARY AND FUTURE WORK

In this dissertation, LaF_3:Ce nanoparticles were synthesized in DMSO which has been proved to be a carrier of drugs across membranes without causing significant damage. The luminescence of LaF_3:Ce powder which was precipitated from the DMSO solution is markedly different from that of the solution sample. The former emission is attributed to Ce^{3+} d-f transitions while the emission of the solution samples is originated from metal-to-ligand charge-transfer excited states. We further investigated the biological application of LaF_3:Ce in DMSO by conjugating the particles with PpIX and then encapsulating the complex into PLGA. The results show efficient uptake and damage to cancer cells. Therefore, this material could be very promising as an agent in photodynamic therapy for cancer treatment.

The case for Eu-DMSO complex is different from above stated. In this complex, very strong characteristic luminescence of Eu was observed but no such emissions induced by metal-to-ligand charge-transfer excited states as observed in LaF_3:Ce in DMSO. It is very interesting to be found that the emission of Eu^{3+} in Eu-DMSO complex becomes hypersensitive when water was introduced into the solution, moreover, the strongest emission at 617 nm had a shoulder peak at 613 nm, and these two peaks were affected by the coupling of Eu ion with O-H oscillators in an opposite way. We found that the ratio of emission intensity of 613 nm to 617 nm has a nearly perfect linear dependence on increasing water concentration in Eu-DMSO, which provides a very convenient and valuable method for water determination in DMSO. This method could be also used for other solvent detection in DMSO such as ethanol, acetone, diethyl ether, benzene, chloroform, phosphate buffered saline (PBS) buffer solutions, and cell culture media which are well worth investigating in the future work.

Water-soluble nanoparticles were synthesized by doping different lanthanide ions in LaF_3. Ce and Tb co-doped LaF_3 with a molecular formula of $La_{0.4}Ce_{0.45}Tb_{0.15}F_3$ had the strongest emissions due to energy transfer from Ce^{3+} to Tb^{3+}. Due to the strong luminescence and long decay lifetime, this material can be used for trace biomaterials detections on surfaces.

Ce^{3+} has been well known as a great activator exhibiting a very fast response in radiation detectors of medical imaging systems for diagnostic radiology. However, its emission within the ultraviolet range limited the environment in which the detection systems work since many materials are not transparent in the UV region. Quantum dots have high luminescence quantum efficiency but their stopping power is low which results in very weak scintillation luminescence. Nanocompound formed by CdTe quantum dots and LaF_3:Ce nanoparticles optimize both stopping power and scintillation efficiency. Energy transfer efficiency was calculated as 53% for the fast component and 49% for the slow component. The energy transfer efficiency could be improved by further optimizing the synthesis process.

Hybrid matrix materials such as ORMOSIL have superior mechanical properties and a better processability than the pure molecular lanthanide complexes. Moreover, embedding a lanthanide complex in a hybrid matrix enhances its thermal stability and luminescence output, We synthesized LaF_3:Ce embedded ORMOSIL by using two different LaF_3:Ce sources, the nanoparticle doping concentration can be reached up to 15.66% to keep its transparent and luminescent properties. Increasing the nanoparticles loading could be a challenge work in the future. Furthermore, it would be promising for the application in radiation detection if the complex of LaF_3:Ce with CdTe could be successfully doped into ORMOSIL. Both synthesis of ORMOSIL and CdTe require certain PH, which makes it harder to coordinate both without quenching the luminescence of CdTe. Synthesis of CdTe in sol at the starting point might be a solution to avoid this problem.

APPENDIX A

PUBLICATIONS

1. Xiaoju Zou, **Mingzhen Yao**, Marius Hossu and Wei Chen, Assessing exposure, uptake and toxicity of PLGA encapsulated LaF_3:Ce/PpIX in human prostate cancer cells, under preparation.
2. **Mingzhen Yao**, Sammynaiken Ramaswami, Hongbing Lu and Wei Chen, Synthesis and Characterization of LaF_3:Ce Nanoparticles Doped ORMOSIL Hybrid Material for Radiation Detection Application, under preparation.
3. **Mingzhen Yao**, Yuebin Li, Marius Hossu, Alan Joly, Zhongxin Liu, Zuli Liu and Wei Chen, Luminescence of Lanthanide-Dimethyl Sulfoxide Compound Solutions, *J. Phys. Chem. B.* 2011, accepted.
4. **Mingzhen Yao** and Wei Chen, Hypersensitive Luminescence of Eu^{3+} in Dimethyl Sulfoxide as a New Probing for Water Measurement, *Anal. Chem.* 2011, 83, 1879-1882
5. **Mingzhen Yao,** Alan G. Joly, and Wei Chen, Formation and Luminescence Phenomena of LaF_3:Ce^{3+} Nanoparticles and Lanthanide-Organic Compounds in Dimethyl Sulfoxide, *J. Phys. Chem. C.* 2010, 114, 826–831
6. **Mingzhen Yao**, Xing Zhang, Yuebin Li, Wei Chen, Alan G. Joly, Jinsong Huang and Qingwu Wang, Luminescence Enhancement of CdTe Nanostructures in LaF_3:Ce/CdTe Nanocomposites. *J. Appl. Phys*. 2010, 108, 103104
7. Yuebin Li, Zhong Sun, LunMa, Xing Zhang, **Mingzhen Yao**, Alan G Joly, Zuli Liu andWei Chen, Synthesis and luminescence of $CePO_4$**:**Tb/$LaPO_4$ core/sheath nanowires, *Nanotechnology* 2010, 21,125604
8. Zhong Sun, Yuebin Li, Xing Zhang, **Mingzhen Yao**, Lun Ma, and Wei Chen, Luminescence and Energy Transfer in Water Soluble CeF_3 and CeF_3:Tb^{3+} Nanoparticles. *J. Nanosci. Nanotechnol* 2009, 9, 6283-6291
9. **Mingzhen Yao**, The Synthesis and Luminescence Properties of Lanthanide-based Nanoparticles for Biological Application, Master Thesis, The University of Texas at Arlington

(August 2008)

10. Kwan H. Cheng, Jacob Aijmo, Lun Ma, **Mingzhen Yao**, Xing Zhang, John Como, Louisa J. Hope-Weeks, Juyang Huang, and Wei Chen, Luminescence Decay Dynamics and Trace Biomaterials Detection Potential of Surface-Functionalized Nanoparticles, *J. Phys. Chem. C* 2008, 112, 17931–17939

APPENDIX B

CONFERENCE PRESENTATIONS

1. **Mingzhen Yao**, Wei Chen and Alan G. Joly. “Luminescence properties of doped LaF_3 nanoparticles”, Academic Research Initiative Grantees Conference, Washington, D.C. April 21-22, 2008
2. **Mingzhen Yao** and Wei Chen. 2007 Joint Fall Meeting of the APS and AAPT, oral presentation entitled “Synthesis of LaF_3:Ce^{3+} Nanoparticles with Tunable Emissions”, College station, TX, 2007.
3. Jacob Ajimo , Lun Ma , **Mingzhen Yao** , Xing Zhang , John Como , Louisa Hope-weeks , Juyang Huang , Wei Chen , Kwan Cheng. 2008 Joint Fall Meeting of the APS and AAPT, EL Paso, Texas.

REFERENCES

1. Taniguchi N. On the basic concept of 'nano-technology' In: Engineering PotICoP, editor; 1974; Tokyo, Japan. Society of Precision Engineering.
2. Dowling A, Clift, R., Grobert, N., Hutton, D., Oliver, R., O'neill, O., Pethica, J., Pidgeon, N., Porritt, J., Ryan, J., Season, A., Tendler, S., Wellland, M., Whatmore, R., . Nanoscience and Nanotechnologies: Opportunities and Uncertainties. London, UK.: The Royal Society and the Royal Academy of Engineering; 2004.
3. Buffat P, Borel JP. Size Effect on Melting Temperature of Gold Particles. Physical Review A 1976;13(6):2287-2298.
4. Akerman ME, Chan WCW, Laakkonen P, Bhatia SN, Ruoslahti E. Nanocrystal targeting in vivo. Proceedings of the National Academy of Sciences of the United States of America 2002;99(20):12617-12621.
5. Gao XH, Cui YY, Levenson RM, Chung LWK, Nie SM. In vivo cancer targeting and imaging with semiconductor quantum dots. Nature Biotechnology 2004;22(8):969-976.
6. Tada H, Higuchi H, Wanatabe TM, Ohuchi N. In vivo real-time tracking of single quantum dots conjugated with monoclonal anti-HER2 antibody in tumors of mice. Cancer Research 2007;67(3):1138-1144.
7. Montet X, Montet-Abou K, Reynolds F, Weissleder R, Josephson L. Nanoparticle imaging of integrins on tumor cells. Neoplasia 2006;8(3):214-222.
8. Cai WB, Shin DW, Chen K, Gheysens O, Cao QZ, Wang SX, Gambhir SS, Chen XY. Peptide-labeled near-infrared quantum dots for imaging tumor vasculature in living subjects. Nano Letters 2006;6(4):669-676.

9. Soltesz EG, Kim S, Laurence RG, DeGrand AM, Parungo CP, Dor DM, Cohn LH, Bawendi MG, Frangioni JV, Mihaljevic T. Intraoperative sentinel lymph node mapping of the lung using near-infrared fluorescent quantum dots. Annals of Thoracic Surgery 2005;79(1):269-277.

10. Ballou B, Ernst LA, Andreko S, Harper T, Fitzpatrick JAJ, Waggoner AS, Bruchez MP. Sentinel lymph node imaging using quantum dots in mouse tumor models. Bioconjugate Chemistry 2007;18(2):389-396.

11. Dhawan D, Ramos-Vara JA, Stewart JC, Zheng R, Knapp DW. Canine invasive transitional cell carcinoma cell lines: In vitro tools to complement a relevant animal model of invasive urinary bladder cancer. Urologic Oncology-Seminars and Original Investigations 2009;27(3):284-292.

12. Knapp DW, Adams LG, DeGrand AM, Niles JD, Ramos-Vara JA, Weil AB, O'Donnell MA, Lucroy MD, Frangioni JV. Sentinel lymph node mapping of invasive urinary bladder cancer in animal models using invisible light. European Urology 2007;52(6):1700-1709.

13. Michalet X, Pinaud FF, Bentolila LA, Tsay JM, Doose S, Li JJ, Sundaresan G, Wu AM, Gambhir SS, Weiss S. Quantum dots for live cells, in vivo imaging, and diagnostics. Science 2005;307(5709):538-544.

14. Medintz IL, Uyeda HT, Goldman ER, Mattoussi H. Quantum dot bioconjugates for imaging, labelling and sensing. Nature Materials 2005;4(6):435-446.

15. Wang CW, Moffitt MG. Use of block copolymer-stabilized cadmium sulfide quantum dots as novel tracers for laser scanning confocal fluorescence imaging of blend morphology in polystyrene/poly(methyl methacrylate) films. Langmuir 2005;21(6):2465-2473.

16. Baumle M, Stamou D, Segura JM, Hovius R, Vogel H. Highly fluorescent streptavidin-coated CdSe nanoparticles: Preparation in water, characterization, and micropatterning. Langmuir 2004;20(10):3828-3831.

17. Meziani MJ, Pathak P, Harruff BA, Hurezeanu R, Sun YP. Direct conjugation of semiconductor nanoparticles with proteins. Langmuir 2005;21(5):2008-2011.

18. Charvet N, Reiss P, Roget A, Dupuis A, Grunwald D, Carayon S, Chandezon F, Livache T. Biotinylated CdSe/ZnSe nanocrystals for specific fluorescent labeling. Journal of Materials Chemistry 2004;14(17):2638-2642.

19. Powe AM, Fletcher KA, St Luce NN, Lowry M, Neal S, McCarroll ME, Oldham PB, McGown LB, Warner IM. Molecular fluorescence, phosphorescence, and chemiluminescence spectrometry. Analytical Chemistry 2004;76(16):4614-4634.

20. Alivisatos P. The use of nanocrystals in biological detection. Nature Biotechnology 2004;22(1):47-52.

21. Daniel MC, Astruc D. Gold nanoparticles: Assembly, supramolecular chemistry, quantum-size-related properties, and applications toward biology, catalysis, and nanotechnology. Chem Rev 2004;104(1):293-346.

22. Penn SG, He L, Natan MJ. Nanoparticles for bioanalysis. Current Opinion in Chemical Biology 2003;7(5):609-615.

23. Shipway AN, Katz E, Willner I. Nanoparticle arrays on surfaces for electronic, optical, and sensor applications. Chemphyschem 2000;1(1):18-52.

24. Kubitschko S, Spinke J, Bruckner T, Pohl S, Oranth N. Sensitivity enhancement of optical immunosensors with nanoparticles. Analytical Biochemistry 1997;253(1):112-122.

25. Kambhampati DK, Knoll W. Surface-plasmon optical techniques. Current Opinion in Colloid & Interface Science 1999;4(4):273-280.

26. Rich RL, Myszka DG. Survey of the 1999 surface plasmon resonance biosensor literature. Journal of Molecular Recognition 2000;13(6):388-407.

27. Schultz S, Smith DR, Mock JJ, Schultz DA. Single-target molecule detection with nonbleaching multicolor optical immunolabels. Proceedings of the National Academy of Sciences of the United States of America 2000;97(3):996-1001.

28. Psaras PA, Langford HD. In: Research AM, editor. US National Academy of Engineering and National Academy of Sciences. Washington, DC: National Academy Press; 1987. p 203.

29. LaMer VK, Dinegar RH. J Am Chem Soc 1950;72:4847.

30. Nielsen F. Spray Drying Pharmaceuticals. Manuf Chemist 1982;53(7):38-&.

31. Real M. Proceedings of the British Ceramic Society 1986;38(59).

32. Rosen MJ. Surfactants in Emerging Technologies. New York: Dekker; 1987.

33. McHale AE. Ceramics and Glasses. Engineered Materials Handbook. Volume 4: Metals Park, OH:ASM; 1991. p 115.

34. Whetten RL, Khoury JT, Alvarez MM, Murthy S, Vezmar I, Wang ZL, Stephens PW, Cleveland CL, Luedtke WD, Landman U. Nanocrystal gold molecules. Advanced Materials 1996;8(5):428-&.

35. Murray CB, Kagan CR, Bawendi MG. Self-Organization of Cdse Nanocrystallites into 3-Dimensional Quantum-Dot Superlattices. Science 1995;270(5240):1335-1338.

36. Simonian AL, Good TA, Wang SS, Wild JR. Nanoparticle-based optical biosensors for the direct detection of organophosphate chemical warfare agents and pesticides. Anal Chim Acta 2005;534(1):69-77.

37. Power JR, Weightman P, Bose S, Shkrebtii AI, Del Sole R. Sensitivity of reflectance anisotropy spectroscopy to the orientation of Ge dimers on vicinal Si(001). Physical Review Letters 1998;80(14):3133-3136.

38. Sabbatini N, Guardigli M, Lehn JM. Luminescent Lanthanide Complexes as Photochemical Supramolecular Devices. Coordination Chemistry Reviews 1993;123(1-2):201-228.

39. Bernardinelli GP, C.; Williams, A.F. Angewandte Chemie-International Edition 1992(31):1622-1624.

40. Piguet C, Hopfgartner G, Williams AF, Bunzli JC. Self-Assembly of the First Heterodinuclear-D-F Triple-Helix in Solution. J Chem Soc Chem Comm 1995(4):491-493.

41. Edder CP, C.; Bunzli, J.C.G. Hopfgartner, G. J. . J Chem Soc, Dalton Trans 1997:4957-4663.

42. Greenwood NN, Earnshaw A. Yew York, NY: Pergamon Press; 1990.

43. Bunzli JCGC, G.R., editor. Lanthanide Plobes in Life Elsever: Amsterdam; 1989.

44. Stein G, Wurzberg E. Energy-Gap Law in Solvent Isotope-Effect on Radiationless Transitions of Rare-Earth Ions. Journal of Chemical Physics 1975;62(1):208-213.

45. Selvin PR. Fluorescence Resonance Energy-Transfer. Biochemical Spectroscopy 1995;246:300-334.

46. Beeby A, Botchway SW, Clarkson IM, Faulkner S, Parker AW, Parker D, Williams JAG. Luminescence imaging microscopy and lifetime mapping using kinetically stable lanthanide(III) complexes. J Photochem Photobiol B-Biol 2000;57(2-3):83-89.

47. Christopoulos TK, Diamandis EP. Enzymatically Amplified Time-Resolved Fluorescence Immunoassay with Terbium Chelates. Analytical Chemistry 1992;64(4):342-346.

48. Diamandis EP. Analyst 1992(117):1879-1884.

49. Beeby A, Clarkson IM, Dickins RS, Faulkner S, Parker D, Royle L, de Sousa AS, Williams JAG, Woods M. Non-radiative deactivation of the excited states of europium, terbium and ytterbium complexes by proximate energy-matched OH, NH and CH oscillators: an improved luminescence method for establishing solution hydration states. Journal of the Chemical Society-Perkin Transactions 2 1999(3):493-503.

50. Kropp JL, Windsor MW. Luminescence and Energy Transfer in Solutions of Rare-Earth Complexes .I. Enhancement of Fluorescence by Deuterium Substitution. Journal of Chemical Physics 1965;42(5):1599-&.

51. Kropp JL, Windsor MW. Comment on Fluorescence of Trivalent Europium in D2o-H2o Mixtures. Journal of Chemical Physics 1966;45(2):761-&.

52. Kropp JL, Windsor MW. Enhancement of fluorescence yield of rare earth ions by heavy water. J Chem Phys 1963;39(10):2769-2770.

53. Haas Y, Stein G. Pathways of Radiative and Radiationless Transitions in Europium(Iii) Solutions - Role of High Energy Vibrations. J Phys Chem-Us 1971;75(24):3677-&.

54. Horrocks WD, Sudnick DR. Lanthanide Ion Probes of Structure in Biology - Laser-Induced Luminescence Decay Constants Provide a Direct Measure of the Number of Metal-Coordinated Water-Molecules. Journal of the American Chemical Society 1979;101(2):334-340.

55. Choppin GR, Peterman DR. Applications of lanthanide luminescence spectroscopy to solution studies of coordination chemistry. Coordination Chemistry Reviews 1998;174:283-299.

56. Bunzli JCC, G.R. Lanthanide Probes in Life: Elsevier, Amsterdam; 1979.

57. Lis S. Luminescence spectroscopy of lanthanide(III) ions in solution. J Alloy Compd 2002;341(1-2):45-50.

58. Elbanowski M, Makowsaka B. The lanthanides as luminescent probes in investigations of biochemical systems. J Photoch Photobio A 1996;99(2-3):85-92.

59. lewin MC, N.; Tung, C.H.; Tang, X.W.; Cory, D.; Scadden, D.T.; Weissleder, R. Tat peptide-derivatized magnetic nanoparticles allow in vivo tracking and recovery of progenitor cells. Nat Biotechnol 2000;18(4):410-414.

60. Lu H, Yi G, Zhao S, Chen D, Guo L-H, Cheng J. Synthesis and characterization of multi-functional nanoparticles possessing magnetic, up-conversion fluorescence and bio-affinity properties. Journal of Materials Chemistry 2004;14(8):1336-1341.

61. Levy L, Sahoo, Y., Kim, K.s., Bergey, E.J., Prasad, P. N. . Chemistry of Materials 2002(14):3715.

62. Lal M, Levy L, Kim KS, He GS, Wang X, Min YH, Pakatchi S, Prasad PN. Silica nanobubbles containing an organic dye in a multilayered organic/inorganic heterostructure with enhanced luminescence. Chemistry of Materials 2000;12(9):2632-2639.

63. Tissue BM. Synthesis and Luminescence of Lanthanide Ions in Nanoscale Insulating Hosts. Chemistry of Materials 1998;10(10):2837-2845.

64. Gordon WO, Carter JA, Tissue BM. Long-lifetime luminescence of lanthanide-doped gadolinium oxide nanoparticles for immunoassays. Journal of Luminescence 2004;108(1-4):339-342.

65. Feng J, Shan GM, Maquieira A, Koivunen ME, Guo B, Hammock BD, Kennedy IM. Functionalized europium oxide nanoparticles used as a fluorescent label in an immunoassay for atrazine. Analytical Chemistry 2003;75(19):5282-5286.

66. Tan M, Wang G, Hai X, Ye Z, Yuan J. J Mater Chem 2004;14:2896.

67. Weber MJ. Probabilities for Radiative and Nonradiative Decay of Er^{3+} in LaF_3. Phys Rev 1967;157(2):262.

68. Klink SI, Hebbink GA, Grave L, Van Veggel FCJM, Reinhoudt DN, Slooff LH, Polman A, Hofstraat JW. Sensitized near-infrared luminescence from polydentate triphenylene-functionalized Nd^{3+},Yb^{3+}, and Er^{3+} complexes. Journal of Applied Physics 1999;86(3):1181-1185.

69. Chen W. Nanomaterials and Nanodevices. Los Angeles: American Scientific: ; 2009.

70. Chen W, Zhang JZ, Joly AG. J Nanosci Nanotechnol 2004;4:919.

71. Goldburt ET, Kulkarni B, Bhargava RN, Taylor J, Libera M. Size dependent efficiency in Tb doped Y_2O_3 nanocrystalline phosphor. Journal of Luminescence 1997;72-4:190-192.

72. Chen D, Wang Y, Yu Y, Ma E. Mater Chem Phys 2007;101:464-469.

73. Liu YF, Chen W, Wang SP, Joly AG, Westcott S, Woo BK. X-ray luminescence of LaF_3 : Tb^{3+} and LaF3 : $Ce3^{+,}$ Tb^{3+} water-soluble nanoparticles. Journal of Applied Physics 2008;103(6):-.

74. Sivakumar S, Diamente PR, van Veggel FC. Silica-coated $Ln(^{3+})$-doped LaF_3 nanoparticles as robust down- and upconverting biolabels. Chemistry-a European Journal 2006;12(22):5878-5884.

75. Stouwdam JW, Hebbink GA, Huskens J, van Veggel FCJM. Lanthanide-doped nanoparticles with excellent luminescent properties in organic media. Chemistry of Materials 2003;15(24):4604-4616.

76. Wang F, Zhang Y, Fan XP, Wang MQ. Facile synthesis of water-soluble LaF_3 : $Ln(^{3+})$ nanocrystals. Journal of Materials Chemistry 2006;16(11):1031-1034.

77. Kompe K, Borchert H, Storz J, Lobo A, Adam S, Moller T, Haase M. Green-emitting $CePO_4$: Th/$LaPO_4$ core-shell nanoparticles with 70% photoluminescence quantum yield. Angewandte Chemie-International Edition 2003;42(44):5513-5516.

78. Meyssamy H, Riwotzki K, Kornowski A, Naused S, Haase M. Wet-chemical synthesis of doped colloidal nanomaterials: Particles and fibers of $LaPO_4$: Eu, $LaPO_4$: Ce, and $LaPO_4$: Ce,Tb. Advanced Materials 1999;11(10):840-+.

79. Shan JN, Chen JB, Meng J, Collins J, Soboyejo W, Friedberg JS, Ju YG. Biofunctionalization, cytotoxicity, and cell uptake of lanthanide doped hydrophobically ligated $NaYF_4$ upconversion nanophosphors. Journal of Applied Physics 2008;104(9):-.

80. Weber MJ. Science and Technology of Laser Glass. J Non-Cryst Solids 1990;123(1-3):208-222.

81. Marion JE, Weber MJ. Phosphate Laser Glasses. Eur J Sol State Inor 1991;28(1):271-287.

82. Reisfeld R. Theory and Application of Spectroscopically Active Glasses Prepared by the Sol-Gel Method. Sol-Gel Optics 1990;1328:29-39

83. Miniscalco WJ. Erbium-Doped Glasses for Fiber Amplifiers at 1500-Nm. J Lightwave Technol 1991;9(2):234-250.

84. Hench LL, West JK. The Sol-Gel Process. Chem Rev 1990;90(1):33-72.

85. Brinker CJ, Bein T, Frye GC, Ashley CS. Sol-Gel Processing of Controlled Pore Films. Abstracts of Papers of the American Chemical Society 1989;197:173-IAEC.

86. Buckley AM, Greenblatt M. The Sol-Gel Preparation of Silica-Gels. Journal of Chemical Education 1994;71(7):599-602.

87. Reisfeld R. Prospects of sol-gel technology towards luminescent materials. Opt Mater 2001;16(1-2):1-7.

88. Reisfeld R. Spectroscopy and Applications of Molecules in Glasses. J Non-Cryst Solids 1990;121(1-3):254-266.

89. Dunn B, Zink JI. Optical-Properties of Sol-Gel Glasses Doped with Organic-Molecules. Journal of Materials Chemistry 1991;1(6):903-913.

90. Sanchez C, Ribot F. Design of Hybrid Organic-Inorganic Materials Synthesized Via Sol-Gel Chemistry. New J Chem 1994;18(10):1007-1047.

91. Sanchez C, Lafuma A, Rozes L, Nakatani K, Delaire JA, Cordoncillo E, Viana B, Escribano P. Molecular design of hybrid organic-inorganic nanocomposites with emission and photochromic properties. Organic-Inorganic Hybrid Materials for Photonics 1998;3469:192-200

92. Escribano P, Julian-Lopez B, Planelles-Arago J, Cordoncillo E, Viana B, Sanchez C. Photonic and nanobiophotonic properties of luminescent lanthanide-doped hybrid organic- inorganic materials. Journal of Materials Chemistry 2008;18(1):23-40.

93. Sanchez C, Lebeau B. Design and properties of hybrid organic-inorganic nanocomposites for photonics. Mrs Bulletin 2001;26(5):377-387.

94. Avnir D. Organic-Chemistry within Ceramic Matrices - Doped Sol-Gel Materials. Accounts of Chemical Research 1995;28(8):328-334.

95. Henderson B, Lmbusch GF. Optical Spectroscopy in Inorganic Solids. Oxford: Oxford University Press; 1989.

96. Blasse G, Grabmaier BC. Luminescent Materials. Berlin: Springer; 1994.

97. Ye Z, Tan M, Wang G, Yuan J. J Mater Chem 2004;14(851-856).

98. Hai XD, Tan MQ, Wang G, Ye ZQ, Yuan JL, Matsumoto K. Preparation and a time-resolved fluoroimmunoassay application of new europium fluorescent nanoparticles. Analytical Sciences 2004;20(2):245-246.

99. Meiser F, Cortez C, Caruso F. Biofunctionalization of fluorescent rare-earth-doped lanthanum phosphate colloidal nanoparticles. Angewandte Chemie-International Edition 2004;43(44):5954-5957.

100. Beaurepaire E, Buissette V, Sauviat MP, Giaume D, Lahlil K, Mercuri A, Casanova D, Huignard A, Martin JL, Gacoin T, Boilot JP, Alexandrou A. Functionalized fluorescent oxide nanoparticles: Artificial toxins for sodium channel targeting and Imaging at the single-molecule level. Nano Letters 2004;4(11):2079-2083.

101. Derfus AM, Chan WCW, Bhatia SN. Intracellular delivery of quantum dots for live cell labeling and organelle tracking. Advanced Materials 2004;16(12):961-966.

102. Wang F, Zhang Y, Fan X, Wang M. Facile synthesis of water-soluble LaF3 : Ln3+ nanocrystals. Journal of Materials Chemistry 2006;16:1031-1034.

103. Stouwdam JW, Hebbink GA, Huskens J, van Veggel F. Lanthanide-doped nanoparticles with excellent luminescent properties in organic media. Chemistry of Materials 2003;15(24):4604-4616.

104. Thomas ED, Shields H, Zhang Y, McCollumb BC, Williams RT. EPR and luminescence studies of LaF, and CeF, under X-ray and laser irradiation. Journal of Luminescence 1997;71:93-104.

105. Rodnyi P, Melchakov E, Zakharov N, Munrob I, Hopkirk A. Fast luminescence of cerium doped lanthanum fluoride. Journal of Luminescence 1995;65:85-89. .

106. Jouda K, Tanaka S, Ichikawa K, Aita O. X-ray photoemission and X-ray emission spectra in rare-earth trifluorides Journal of The Physical Society of Japan 1996;65:2585-2589.

107. Liu YF, Chen W, Wang SP, Joly AG, Westcott S, Woo BK. X-ray Luminescence of LaF3:Tb and LaF3:Ce, Tb Water Soluble Nanoparticles. J Appl Phys 2008;103(6):63105.

108. Chen W. Nanoparticle Fluorescence Based Technology For Biological Applications. J Nanosci Nanotechnol 2008;8(3):1019-1051.

109. Jacob SW, Wood DC. Dimethyl Sulfoxide (DMSO). Am J Surgery 1967;114:414-426.

110. Pope DC, Oliver WT. Dimethyl Sulfoxide (DMSO). Can J Comp Med Vet Sci 1966;30:3--8.

111. Yu Z-W, Quinn PJ. Dimethyl Sulphoxide: A Review of Applications in Cell Biology. Biosci Rep 1994;14:259-281.

112. Parkin J, Shea C, Sant G. Intravesical dimethyl sulfoxide (DMSO) for interstitial cystitis—a practical approach. Urol 1997;49:105-107.

113. DMSO - The Magic Bullet For Cancer, http://cancertutor.com/Cancer/DMSO.htm.

114. Broadwell R, Salcman M, Kaplan R. Morphologic Effect of Dimethyl Sulfoxide on the Blood–Brain Barrier Science 1982;217:164-166.

115. Schrijvers DL. Extravasation: A Dreaded Complication of Chemotherapy. Annals of Oncology 2003;14:26-30.

116. Lebredo L, Barrie R, Woltering E. DMSO Protects Against Adriamycin-Induced Tissue Necrosis. J Surgical Res 1992;53:62-65.

117. Leon AS, Bloor CM, Pitt B. The Effects of Dimethylsulfoxide (DMSO) on the Healing of Experimental Myocardial Necrosis. Am heart J 1970;79:384-389.

118. Wang K, Adelstein SJ, Kassis AI. DMSO Increases Radioiodination Yield of Radiopharmaceuticals. Appl Radiat Isot (UK) 2008;66:50-59.

119. Raposio E, Santi PL. Topical Application of DMSO As an Adjunct to Tissue Expansion for Breast Reconstruction. British J Plastic Surgery 1999;52:194-197.

120. Regelson W, Harkins S. Amyloid Is Not A Tombstone—A Summation. The Primary Role For Cerebrovascular And CSF Dynamics As Factors In Alzheimer's Disease (AD): DMSO, Fluorocarbon Oxygen Carriers, Thyroid Hormonal, And Other Suggested Therapeutic Measures. Ann NY Acad Sci 1997;826:348–374.

121. Wood DC, Wood J. Pharmacologic and Biochemical Consideration of Dimethyl Sulfoxide. Ann NY Acad Sci 1975;243:7-19.

122. Yoshiike T, Aikawa Y, Sindhvananda J, Suto H, Kawamoto T, Odawa H. Skin Barrier Defect in Atopic Dermatitis: Increased Permeability of the Stratum Corneum Using Dimethyl Sulfoxide and Theophylline. J Dermatol Sci 1993;5:92-96.

123. Lehmann P, Holzle E, Melnik B, Plewig G. Effects of Ultraviolet A and B on the Skin Barrier: a Functional,Eelectron Microscopic and Lipid Biochemical Study. Photodermatol Photoimmunol Photomed 1991;8:129-134.

124. Hakura A, Mochida H, Yamatsu K. Dimethyl Sulfoxide (DMSO) is Mutagenic For Bacterial Mutagenicity Tester Strains. Mutation Research 1993;303:127-133.

125. Wankhede ME, Haram SK. Synthesis and Characterization of Cd-DMSO Complex Capped CdS Nanoparticles Chem Mater 2003;15(6):1296 -1301.

126. Diaz D, Rivera M, Ni T, Rodriguez J-C, Castillo-Blum S-E, Nagesha D, Robles J, Alvarez-Fregoso O-J, Kotov* NA. Conformation of Ethylhexanoate Stabilizer on the Surface of CdS Nanoparticles J Phys Chem B 1999;104(45):9854 -9858.

127. Elbaum R, Vega S, Hodes G. Preparation and surface structure of nanocrystalline cadmium sulfide (sulfoselenide) precipitated from dimethyl sulfoxide solutions. Chemistry of Materials 2001;13(7):2272-2280.

128. Li YB, Ma L, Zhang X, Chen W, Joly AG, Z. Liu. Synthesis and Optical Properties of Sulfide Nanoparticles Prepared in Dimethyl Sulfoxide. J Nanosci Nanotechnol 2008;8(11):5646.

129. Chen D, Wang Y, Yu Y, En Ma. Influence of Yb3+ content on microstructure and fluorescence oxyfluoride glass ceramics containing LaF3 nano-crystals Materials Chemistry and Physics 2007;101 464-469.

130. Pi D, Wang F, Fan X, Wang M, Zhang Y. Luminescence behavior of Eu3+ doped LaF3 nanoparticles 2005, A. Spectrochimica Acta Part A 2005;61:2455-2459. .

131. Zhang YW, Sun X, Si R, You LP, Yan CH. Single-crystalline and monodisperse LaF3 triangular nanoplates from single-source precursor. J Am Chem Soc 2005;127:3260.

132. Wojtowicz AJ, Balcerzyk M, Wisniewski D, Lempicki A. Scintillation light trapping and rdaiation damage in CeF3. IEEE TRANSACTIONS ON NUCLEAR SCIENCE, 1994;41(4):713.

133. Elias LR, Heaps WS, Yen WM. Excitation of uv Fluorescence in LaF3 Doped with Trivalent Cerium and Praseodymium. Physical Review B 1973;8(11):4989.

134. Pedrinit C, Moinet B, Gacon JC, Jacquier B. One- and two-photon spectroscopy of Ce3+ ions in LaF3-CeF3 mixed crystals. J Phys: Condens Matter 1992;4:5461.

135. Mandal PK, Paul A, Samanta A. Excitation wavelength dependent fluorescence behavior of the room temperature ionic liquids and dissolved dipolar solutes. J Photochem Photobio A 2006;182:113-120.

136. Yang J, Gautam S, Zhang Y, Li L, Dey J, Chen W, Mason RP, Tang L. Development of non-phenyl containing biodegradable photoluminescent polymers. Proc Natl Acad Sci U S A 2009;106:10086-10091.

137. Sun Y-P, Zhou B, Lin Y, Wang W, Fernando KAS, Pankaj Pathak, Meziani MJ, Harruff BA, Wang X, Wang H, Luo PG, Yang H, Kose ME, Chen B, Veca LM, Xie S-Y. Quantum-Sized Carbon Dots for Bright and Colorful Photoluminescence. J AM CHEM SOC 2006;128:7756-7757.

138. Lakowicz JR. Principles of Fluorescence Spectroscopy Springer; 2006.

139. Shionoya S, Yen WM, editors. Phosphor Handbook. New York: CRC Press; 1999.

140. Vogler A, Kunkely H. excited state properties of lanthanide complexes: Beyond ff states. Inorganica Chimica Acta 2006;359:4130.

141. Liu Y, Chen W, Joly AG, Wang Y, Pope C, Zhang Y, Bovin JO, Sherwood P. Comparison of water-soluble CdTe nanoparticles synthesized in air and in nitrogen. J Phys Chem B Condens Matter Mater Surf Interfaces Biophys 2006;110(34):16992-17000.

142. Peng XG. Green chemical approaches toward high-quality semiconductor nanocrystals. Chemistry-A European Journal 2002;8(2):335-339.

143. Schachar R, Chen W, Woo BK, Pierscione B, Zhang X, Ma L. Diffusion of nanoparticles into the capsule and cortex of crystalline lens. Nanotechnology 2008;19:25102.

144. Kennedy JC, Pottier RH. New trends in photobiology: Endogenous protoporphyrin IX, a clinically useful photosensitizer for photodynamic therapy. Journal of Photochemistry and Photobiology B: Biology 1992;14(4):275-292.

145. Diamandis EP. EUROPIUM AND TERBIUM CHELATORS AS CANDIDATE SUBSTRATES FOR ENZYME-LABELED TIME-RESOLVED FLUOROMETRIC IMMUNOASSAYS. Analyst 1992;117(12):1879-1884.

146. Horrocks WD, Sudnick DR. Lanthanide Ion Luminescence Probes of the Structure of Biological Macromolecules. Accounts of Chemical Research 1981;14(12):384-392.

147. Freed S, Weissman SI, Fortess FE, Jacobson HF. Ions of Europium Distributed Between Different Configurations in Homogeneous Solutions. The Journal of Chemical Physics 1939;7(9):824-828.

148. Barthelemy PP, Choppin GR. Luminescence Study of Complexation of Europium and Dicarboxylic-Acids. Inorganic Chemistry 1989;28(17):3354-3357.

149. Breen PJ, Dehorrocks W. Europium(Iii) Luminescence Excitation Spectroscopy - Inner-Sphere Complexation of Europium(Iii) by Chloride, Thiocyanate, and Nitrate Ions. Inorganic Chemistry 1983;22(3):536-540.

150. Richardson FS. TERBIUM(III) AND EUROPIUM(III) IONS AS LUMINESCENT PROBES AND STAINS FOR BIOMOLECULAR SYSTEMS. Chem Rev 1982;82(5):541-552.

151. Albin M, Farber GK, Horrocks WD. Europium(Iii) Luminescence Excitation Spectroscopy - a Species-Specific Method for the Quantitation of Lanthanide Ion Binding to Chelating-Agents - Complexes of (1,2-Ethanediyldioxy)Diacetate. Inorganic Chemistry 1984;23(12):1648-1651.

152. Bryden CC, Reilley CN. Europium Luminescence Lifetimes and Spectra for Evaluation of 11 Europium Complexes as Aqueous Shift-Reagents for Nuclear Magnetic-Resonance Spectrometry. Analytical Chemistry 1982;54(4):610-615.

153. Lis S, Choppin GR. Determination of Small Amounts of Water in Dimethylformamide and Dimethylsulfoxide Using Luminescence Lifetime Measurements of Europium(Iii). Analytical Chemistry 1991;63(21):2542-2543.

154. Yao MZ, Joly AG, Chen W. Formation and Luminescence Phenomena of LaF3:Ce3+ Nanoparticles and Lanthanide-Organic Compounds in Dimethyl Sulfoxide. J Phys Chem C 2010;114(2):826-831.

155. Pires AM, Davolos MR, Malta OL. EU3+-O2- associates luminescence in Ba2SiO4. Journal of Luminescence 1997;72-4:244-246.

156. Jouart JP, Bouffard M, Klein G, Mary G. CUBIC EU-3+ CENTERS IN FLUORITE-TYPE CRYSTALS. Journal of Luminescence 1991;50(5):273-277.

157. Bang J, Yang H, Abrams B, Holloway PH. Effects of electron beam current density and temperature on peak height ratios D-5(j)/D-5(0) for cathodoluminescence of Ln(2)O(2)S : Eu3+. Journal of Luminescence 2007;126(2):629-635.

158. Reisfeld R, Zigansky E, Gaft M. Europium probe for estimation of site symmetry in glass films, glasses and crystals. Molecular Physics 2004;102:1319-1330.

159. Lu HC, Yi GS, Zhao SY, Chen DP, Guo LH, Cheng J. Synthesis and characterization of multi-functional nanoparticles possessing magnetic, up-conversion fluorescence and bio-affinity properties. Journal of Materials Chemistry 2004;14(8):1336-1341.

160. Stouwdam JW, van Veggel FCJM. Near-infrared emission of redispersible Er3+, Nd3+, and Ho3+ doped LaF3 nanoparticles. Nano Letters 2002;2(7):733-737.

161. Diamente PR, Burke RD, van Veggel FCJM. Bioconjugation of Ln(3+)-doped LaF3 nanoparticles to avidin. Langmuir 2006;22(4):1782-1788.

162. Yu WW, Chang E, Drezek R, Colvin VL. Water-soluble quantum dots for biomedical applications. Biochemical and Biophysical Research Communications 2006;348(3):781-786.

163. Franzo G, Iacona F, Vinciguerra V, Priolo F. Enhanced rare earth luminescence in silicon nanocrystals. Mat Sci Eng B-Solid 2000;69:335-339.

164. Fan WL, Zhao W, You LP, Song XY, Zhang WM, Yu HY, Sun SX. J Solid State Chem 2004;177:4399.

165. Haase M, Riwotzki K, Meyssamy H, Kornowski A. Synthesis and properties of colloidal lanthanide-doped nanocrystals. J Alloy Compd 2000;303:191-197.

166. Marrero-Lopez D, Nunez P, Abril M. J Non-Cryst Solids 2004;345:377.

167. Xie YB, Yuan CW. Characterization and photocatalysis of Eu3+-TiO2 sol in the hydrosol reaction system. Mater Res Bull 2004;39(4-5):533-543.

168. Chen LM, Liu YN, Li YD. Preparation and characterization of ZrO2 : Eu3+ phosphors. J Alloy Compd 2004;381(1-2):266-271.

169. Song HW, Yu LX, Yang LM, Lu SZ. Luminescent properties of rare earth ions in one-dimensional oxide nanowires. Journal of Nanoscience and Nanotechnology 2005;5(9):1519-1531.

170. Yu LX, Song HW, Liu ZX, Yang LM, Zheng SZLZH. Electronic transition and energy transfer processes in LaPO4-Ce3+/Tb3+ nanowires. J Phys Chem B 2005;109(23):11450-11455.

171. Yanes AC, Del-Castillo J, Mendez-Ramos J, Rodriguez VD, Torres ME, Arbiol J. Luminescence and structural characterization of transparent nanostructured Eu3+-doped LaF3-SiO2 glass-ceramics prepared by sol-gel method. Opt Mater 2007;29(8):999-1003.

172. Cheng KH, Aijmo J, Ma L, Yao M, Zhang X, Como J, Hope-Weeks LJ, Huang J, Chen W. Luminescence Decay Dynamics and Trace Biomaterials Detection Potential of Surface-Functionalized Nanoparticles. The Journal of Physical Chemistry C 2008;112(46):17931-17939.

173. Chen W. Nanoparticle Self-Lighting Photodynamic Therapy For Cancer Treatment. J Biomed Nanotechnol 2008;4:369-276.

174. Chen W, Zhang J. Using Nanoparticles to Enable Simultaneous Radiation and Photodynamic Therapies for Cancer Treatment. J Nanosci Nanotechnol 2006;6:1159-1166.

175. Chen W, Westcott SL, Wang S, Liu Y. Dose Dependent X-Ray Luminescence in MgF_2:Eu^{2+}, Mn^{2+} Phosphors. J Appl Phys 2008;103:113103.

176. Knoll GF. Radiation detection and Measurement, Third Edition: John Wiley & Sons, Inc.; 2000.

177. Derenzo SE, Weber MJ, Bourret-Courchesne E, Klintenberg MK. The quest for the ideal inorganic scintillator. Nuclear Instruments and methods in Physics Research A 2003;505:111-117.

178. Birowosuto MD, Dorenbos P, Eijk CWEv, Kramer KW, Gudel HU. Scitillation properties of $LuI_3:Ce^{3+}$ -high light yield scitillators. IEEE Transactions on nuclear science 2005;52(4):1114-1118.

179. Khaidukova NM, Lamb SK, Lob D, Makhov VN. Observation of Time-transient spectral narrowing at 309 nm in Ce^{3+} doped SrF_2 crystal. Opt Commun 2005;205:415-420.

180. Radzhabov E. Charge transfer luminescence in Ce-doped fluorides. Radiation Effects & Defects in Solids 2003;158(1-6):203-207.

181. Zhang MS, Yu J, Chen WC, Yin Z. Optical and structral properties of pure and Ce-doped nanocrystals of barium titanate. Progress in Crystal Growth & Characterization 2000;40(1-4):33-42.

182. Dabbousi BO, RodriguezViejo J, Mikulec FV, Heine JR, Mattoussi H, Ober R, Jensen KF, Bawendi MG. (CdSe)ZnS core-shell quantum dots: Synthesis and characterization of a size series of highly luminescent nanocrystallites. Journal of Physical Chemistry B 1997;101(46):9463-9475.

183. Chen W, Zhang JZ, Joly AG. Optical properties and potential applications of doped semiconductor nanoparticles. J Nanosci Nanotechnol 2004;4(8):919-947.

184. He Y, Sai L-M, Lu H-T, Hu M, Lai W-Y, Fan Q-L, Wang LH, Huang W. Microwave-Assisted Synthesis of Water-Dispersed CdTe Nanocrystals with High Luminescent Efficiency and Narrow Size Distribution. Chemistry of Materials 2007;19:359-365.

185. Joly AG, Chen W, McCready DE, Malm J-O, Bovin J-O. Upconversion luminescence of CdTe nanoparticles. Phys Rev B 2005;71(16):165304.

186. Chen W, Joly AG, McCready DE. Upconversion luminescence from CdSe nanoparticles. J Chem Phys 2005;122(22):224708.

187. Ouyang J, Ripmeester JA, Wu X, Kingston D, Yu K, Joly AG, Chen W. Upconversion Luminescence of Colloidal CdS and ZnCdS Semiconductor Quantum Dots. J Phys Chem C 2007;111:16261-16266.

188. Chen W, Zhang J, Westcott SL, Joly AG, Malm J-O, Bovin J-O. The Origin of X-ray Luminescence from CdTe Nanoparticles in CdTe/BaFBr:Eu^{2+} Nanocomposite Phosphors. Journal of Applied Physics 2006;99:34302 34301-34305.

189. Gaponik N, Talapin DV, Rogach AL, Hoppe K, Shevchenko EV, Kornowski A, Eychmuller A, Weller H. Thiol-Capping of CdTe Nanocrystals: An Alternative to Organometallic Synthetic Routes. J Phys Chem B 2002;106(29):7177-7185.

190. Hu H, Chen Z, Cao T, Zhang Q, Mengxiao Yu, Li F, Yi T, Huang C. Hydrothermal synthesis of hexagonal lanthanide-doped LaF_3 nanoplates with bright upconversion luminescence. Nanotechnology 2008(19):375702-375711.

191. Tang ZY, Kotov NA, Giersig M. Spontaneous organization of single CdTe nanoparticles into luminescent nanowires. Science 2002;297(5579):237-240.

192. Peng XG, Manna L, Yang WD, Wickham J, Scher E, Kadavanich A, Alivisatos AP. Shape control of CdSe nanocrystals. Nature 2000;404(6773):59-61.

193. Scher EC, Manna L, Alivisatos AP. Shape control and applications of nanocrystals. Phil Trans R Soc Lond A 2003;361:241-257.

194. Leitsmann R, Bechstedt F. Influence of the quantum confined Stark effect on photoluminescence spectra of PbTe nanodots embedded in a CdTe matrix. Phys Rev B 2009;80:165402.

195. Leitsmann R, Bechstedt F. Characteristic Energies and Shifts in Optical Spectra of Colloidal IV−VI Semiconductor Nanocrystals. ACS Nano 2009;3(11):3505.

196. Mastro MA, Jr. JAF, Holm RT, Jr CRE, Caldwell J, Liu K, Glembocki O, Henry RL, Kim J. Rare-earth chloride seeded growth of GaN nano- and micro-crystals. appl Suf Sci 2007;253:6157-6161.

197. Yao M, Liu B, Zou Y, Wang L, Cui T, Zou G, Li J, Sundqvist B. Effect of Rare-Earth Component of the RE/Ni Catalyst on the Formation and Nanostructure of Single-Walled Carbon Nanotubes. J Phys Chem B 2006;110:15284-15290.

198. Watanabe K, Sunagawa I. Effects of trivalent rare-earth ions upon the morphology of corundum crystals J Cryst Grow 1983;65:568-575.

199. Lev O, Tsionsky M, Rabinovich L, Glezer V, Sampath S, Pankratov I, Gun J. Organically Modified Sol-Gel Sensors. Analytical Chemistry 1995;67(1):A22-A30.

200. Brinker CJ. Hydrolysis and Condensation of Silicates - Effects on Structure. J Non-Cryst Solids 1988;100(1-3):31-50.

201. Brinker CJ, Scherer G. Sol-Gel Science. New York: Academic Press; 1989.

202. Kozuka H. Proc SPIE. Volume 3236; 1994. p 304.

203. Cai W, Z. L. Characerization and the optical seitching phenomenon of porous silica dispersed with silver nano-particles within its pores. Journal of physics: Condensed Matter 1996;8(40):L591-L596.

204. Ritzer B, Villegas MA, Navarro JMF. Influence of temperature and time on the stability of silver in silica sol-gel glasses. J Sol-Gel Sci Techn 1997;8(1-3):917-921.

205. Ricard D, Roussignol P, Flytzanis C. Surface-Mediated Enhancement of Optical-Phase Conjugation in Metal Colloids. Optics Letters 1985;10(10):511-513.

206. Chia C, Kao YH, Xu YH, Mackenzie JD. Cadmium telluride quantum dot-doped glass by the sol-gel technique. Sol-Gel Optics Iv 1997;3136:337-347

207. Ou DL, Seddon AB. Cadmium selenide quantum dot doping of organic-inorganic hybrid materials derived by sol-gel processing. Sol-Gel Optics Iv 1997;3136:348-357

208. Guo L, Hyeon-Lee J, Beaucage G. J Non-Cryst Solids 1999;243:61.

209. Collinson MM, Howells AR. Sol-gels and electrochemistry: Research at the intersection. Analytical Chemistry 2000;72(21):702a-709a.

210. Collinson MM. Analytical applications of organically modified silicates. Mikrochim Acta 1998;129(3-4):149-165.

211. Jin T, Tsutsumi S, Deguchi Y, Machida K, Adachi G. Luminescence characteristics of the lanthanide complex incorporated into an ORMOSIL matrix using a sol-gel method. J Electrochem Soc 1996;143(10):3333-3335.

212. Jin T, Inoue S, Tsutsumi S, Machida K, Adachi GY. Luminescence properties of lanthanide complexes incorporated into sol-gel derived inorganic-organic composite materials. J Non-Cryst Solids 1998;223(1-2):123-132.

213. Machida K, Li H, Ueda D, Inoue S, Adachi G. Preparation and application of lanthanide complex incorporated ormosil composite phosphor films. Journal of Luminescence 2000;87-9:1257-1259.

214. Birowosuto MD, Dorenbos P, van Eijk CWE, Kramer KW, Gudel HU. Scintillation properties of LuI_3 : Ce^{3+}-high light yield scintillators. Ieee T Nucl Sci 2005;52(4):1114-1118.

215. Khaidukova NM, Lamb SK, Lob D, Makhov VN. Opt Commun 2005;205:415.

216. Radzhabov E. Charge transfer luminescence in Ce-doped fluorides. Radiat Eff Defect S 2003;158(1-6):203-207.

217. Zhang MS, Yu J, Chen WC, Yin Z. Optical and structral properties of pure and Ce-doped nanocrystals of barium titanate. Prog Cryst Growth Ch 2000;40(1-4):33-42.

218. Kang KS, Kim JH. Origin of blue luminescence from a hybrid sol-gel after thermal processing. J Phys Chem C 2008;112(2):618-620.

219. Green WH, Le KP, Grey J, Au TT, Sailor MJ. White phosphors from a silicate-carboxylate sol-gel precursor that lack metal activator ions. Science 1997;276(5320):1826-1828.

BIOGRAPHICAL INFORMATION

Mingzhen Yao received her Master degree in physics from Tongji University in China in 2002; she continued her graduate study in the University of Texas at Arlington in 2006 and earned another Master degree in applied physics in 2008 and a Ph.D degree in 2011. Her research interest focuses on developing nanomaterials for radiation detection and biomedical applications.